Dissertation

Theoretical Modeling of Quantum Dots Nanolasers and Disordered Coupled-Cavity Arrays

Mawussey Segnon
University of Bremen

Theoretical Modeling of Quantum Dots Nanolasers and Coupled-Cavity Arrays

dem Fachbereich Physik/Elektrotechnik
der Universität Bremen

zur Erlangung des akademischen Grades
Doktor der Naturwissenschaften (Dr. rer. nat.)
vorgelegte Dissertation

von

M. Sc. Mawussey Segnon
aus Lomé

Bremen, Oktober 2018

This work was typset in LateX.
Figures were generated by means of TikZ, the vector graphics language,
mathematica, the technical computing sofware, and Veusz, the scientific plotting package.

Liste der Gutachter:

Prof. Dr. Frank Jahnke
Institut für Theoretische Physik
Universität Bremen,
Otto-Hahn-Allee 1 (NW1) ,
28334 Bremen,
Germany

Prof. Dr. Tim Wehling
Institut für Theoretische Physik
Universität Bremen,
Otto-Hahn-Allee 1 (NW1) ,
28334 Bremen,
Germany

Datum der mündlichen Prüfung: 18. Januar 2019

Zum Druck genehmigt: 18. Januar 2019

Abstract

Ultrasmall semiconductor lasers have emerged as strong candidates for the implementation of quantum information processing devices. Manufacturing such nanophotonic light sources heavily relies on the use of cavity quantum electrodynamic effects to enhance spontaneous emission and enable the lasing threshold to be crossed with gain contributions from only a few solid-state emitters. In the cavity quantum electrodynamic regime, the emission dynamics of nanolasers is governed by photonic and electronic correlation and fluctuations effects. This thesis accompanies some of the advancements in ultrasmall lasers by using microscopic quantum-optical models to enable a better understanding of the underlying physical effects.

The first main topic of this thesis draws on time-resolved photon-correlation spectroscopy to investigate the build up of second-order coherence, associated with lasing, on a different timescale than the emission itself in a quantum-dot photonic-crystal nanolaser emitting in the telecom band. By combining measurements perfomed by *Dr. Galan Moody* at the National Institute of Standards and Technology, Colorado, USA, with a microscopic semiconductor laser theory, the non-Markovian behavior of the emission dynamics is attributed to carrier-photon correlations that are not amenable by using laser rate-equation formalism. The obtained insights have direct implications with respect to the modulation response, repetition rate, noise characteristics, and coherence properties of nanolasers for device applications.

The second main topic concerns a theoretical modeling of single-emitter lasing effects in a quantum dot (QD)-microlaser under controlled variation of background gain provided by off-resonant discrete gain centers. In the framework of a judicious two-color excitation scheme, recently put forward by the group of *Prof. Stephan Reitzenstein* in Berlin, the background gain contribution of off-resonant QDs can be continuously tuned by precisely balancing the relative excitation power of two lasers emitting at different wavelengths. In this thesis, a multi-component gain medium semiconductor laser theory has been developed, which in conjunction with the measurements allows for identifying distinct single-QD signatures in the lasing characteristics, and for distinguishing between gain contributions of a single resonant emitter and a countable number of off-resonant background emitters to the optical output of the microlaser. The upshot of the joint theoretical and experimental investigation is that in experimentally accessible systems, and in the investigated micropillar in particular, the single-QD gain needs to be supported by the background gain contribution of off-resonant QDs to reach the transition

to lasing. Theoretical calculations based on the developed model reveal that while a single QD cannot drive the investigated micropillar into lasing, its relative contribution to the emission can be as high as 70 % and it dominates the statistics of emitted photons in the intermediate excitation regime below threshold.

The last part of the dissertation deals with the analytical and numerical investigation of collective lasing in disordered coupled-cavity arrays. These systems are an interesting physical architectures, wherein the optical coupling between their building blocks allows for exploring some exotic states of photons including the Mott insulator and the fractional quantum Hall effect. The analysis focuses on the Jaynes-Cummings-Hubbard Hamiltonian, where each cavity contains a single two-level quantum dot interacting with the confined local mode and contiguous cavities are mutually coupled by photon hopping. By introducing a diagonal average approximation, it can be show that results for translation invariant coupled cavities, i.e. homogeneous coupled cavities, can be extended for weak photonic disordered array of cavities.

Contents

Part

I

Motivation and Introduction

1 Motivation and Outline

It is an intriguing fact that the spontaneous emission (SE) is not a rigid property of an atom, but is orchestrated by the interaction of the atom with the ambient light field. Since the effect has been demonstrated by the pioneering work of E. M. Purcell in 1946 [1], the study of light-matter interaction in cavities and that of exerting control over the SE has blossomed into a vivid field of research commonly termed *cavity quantum electrodynamic* (cQEQ). Besides providing a solid framework for testing some paradoxical concepts of the quantum mechanics [2], cQED concept harbors a huge amount of potential for quantum information science [3–6].

Self-assembled Stranski–Krastanov semiconductor quantum dots (QDs) are engineered quantum systems allowing for a 3D carrier confinement giving rise to a strong localization of electron-hole pairs, the level spacing of which can be tuned by the size, the geometry and the composition of the QDs. Implementation of cQED using semiconductor QDs has paved the way for the fabrication of ultrasmall nanolasers constituting the building block of applications in on-chip integration of nanophotonics and nanoelectronics [7–10]. The small mode volume provided by the optical cavities, such as micropillars [11, 12], microdisks [13, 14] and photonic crystals [15, 16] being designed for a three-dimensional (3D) confinement of light and thereby a discretization of the mode spectrum, allows for a single-mode lasing with a few emitters [17–19] or even a single emitter [20–22]. In contrast to conventional lasers, nanolasers operate in the cQED regime and take advantage of the *Purcell effect* [1] to channel a large fraction of the spontaneously emitted photons into the lasing mode, visible in the output intensity as a vanishing of the threshold jump [17–19]. In this regime, the emission dynamics of nanolasers is governed by photonic and electronic excitation correlation, and fluctuations effects. A sophisticated theoretical basis for understanding such correlations and effects is of salient relevance for the lasing transition, especially in the ultimate limit of single QD nanolaser. The purpose of this thesis is to use a microscopic semiconductor quantum dot laser theory to investigate non-Markovian delay in the formation of coherence in quantum-dot nanolasers operating in the cavity-QED regime, and the influence of background emitters on lasing in quantum dot micropillars.

The first main topic of this thesis draws on time-resolved photon-correlation spectroscopy to investigate the build up of second-order coherence, associated with lasing, on a different timescale than the emission itself in a quantum-dot photonic-crystal nanolaser emitting in the telecom band. By combining measurements, perfomed by *Dr. Galan Moody* at the National

Institute of Standards and Technology, Colorado, USA, with a microscopic semiconductor laser theory, the non-Markovian behavior of the emission dynamics is attributed to carrier-photon correlations that are not amenable by using laser rate-equation formalism.

The second main topic concerns a theoretical modeling of single-emitter lasing effects in a quantum dot (QD)-microlaser under controlled variation of background gain provided by off-resonant discrete gain centers. In the framework of a judicious two-color excitation scheme, recently put forward by the group of *Prof. Stephan Reitzenstein* in Berlin, the background gain contribution of off-resonant QDs can be continuously tuned by precisely balancing the relative excitation power of two lasers emitting at different wavelengths. In this thesis, a multi-component gain medium semiconductor laser theory has been developed, which in conjunction with the measurements allows for identifying distinct single-QD signatures in the lasing characteristics, and for distinguishing between gain contributions of a single resonant emitter and a countable number of off-resonant background emitters to the optical output of the microlaser.

Quantum networks based on coupled high-quality cavities constitute an interesting physical architecture, wherein the optical coupling between its building blocks allows for investigating the realm of strongly correlated states of light [23–25]. In contrast to their counterparts *Josephson junctions and optical lattices*, they allow for the control and the addressability of single-sites and therefore open the door to many applications in quantum information science [26, 27]. The last part of the dissertation deals with the analytical and numerical investigation of collective lasing in disordered coupled-cavity arrays. The analysis focuses on the Jaynes-Cummings-Hubbard Hamiltonian, where each cavity contains a single two-level quantum dot interacting with the confined local mode and contiguous cavities are mutually coupled by photon hopping. By introducing a diagonal average approximation, it can be shown that results for translation invariant coupled cavities, i.e. homogeneous coupled cavities, can be extended for weak photonic disorder in an array of cavities.

Outline of the thesis

The present thesis is divided into nine chapters. **Chapter** 2 serves as an introduction to the physics of the cavity quantum electrodynamic. Here the different physical effects arising in limits of weak and strong coupling regime will be succinctly addressed. This includes the *Purcell effect*, being the modification of the spontaneous emission pattern of an emitter in a single mode cavity and the *vacuum rabi-splitting* which is the modification of the cavity spectrum.

Chapter 3 is devoted to the theoretical framework underlying the study of open quantum systems. Firstly the time evolution in closed quantum systems is discussed. The remaining part of the chapter focuses on the derivation of the set of equations underlying the analysis of the dynamical behavior of quantum systems interacting with their surrounding.

The ensuing **Chap**. 4 deals with the light-matter interaction in semiconductor quantum dots.

The first part sets up the model Hamiltonian of the system under consideration. Because solving the *Quantum Markovian Master Equation* is intractable when it comes to dealing with many-body systems, the second part discusses the expectation value approach and its intimately related hierarchy problem. Here, concept such the cluster expansion will be alluded. To exemplify the mean value scheme, the last part presents the derivation of the semiconductor luminescence equations which constitute the starting point of the semiconductor quantum-dots laser model.

Chap. 5 draws on the semiconductor luminescence equations outlined in Chap. 4 to derive the theory for semiconductor quantum-dots nanolasers. Upon considering high-order carrier-photon correlations, access to the second-order photon correlation function being a powerful tool for the characterization of the threshold properties in nanolasers, is amenable.

Chapter 6 dwells on the theoretical modeling of the non-Markovian effect in the lasing dynamics of high-Q nanolasers. Here it can be theoretically and experimentally shown that in cavity quantum electrodynamic dynamics regime, carrier-photon correlations delays the response of the photon-autocorrelation to the onset of the stimulated emission. An adiabatic elimination of these correlations in the semiconductor quantum dots laser model restores the mainstream picture of lasing in which the coherent emission is intimately connected to the presence of stimulated emission.

Chap. 7 is devoted to the theoretical and experimental understanding, and controlling of the off-resonant emitters contribution to the gain medium in single quantum-dot microlasers. In the framework of a judicious two-color excitation scheme, put forward by the group of *Prof. Stephan Reitzenstein* in Berlin, which consists in selectively exciting resonantly the spectrally narrow p-shell of a target QD, while the gain of the off-resonantly coupled QDs is controlled simultaneously by above-band excitation, the gain contribution of background emitters can be tuned.

The theoretical and numerical analysis of lasing in an array of disordered coupled cavities are presented in **Chap**. 8. By resorting to the diagonal average approximation, it can be shown that for some parameters regime, the translation invariant result can be extended for weak disorder.

Chapter 9 ends the thesis with a summary of the points that have been addressed.

In the **Appendix**, the reader will find useful supplementary information. Appendix A presents the definition of the *Banach or Liouville space* and the proof of the *Lindblad representation.* **Appendix** B deals with the derivation of the equations of motion for the relevant correlation functions in coupled-cavity array.

2 Introduction–Cavity Quantum Electrodynamic

The field of *cavity quantum electrodynamic* (cQED) deals with the interaction between a dipole and the states of an electromagnetic field stored in a single-mode resonant cavity. The dipole may be a genuine atom, or may be based on engineered systems including, inter alia[1] quantum dots, nitrogen vacancy centers in diamond, superconducting systems. Figure 2.1 displays the core ingredients of the concept of cQED. Depending on the quality factor Q of the cavity and the dipole moment of the two-level system two communication regimes may be distinguished: the *weak coupling* and *strong coupling regime* [28, 29].

In the weak coupling regime, a modification of the spontaneous emission pattern of the dipole arises, a phenomenon commonly referred to as the Purcell effect [1] being instrumental in manufacturing nanolasers [7, 21, 22, 30]. On the other hand, the strong coupling regime leads to the reversibility of the spontaneous transition of the dipole. Here a periodic exchange of photons between the dipole and the cavity mode is observed [12, 31]. This entanglement of the emitter and the ambient cavity field constitutes the foundation of a variety of interesting phenomena which are essential for applications in quantum information processing.

The purpose of this chapter is to introduce the physics of cQED. After discussing the effect of the cavity on the emitter spontaneous emission dynamics in section 2.1, we proceed further to review the strong coupling regime in section 2.2.

2.1 Weak Coupling Regime

2.1.1 Free-space Spontaneous Emission

Let us consider a two-level emitter (TLE) as depicted in Fig. 2.1 with $|g\rangle$ being its ground state and $|e\rangle$ the excited state separated by an energy interval ω_{eg}. Then, the spontaneous emission is an irreversible process, wherein the TLE is demoted from its excited state to its ground state by radiating a photon. This process comes about as a result of the ineluctable coupling of the TLE to the surrounding electromagnetic field in its vacuum state. To describe the coupling between

[1] Latin for *Among others*

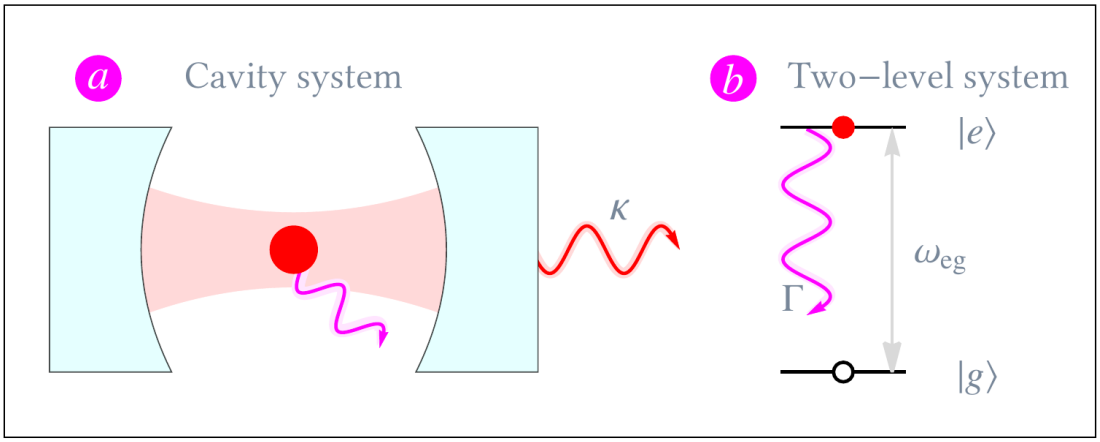

Figure 2.1 | A pictorial description of the cavity QED. The cavity system is described by three parameters including the light-matter coupling g_0, the photon leaking rate from the cavity κ and the non-resonant decay rate Γ of the emitter from its excited state $|e\rangle$ to the ground state $|g\rangle$.

the emitter and a field mode, the so-called *Rabi frequency* is usually used. It is given by [32]

$$\Omega_{eg} = \frac{d_{eg}\mathcal{E}_{\text{vac}}}{\hbar} \tag{2.1}$$

and encodes the frequency at which the emitter and the field would exchange energy if there field contained only a single mode. In Eq. (2.1), d_{eg} represents the matrix element of the electric dipole of the emitter between the two levels, while $\mathcal{E}_{\text{vac}}$ is the vacuum electric-field amplitude in a mode of frequency ω. It is expressible as [32]

$$\mathcal{E}_{\text{vac}} = \left(\frac{\hbar\omega}{2\varepsilon_0 V}\right)^{1/2}, \tag{2.2}$$

where ε_0 is the permittivity of free space and V is the volume of the cavity which is assumed to be large enough so that it has a negligible effect on the properties of the emitter. It is instructive to mention that in free space the radiation field is described in terms of an infinite set of harmonic oscillators, one for each mode of the radiation.

According to the Fermi's golden rule, the transition rate for spontaneous emission reads as

$$\Gamma_0 = \frac{2\pi}{3}\Omega_{eg}^2 g(\omega) = \frac{\omega^3}{3\pi\hbar c^3}\frac{|d_{eg}|^2}{\varepsilon_0}. \tag{2.3}$$

Here $g(\omega) = \omega^2 V/(\pi^2 c^3)$ represents local the density of state (LDOS) of the light field at the position of the emitter.

2.1.2 Spontaneous Emission Engineering

The dependence of the spontaneous emission on the LDOS of the radiation field suggests that a modification of the mode structure of the vacuum field may leads to the alteration of the

emission pattern of the the two-level emitter. Indeed, by loading the TLE into a single-mode[2] cavity whose size is comparable to the wavelength of the light field, the spontaneous emission rate can be enhanced [1] inhibited [33] depending on the magnitude of the spectral detuning between the cavity the emitter.

The effect of the single-mode cavity on the spontaneous emission dynamics of the emitter can be parametrized in terms of the so-called *Purcell factor*, F_P. It is given by

$$F_P = \frac{\Gamma_c}{\Gamma_0}, \tag{2.4}$$

where Γ_c and Γ_0 denote the spontaneous emission rate of the emitter in the cavity and in the free-space, respectively. In 1D single-mode cavity, where the density of modes around the fundamental cavity mode ω_c can be approximated by a normalized Lorentzian function [28],

$$g(\omega) = \frac{2}{\pi} \frac{\Delta\omega_c^2}{4\left(\omega - \omega_c\right)^2 + \Delta\omega_c^2} \tag{2.5}$$

with $\Delta\omega_c$ being the cavity bandwidth which is traditionally associated with the quality factor of the cavity as $Q = \omega_c/\Delta\omega_c$, the Purcell factor reads as

$$F_P = \frac{3Q(\lambda_c/n)^3}{4\pi^2 V_0} \xi^2 \frac{\Delta\omega_c^2}{4\left(\omega_{eg} - \omega_c\right)^2 + \Delta\omega_c^2}, \quad \text{with} \quad \xi = \frac{|\boldsymbol{d} \cdot \boldsymbol{E}(\boldsymbol{r}_e)|}{|\boldsymbol{d}|}. \tag{2.6}$$

Here λ_c denotes the wavelength of the cavity, n its refractive index, and V_0 its effective volume. At resonance and when the electric dipole of the emitter is oriented along the cavity field, the Purcell factor reduces to [29]

$$F_P = \frac{3Q(\lambda_c/n)^3}{4\pi^2 V_0}, \tag{2.7}$$

which depends only on the parameters of the cavity and suggests that high quality factor Q cavities with small modal volumes is required for large Purcell factors.

Alternatively, the effect of the cavity on the emitter emission dynamics can be described in terms of the *spontaneous emission factor* β which encodes the fraction of the number of photons loaded into the cavity mode to the total radiated photons. It is given by

$$\beta = \frac{\Gamma_l}{\Gamma_{nl} + \Gamma_l} = \frac{F_P}{1 + F_P}, \tag{2.8}$$

where Γ_{nl} and Γ_l denote the rate of photons into the leaking, and the lasing mode, respectively. Their derivation will be addressed in Chap. 5.

[2]Here single-mode means that there is only one resonant cavity mode being in the vicinity of the transition frequency of the emitter. The other modes are assumed to be far from resonance.

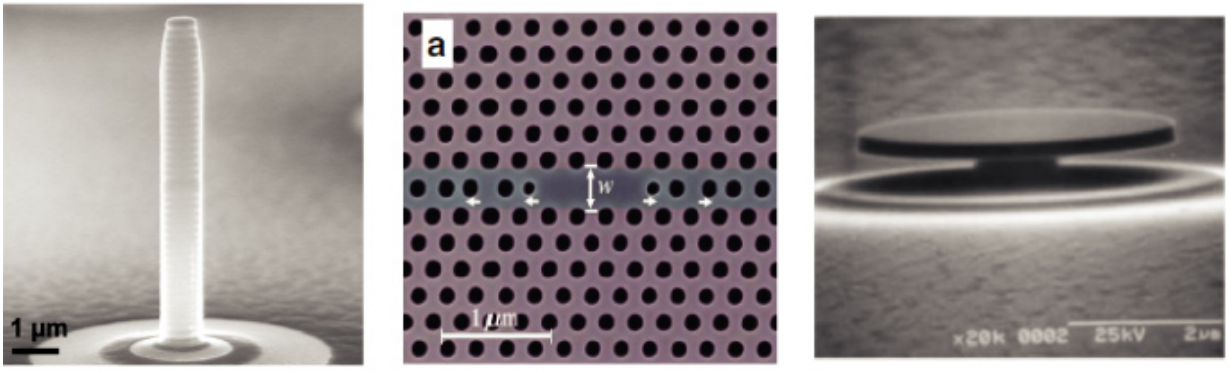

Figure 2.2 | Gallery of the most prominent type of optical resonators. Scanning electron microscopy images of quantum dot optical cavitie. The left panel displays the micropillar cavity, the middle and the right panel show the photonic crystal and microdisc cavity, respectively. Figure taken from Ref. [37].

Experimental implementation of the Purcell effect was carried out by *Drexhage* in the late 1960s in a fluorescence experiment using a rare earth ion placed in front of a mirror [34]. Over the years, due to the technological advancements in the solid-state physics, microcavities, such as the *micropillar, photonic crystal cavities*, which can be seen in Fig. 2.2, have emerged as platforms for engineering the LDOS. With them, single-mode light sources with β reaching 1 have been designed [17, 18, 35, 36]. In this thesis, some effects that arise due their small modal volumes of the order of the fraction of cubic wavelength will be investigated.

2.2 Strong Coupling Regime

When the coupling between the emitter and the empty cavity mode overpowers the dissipation channels, thus the spontaneous decay rate and the cavity loss, the cavity field and the dipole become entangled. An interesting feature of the strong coupling regime is coherent exchange of quanta between both subsystems, something that is commonly referred to as the vacuum Rabi oscillation. In the strong coupling (SC) regime , the interaction between the resonant cavity mode and the dipole is conveniently describe in terms of the so-called *dressed states*, $\psi_n^{\pm} = \frac{1}{\sqrt{2}}(|g,n\rangle + |e,n+1\rangle)$, which are the eigenstates of the Jaynes-Cummings model which encodes the interaction of two-level emitter with a single quantized mode of the radiation field [38],

$$H = \hbar\omega_{eg}\hat{\sigma}^{\dagger}\hat{\sigma} + \hbar\omega_b\left(\hat{b}^{\dagger}\hat{b} + \frac{1}{2}\right) + ig\left(\hat{\sigma}\hat{b}^{\dagger} - \hat{\sigma}^{\dagger}\hat{b}\right). \tag{2.9}$$

Here $\hat{\sigma}^{\dagger}(\hat{\sigma})$ is the emitter excitation (de-excitation) operator, g the light-matter coupling constant, and ω_{eg} and ω_b are the resonance frequency for the emitter and the cavity mode, respectively. The dressed states are split by an energy $2g\sqrt{n+1}$, which depends on th number of photons in the cavity mode n. The case of $n = 0$ is termed the *vacuum Rabi splitting* (VRS). By

treating the cavity loss and the emitter decay rate in the limit of weak damping, the energies of the two eigenmodes at resonance are expressible as [38–40]

$$E_{1,2} = E_0 - \mathrm{i}\lambda \pm \sqrt{g^2 - \lambda^2}, \quad \text{with} \quad \lambda = \frac{(\Gamma_0 + \kappa)}{4} \tag{2.10}$$

Here E_0 is the transition energy of the free dipole and the cavity mode in unity of $\hbar$, and Γ_0 and κ are their decay rates respectively. From the above expression follows the VRS for the composite system,

$$\Delta E = 2\sqrt{g^2 - \lambda^2} \tag{2.11}$$

yielding the condition for the strong coupling $4g > |\Gamma + \kappa|$. The SC regime plays a key role in the practical implementation of quantum information processing [41–44]. In the last part of this thesis, collective lasing in network of coupled cavities in SC regime will be analyzed.

Part

II

Theory

3 Quantum Markovian Master Equation

Since *bona fide*[1] world quantum systems are ineluctably coupled to their surroundings, any attempt to genuinely record their dynamics must stay clear of the Hamiltonian dynamics if there is no way to isolate the system from its environment. To account for this inherent openness, the theory of open quantum systems (TOQS) has been devised for a truly description of such a system without taking explicitly the environment into account [45]. The main idea of this theory is to conceive a global quantum system as a bipartite system and try to describe the time evolution of one of them by extending its Hamiltonian in order to account for the effect of the other system [45, 46] . TOQS has suggested many evolution equations depending on the nature of the environment. One, which is widely and extensively used in quantum information theory and quantum optics, see e.g Ref. [47] and references therein, in photochemistry, and in quantum measurement process [48, 49], is the so-called quantum dynamical semigroup (QDS) [46, 50]. In contrast to other approaches suggested by TOQS, such as the Redfield method[45], the QDS has the ability to maintain the von Neumann conditions of hermiticity, trace-preservation and positivity of any density operator. It has been pioneered by Lindblad, Gorini, Kossakowski and Sudarshan and is based on the assumption of Markovian dynamics. The Markovianess means that the time window between the build-up and the subsequent dispersion of the correlation function of the surrounding is so small that on a coarse-grained time scale the time evolution of the system state is unequivocally describable by the present state [51].

The present chapter aims at giving a survey of a basis knowledge required to deal with open quantum systems. Specifically, the focus will be on the derivation of the most general form of the quantum Markovian master equation (QMME) of the Lindblad-type. The QMME will be used in the subsequent chapters for deriving the equations of motion for the expectation value. More details on the all the subjects alluded to in this chapter can be found in [46–48, 52] and references therein.

3.1 Closed Quantum System

Before embarking on the derivation of the quantum Markovian master equation, it is worth taking a look at the dynamics in closed quantum systems in terms of the pure states and the

[1] Latin for *real*

density operator, as this constitutes its starting point.

From the mathematical point of view, the time evolution of any closed quantum mechanical system is described by the time-dependent Schrödinger equation (TDSE), which reads

$$\mathrm{i}\hbar\frac{\partial}{\partial t}|\psi\rangle = \hat{H}(t)|\psi\rangle. \tag{3.1}$$

Here $|\psi\rangle \in \mathcal{H}$ represents the state vector of the closed system at any time t, where $\mathcal{H}$ is the associated Hilbert space. $\hat{H}(t)$ is the Hamiltonian of the system, being self adjoint, i.e. $\hat{H}^\dagger(t) = \hat{H}(t)$. Hereafter, Planck's constant will be set equal to 1. Since the TDSE is a linear differential equation, its formal solution may be expressed in terms of the unitary time-evolution operator $\hat{U}$ whose operation transforms a state $|\psi_0\rangle$ at some initial time $t_0 = s$ to the state $|\psi\rangle$ at time t:

$$|\psi\rangle = \hat{U}(t,s)|\psi_0\rangle. \tag{3.2}$$

From the Schrödinger equation, an operator equation for the time evolution operator may be obtained [52, 53]

$$\begin{cases} \mathrm{i}\dfrac{\partial}{\partial t}\hat{U}(t,s) &= \hat{H}(t)\hat{U}(t,s) \\ \hat{U}(s,s) &= \hat{\mathbb{1}}. \end{cases} \tag{3.3}$$

By combining Eq. (3.2) and (3.3), the following crucial relation can be obtained

$$\hat{U}^\dagger(s,t)\hat{U}(t,s) = \hat{U}(t,s)\hat{U}^\dagger(s,t) = \hat{\mathbb{1}}, \tag{3.4}$$

which means $\hat{U}(t,s)$ is a norm-preserving map, in other words, the information encoded in the initial state is conserved in every solution to the Schrödinger equation at later times [54].

If the dynamical evolution is generated by a time independent Hamiltonian, which is the case encountered in closed, isolated quantum systems, the unitary map is easily obtained as

$$\hat{U}(t,s) = e^{-\mathrm{i}\hat{H}(t-s)}. \tag{3.5}$$

The situation is somehow subtle when the system under study is driven by an optical pulse, for instance. In this case the propagation operator can be formally written as

$$\hat{U}(t,s) = \hat{T}_t \exp\left(-\mathrm{i}\int_s^t \hat{H}(\tau)\,d\tau\right). \tag{3.6}$$

Here, $\hat{T}_t$ is the time ordering operator whose definition reads [54] :

Definition 3.1.1. *The time ordering operator $\hat{T}_t$ of a product of two operators $\hat{A}(t_1)\hat{A}(t_2)$ is defined by*

$$\hat{T}_t[\hat{A}(t_1)\hat{A}(t_2)] = \Theta(t_1 - t_2)\hat{A}(t_1)\hat{A}(t_2) + \Theta(t_2 - t_1)\hat{A}(t_1)\hat{A}(t_2), \tag{3.7}$$

where $\Theta(x)$ is the Heaviside step function:

$$\Theta(x) = \begin{cases} 1 & for \quad x \geq 0 \\ 0 & otherwise. \end{cases} \tag{3.8}$$

For a product of k operators $\hat{A}(t_1) \cdots \hat{A}(t_k)$ we can write:

$$\hat{T}_t[\hat{A}(t_1) \cdots \hat{A}(t_k)] = \sum_{\pi} \Theta[t_{\pi(1)} - t_{\pi(2)}] \cdots \Theta[t_{\pi(k-1)} - t_{\pi(k)}] \hat{A}[t_{\pi(1)}] \cdots \hat{A}[t_{\pi(k)}], \tag{3.9}$$

whereby π denotes a permutation of k indexes and the sum extends over all k! different permutations.

Hitherto, we have been monitoring the behavior of closed quantum systems in terms of state vectors. Alternatively, information about the state of a quantum system can be encoded in a density operator $\hat{\rho}$, which is a statistical operator. This approach is more general, as it allows for the description of mixture. Mixture is the term used to refer to a quantum system described by an ensemble of pure states $\{|\psi_n\rangle\}$, each one with a probability $\{p_n\}$ [55]. This set of states are not required to be orthogonal to each other. Formally speaking, the density operator, at some time t, is given as a convex combination of these pure states,

$$\hat{\rho}(t) = \sum_k p_k |\psi_k(t)\rangle \langle \psi_k(t)|. \tag{3.10}$$

Starting from the solution of the TDSE in terms of the unitary operator, the time evolution of the density operator at any time may be written as

$$\begin{aligned} \hat{\rho}(t) &= \sum_k p_k \hat{U}(t,s) |\psi_k(s)\rangle \langle \psi_k(s)| \hat{U}^\dagger(s,t), \\ &= \hat{U}(t,s) \hat{\rho}_0 \hat{U}^\dagger(s,t), \end{aligned} \tag{3.11}$$

when assuming that the initial state of the system is described by the density operator

$$\hat{\rho}_0 = \sum_k p_k |\psi_k(s)\rangle \langle \psi_k(s)|. \tag{3.12}$$

The time derivative of Eq. (3.10) yields the equation governing the time evolution of the density operator:

$$\frac{\partial}{\partial t} \hat{\rho} = -\mathrm{i}[\hat{H}, \hat{\rho}], \tag{3.13}$$

which is sometimes referred to as the von Neumann or Liouville-von Neumann equation. Equation. (3.13) may be succinctly written by introducing the Liouville operator L

$$\frac{\partial}{\partial t} \hat{\rho} = \hat{L} \hat{\rho}, \tag{3.14}$$

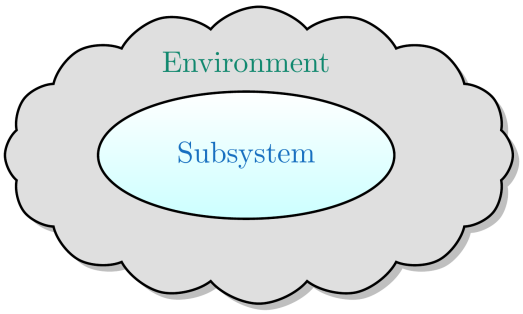

Figure 3.1 | Sketch of open quantum systems. The state of the subsystem $\mathcal{S}$ is described by the density operator $\hat{\rho}_s$ acting on the associated Hilbert space $\mathcal{H}_\mathcal{S}$. Access to information pertaining to the environment $\mathcal{E}$ can be done via $\hat{\rho}_\mathcal{E}$ in the Hilbert space $\mathcal{H}_\mathcal{E}$. The Hilbert space of the composite system $\mathcal{S} + \mathcal{E}$ is given by the tensor product space $\mathcal{H}_\mathcal{S} \otimes \mathcal{H}_\mathcal{E}$.

where $\hat{L} = -\mathrm{i}[\hat{H}, \bullet]$, and $[\hat{H}, \bullet]\hat{A} = [\hat{H}, \hat{A}]$.

Before closing this section, let us collect the properties of a density matrix operator: It must be self-adjoint (Hermitian), i.e $\hat{\rho}^\dagger = \hat{\rho}$. Moreover, it must be positive definite, i.e $\langle\psi|\hat{\rho}|\psi\rangle \geq 0$ for all state vectors $|\psi\rangle$ and its trace must be equal to 1, i.e $\mathrm{Tr}(\hat{\rho}) = 1$. For a given observable A, its expectation value is given by

$$\langle A\rangle = \mathrm{Tr}(A\hat{\rho}). \tag{3.15}$$

3.2 Dynamics in Open Quantum Systems

The previous section was concerned with the time evolution of quantum systems, disregarding any explicit interaction of the system under study with its surrounding. And we have seen that such quantum systems evolve unitarily. Still, this is just an approximation which does not echo the real world. It is intuitively clear that in open quantum systems the unitary time evolution will break down. In this section, the focus will be on the set of equations necessary for a genuine monitoring of the dynamics of such open quantum systems.

3.2.1 Concept of Open Quantum Systems

By definition, an open quantum system, which will be denoted $\mathcal{S}$ throughout the present work, is a system interchanging information (e.g. energy and/or matter) with its environment $\mathcal{E}$ [52, 54]. Figure 3.1 displays a pictorial representation of the concept of open quantum system (OQS). This flow of information between $\mathcal{S}$ and $\mathcal{E}$ complicates somehow the quantification of the dynamics in OQS, which is no longer describable in terms of Hamiltonian dynamics. Nevertheless, the bipartite system consisting of $\mathcal{S}$ and $\mathcal{E}$ may still undergo an unitary evolution [47]. This assumption is the starting point of the theory of open quantum systems.

The Hilbert space in which the unitary dynamics of the composite system $\mathcal{S} + \mathcal{E}$ plays out is given by the tensor product space

$$\mathcal{H} = \mathcal{H}_\mathcal{S} \otimes \mathcal{H}_\mathcal{E}, \tag{3.16}$$

whereby $\mathcal{H}_\mathcal{S}$ and $\mathcal{H}_\mathcal{E}$ denote the Hilbert space of the subsystems $\mathcal{S}$ and $\mathcal{E}$, respectively. The Hamiltonian governing the reversible evolution of the bipartite system is given by

$$\hat{H} = \hat{H}_s \otimes \hat{\mathbb{1}}_e + \hat{\mathbb{1}}_s \otimes \hat{H}_e + \hat{H}_{se}. \tag{3.17}$$

In this equation, $\hat{H}_{se}$ encodes the information about the interaction between the open quantum system $\mathcal{S}$ and the environment $\mathcal{E}$. $\hat{H}_s$ and $\hat{H}_e$ are the respective Hamiltonians of $\mathcal{S}$ and $\mathcal{E}$. $\hat{\mathbb{1}}_s$ and $\hat{\mathbb{1}}_e$ denote the identity operators in $\mathcal{H}_\mathcal{S}$ and $\mathcal{H}_\mathcal{E}$. It should be noted that the boundary between $\mathcal{S}$ and $\mathcal{E}$ has to be aptly chosen so that the Hamiltonian of the system in question is assured to be well defined. The choice must also make allowances for the stability of the environment and not yield a singular interaction between the two subsystems [45].

3.2.2 Partial Trace

In this section, we elaborate on a device which is of fundamental importance for the theory of open quantum systems.

As mentioned above, when describing the state of the closed composite system within the framework of the density matrix, the time evolution is given by the unitary transformation

$$\hat{\rho}(t) = \hat{U}(t,s)\hat{\rho}(s)\hat{U}^\dagger(s,t), \tag{3.18}$$

with $\hat{\rho} = \hat{\rho}_{se}$ being the joint density matrix of the bipartite system and $\hat{U}(t,s) = e^{-\mathrm{i}\hat{H}(t-s)}$. We recall that the generator of the dynamics, H, is the full Hamiltonian of the composite system, see Eq. (3.17).

However, since the focus is on observables pertaining to $\mathcal{S}$, there is no need to keep working with the joint density operator. Instead, it is convenient to seek a map which, when acting linearly on the joint density matrix, should yield a density operator which accounts for the statistical properties of the subsystem $\mathcal{S}$. Such a map exists and is known as the partial trace over the Hilbert space of the surrounding [52].

More formally, let $\hat{\rho}$ be a joint density matrix of a bipartite system $\mathcal{S} + \mathcal{E}$. The linear map

$$\mathrm{Tr}_\mathcal{E} : \mathcal{T}(\mathcal{H}_\mathcal{S} \otimes \mathcal{H}_\mathcal{E}) \to \mathcal{T}(\mathcal{H}_\mathcal{S}), \tag{3.19}$$

which yields an unique operator $\hat{\rho}_s = \mathrm{Tr}_\mathcal{E}(\hat{\rho}_{se})$ on $\mathcal{S}$ fulfilling

$$\mathrm{Tr}\left[\hat{\rho}\hat{A}_s \otimes \hat{\mathbb{1}}_s\right] = \mathrm{Tr}_\mathcal{S}\left[\hat{A}_s\hat{\rho}_s\right], \tag{3.20}$$

is called a partial trace. Here Tr is the trace in the joint space $\mathcal{H}_\mathcal{S} \otimes \mathcal{H}_\mathcal{E}$ and $\mathrm{Tr}_\mathcal{S}$ denotes the trace in the subsystem $\mathcal{S}$ alone. $\mathcal{T}(\mathcal{H})$ is the so-called Banach space or the Liouville space of the self-adjoint trace-class operator for some Hilbert space $\mathcal{H}$ [48].

To be more specific, the mapping procedure is given by

$$\hat{\rho}_s = \sum_m \langle m|\hat{\rho}|m\rangle, \tag{3.21}$$

where $\{|m\rangle\}$ being an orthonormal basis in $\mathcal{H}_\mathcal{E}$. The obtained density matrix is called the *reduced* density, or the *marginal* of $\hat{\rho}$,

$$\hat{\rho}_s(t) = \mathrm{Tr}_\mathcal{E}\left[\hat{U}(t,s)\hat{\rho}(s)\hat{U}^\dagger(s,t)\right]. \tag{3.22}$$

It is instructive to mention that the operation of the partial trace is to reduce the dimensionality of a given operator to a lower dimension and constitutes the only possible way forward to retrieve the state of the subsystem $\mathcal{S}$ from the joint density operator [52]

3.2.3 Dynamical Map

In the previous subsection, we have seen that by drawing on the partial trace over the Hilbert space of the surrounding, a reduced density operator of the subsystem in question can be obtained, which describes completely its statistical properties. It is worthwhile mentioning that the obtained reduced density operator does not make use of any assumptions and therefore represents a realistic and general way of tackling the dynamical behaviour of an open quantum system. In practice, however, a direct application of this tranquil picture may be intractable [45], as it entails to solve the Schrödinger equation for the composite system. On the other hand, as only observables belonging to the subsystem of interest matter, it is desirable and reasonable to avoid this approach, Eq. (3.22), and seek another mathematical relation which still accounts for the openness of the subsystem without taking the degrees of the surrounding $\mathcal{E}$ explicitly into account.

This section discusses the derivation of such a theoretical relation which may be interpreted as a generalization of the unitary dynamics, Eq. (3.14), and is known as Kraus operator sum representation [46, 48].

Kraus Operator Sum Representation

The prerequisite for the derivation of the Kraus representation of the reduced density operator is a zero correlation between the subsystem $\mathcal{S}$ and its surrounding $\mathcal{E}$ at the outset of the time evolution [52]. It should be noted that such a limiting procedure will not cause a loss of generality of the Kraus representation. Based on this assumption, the initial joint density operator may be written as [52]

$$\hat{\rho}(0) = \hat{\rho}_s(0) \otimes \hat{\rho}_e(0), \tag{3.23}$$

where $\hat{\rho}_s(0)$ is the initial state of the subsystem under study and $\hat{\rho}_e(0)$ denotes some reference state of the surrounding. The respective spectral decomposition reads

$$\begin{aligned}\hat{\rho}_s(0) &= \sum_m a_m |\varphi_m\rangle\langle\varphi_m|,\\ \hat{\rho}_e(0) &= \sum_\beta b_\beta |\phi_\beta\rangle\langle\phi_\beta|,\end{aligned} \tag{3.24}$$

with $\{|\varphi_m\rangle\}$ and $\{|\phi_\beta\rangle\}$ being an orthonormal basis in $\mathcal{H}_\mathcal{S}$ and $\mathcal{H}_\mathcal{E}$ respectively. a_m and b_β are non-negative real numbers fulfilling

$$\sum_m a_m = 1, \quad \sum_\beta b_\beta = 1. \tag{3.25}$$

By inserting Eq. (3.24) into the equation for the reduced density, Eq. (3.22), one obtains

$$\begin{aligned}\hat{\rho}_s(t) &= \mathrm{Tr}_\mathcal{E}(\hat{U}(t)\hat{\rho}\hat{U}^\dagger(t)),\\ &= \sum_\alpha \langle\phi_\alpha|\hat{U}[\hat{\rho}_s(0)\otimes\hat{\rho}_e(0)]\hat{U}^\dagger|\phi_\alpha\rangle,\\ &= \sum_{\alpha\beta m} a_m b_\beta \langle\phi_\alpha|\hat{U}[|\varphi_m\rangle\langle\varphi_m|\otimes|\phi_\beta\rangle\langle\phi_\beta|]\hat{U}^\dagger|\phi_\alpha\rangle,\\ &= \sum_{\alpha\beta m} a_m b_\beta (\langle\phi_\alpha|\hat{U}|\varphi_m\rangle\otimes|\phi_\beta\rangle)(\langle\varphi_m|\otimes\langle\phi_\beta|\hat{U}^\dagger|\phi_\alpha\rangle,\\ &= \sum_{\alpha\beta m} a_m b_\beta \hat{U}_{\alpha\beta}|\varphi_m\rangle\langle\varphi_m|\hat{U}^\dagger_{\alpha\beta},\\ &= \sum_{\alpha\beta} b_\beta \hat{U}_{\alpha\beta}\hat{\rho}_s(0)\hat{U}^\dagger_{\alpha\beta},\end{aligned} \tag{3.26}$$

where $\hat{U}_{\alpha\beta} = \langle\phi_\alpha|\hat{U}|\phi_\beta\rangle$ is an operator acting on the Hilbert space of the active system $\mathcal{S}$. Since the coefficients b_β are non-negative, the operator $\hat{U}_{\alpha\beta}$ may be rescaled as

$$\hat{M}_{\alpha\beta} = \sqrt{b_\beta}\hat{U}_{\alpha\beta}. \tag{3.27}$$

Plugging this into the last line of Eq. (3.24), one obtains the following representation

$$\hat{\rho}_s(t) = \sum_{\alpha\beta} \hat{M}_{\alpha\beta}(t)\hat{\rho}_s\hat{M}^\dagger_{\alpha\beta}(t), \tag{3.28}$$

where $\hat{M}_{\alpha\beta}$ are operation elements fulfilling the condition

$$\sum_{\alpha\beta} \hat{M}^\dagger_{\alpha\beta}\hat{M}_{\alpha\beta} = \hat{\mathbb{1}}, \tag{3.29}$$

as the time evolution operator $\hat{U}(t)$ for the composite system is unitary. By introducing a multi-index $\sigma \to (\alpha, \beta)$, the Kraus operator sum representation emerges

$$\hat{\rho}(t) = \sum_{\sigma} \hat{M}_{\sigma}(t)\hat{\rho}_0\hat{M}_{\sigma}^{\dagger}(t), \tag{3.30}$$

where we omit the subscript s and replace $\hat{\rho}(0)$ by $\hat{\rho}_0$. Interestingly, the reversible dynamics represents a special case of the Kraus decomposition. This becomes transparent when there is only one term in the sum, Eq. (3.30), [52]. Moreover, it can be easily shown that such a decomposition preserves the selfadjointness, trace and the positivity property of the density operator [55]. Therefore, it can be considered as the most general evolution maintaining all the properties of a density operator. Despite the fact that both reversible and irreversible processes may be explored by using this mathematical representation, Eq. (3.30), it cannot allow for disentangling the unitary part from the non-unitary one. Hence, the Kraus decomposition is rather tough to be interpreted [55].

Superoperator

The Kraus decomposition can be interpreted as a quantum operation transforming the initial density matrix to the evolved one [52]

$$\hat{\rho}(t) = V(t, s)\hat{\rho}(s). \tag{3.31}$$

By fixing the final time t as well as the initial density of the surrounding, the quantum operator V defines a map from the Banach space $\mathcal{T}(\mathcal{H}_{\mathcal{S}})$ of the reduced density operator into itself,

$$V : \mathcal{T}(\mathcal{H}_{\mathcal{S}}) \to \mathcal{T}(\mathcal{H}_{\mathcal{S}}). \tag{3.32}$$

As the map is an operator acting on an operator to change it over the time, it is referred to as a dynamical map or superoperator [52].

This understanding of the Kraus sum representation suggest that a more general quantum operator $V(t, s)$ for recording the time development of the density may be defined. However, to be in agreement with the fundamental laws of quantum mechanics and its statistical description, it is clear that some requirements must be imposed on the definition of $V(t, s)$ [46]. Indeed, to yield a physically meaningful density matrix, the map $V(t, s)$ must fulfill the following conditions:*linear*, *trace-preserving*, and *positive and completely positive*.

It might be interesting to put flesh on such requirements. The linearity means that

$$V\{a_1\hat{\rho}_1 + a_2\hat{\rho}_2 + \ldots + a_m\hat{\rho}_m\} = \sum_m a_m V(\hat{\rho}_m), \quad \sum_m a_m = 1. \tag{3.33}$$

From this mathematical relation, it is clear that the linearity condition is tantamount to allowing a statistical interpretation of the image $V(\hat{\rho})$ of $\hat{\rho} = \sum_m a_m \hat{\rho}_m$. The trace preserving property is given by

$$\mathrm{Tr}[V(\hat{\rho})] = \mathrm{Tr}(\hat{\rho}), \tag{3.34}$$

is also related to the probabilistic interpretation and ensures that the following condition $\sum_m a_m = 1$, must hold true for the evolved density. Concerning the positivity condition, it means that if $\hat{\rho}$ is positive, i.e $\langle\psi|\hat{\rho}|\psi\rangle \geq 0$ for all state $|\psi\rangle$, the action of the map V must yield a positive density matrix. However this condition breaks down when we consider composite system. More precisely, if the system under question is part of a bipartite system, then the state of the composite system may evolve via

$$V_1 \otimes \mathbb{1}_2 : \mathcal{T}(\mathcal{H}_1 \otimes \mathcal{H}_2) \to \mathcal{T}(\mathcal{H}_1 \otimes \mathcal{H}_2). \tag{3.35}$$

Here $\mathcal{H}_1$ and $\mathcal{H}_2$ denote the Hilbert space of the system under study and its extension respectively. In order for the evolved state being positive, V_1 must be completely positive [46].

3.2.4 Markovian Master Equation

The aim of this subsection is to provide a survey of an important class of time evolution equations for recording the dynamics in open quantum systems. As will be seen, such set of equations, which are termed quantum dynamical semigroup (QDS), see Refs. [46, 50, 52], may be derived from the Kraus operator sum, Eq. (3.30), by assuming an important concept: Markovianness of the dynamical map emerging from the Kraus decomposition. The former means that the environmental correlation function must be δ–correlated [52] synonymously the surrounding behaves memoryless.

Markovianness

In order to derive from the Kraus operator sum representation a differential equation describing the dynamics of the reduced system, we must assume the Markovian property of the system [46, 50, 52]. More formally, for any pair of times $t, s \geq 0$, the following relation must hold true

$$\hat{\rho}(t) = V(t,s)\hat{\rho}(s), \tag{3.36}$$

which means that knowing the state of the system in question at time s, the determination of a posterior state at the time t can be achieved via the above procedure. Such endomorphisms or superoperators, $V(t,s)$, are called quantum dynamical semigroup if they are trace preserving, completely positive and satisfies the following composition law [56]

$$V(t,s)V(s,v) = V(t,v), \quad v < s < t. \tag{3.37}$$

In general, due to the openness of the reduced system Eq. (3.36) is not expected to yield a positive density matrix. Indeed, by interacting with its surrounding, the latter can function as a memory which retains information for a while, so that a sound computation of $\hat{\rho}(t)$ must not only consider $\hat{\rho}(s)$ but also takes into account $\hat{\rho}$ at earlier times stemming from a possible flow back of information from environment to system.

However, by introducing a coarse-grained time scale on which the surrounding has no way to contaminate the time evolution of the system, the Markovianness turns out to be a good approximation [50, 52]. Consequently, the two-parameter convex endomorphisms $V(t,s)$ only depends on time differences $V(t,s) = V(t-s)$ and is completely positive. Correspondingly, Eq. (3.37) becomes [46, 48, 50, 52]

$$V(t)V(s) = V(t+s), \quad \text{for} \quad t,s \geq 0. \tag{3.38}$$

It might be interesting to mention that the concept of semigroup is the same as group with the exception that the semigroup elements do not necessarily feature an inverse.

For the QDS $V(t)$, a Markovian generator L_t can be defined as [46, 48, 50]

$$L_t = \frac{d}{ds} V_{t,s}\Big|_{s=t}. \tag{3.39}$$

By combining this definition with Eq. (3.36), a generalization of the Liouville-von Neumann equation governing the dynamics of the reduced density emerges

$$\frac{\partial}{\partial t}\hat{\rho} = L_t\hat{\rho}. \tag{3.40}$$

The question of which structure the above generator does feature will be discussed below.

Lindblad Representation

Having discussed the condition under which a differential equation for the reduced density operator can be obtained from the Kraus map, we now turn our attention to the structure of the generator of QDS which is given by the Lindblad form [46, 50, 56]. It was first derived independently by Lindblad [46] by Gorini, Kossakowski and Sudarshan [50] by assuming a bounded generator.

Theorem 3.2.1. *A linear operator L: $\mathcal{T}(\mathcal{H}) \to \mathcal{T}(\mathcal{H})$ is the generator of a completely positive dynamical semigroup of $\mathcal{T}(\mathcal{H})$ if it can be expressed in the form*

$$L : \hat{\rho} \to L\hat{\rho} = -\mathrm{i}[\hat{H},\hat{\rho}] + \sum_{\alpha\beta} c_{\alpha\beta}\left(\hat{F}_\alpha\hat{\rho}\hat{F}_\beta^\dagger - \frac{1}{2}\hat{F}_\alpha\hat{F}_\beta^\dagger\hat{\rho} - \frac{1}{2}\hat{\rho}\hat{F}_\alpha\hat{F}_\beta^\dagger\right), \tag{3.41}$$

where $\hat{H}^\dagger = \hat{H}$, $\mathrm{Tr}(\hat{H}) = 0$, $\mathrm{Tr}(\hat{F}_\alpha) = 0$, $\mathrm{Tr}(\hat{F}_\alpha\hat{F}_\beta) = \delta_{\alpha\beta}$, $(\alpha,\beta = 0,1,2,..,N^2-1)$, and $c_{\alpha\beta}$ is a positive semidefinite matrix.

This is the first standard form of the generator of the quantum dynamical semigroup. The proof of this theorem can be found in the appendix. In this form, the generator may be somehow inconvenient to manipulate. However as the coefficients matrix $c_{\alpha\beta}$ is hermitian, the Lindblad representation, Eq. (3.41), may be cast into a diagonal form. To achieve this, $c_{\alpha\beta}$ has to be diagonalized by having recourse to a suitable unitary transformation U, fulfilling the following relation

$$\sum_{\alpha\beta} U_{\alpha'\alpha} c_{\alpha\beta} U^{\dagger}_{\beta\beta'} = \gamma_{\alpha'} \delta_{\alpha'\beta'}, \tag{3.42}$$

where $\gamma_{\alpha'} \geq 0$ denote the positive eigenvalues of the matrix $c_{\alpha\beta}$.

This unitary operation suggests to introduce a new set of operators according to,

$$\hat{F}_{\alpha} = \sum_{\alpha'} U_{\alpha'\alpha} \hat{A}_{\alpha'}. \tag{3.43}$$

Plugging this in the Eq. (3.41), we obtain the quantum markovian master equation in the Lindblad form

$$\frac{\partial}{\partial t}\hat{\rho} = -\mathrm{i}[\hat{H}, \hat{\rho}] + \sum_{\alpha} \gamma_{\alpha} \left(\hat{A}_{\alpha} \hat{\rho} \hat{A}^{\dagger}_{\alpha} - \frac{1}{2} \hat{A}^{\dagger}_{\alpha} \hat{A}_{\alpha} \hat{\rho} - \hat{\rho} \frac{1}{2} \hat{A}^{\dagger}_{\alpha} \hat{A}_{\alpha} \right), \tag{3.44}$$

which describes the time evolution of the density operator. In the above equation, Eq. (3.44), the commutator term generates the unitary part of the dynamics. However, it should be noted that $\hat{H}$ has to be thought of as an effective Hamiltonian, as it cannot be identified with the free Hamiltonian of the reduced system [55].The remaining part accounts for the non-unitary dynamics. The so-called quantum jump or the Lindblad operators $\hat{A}_{\alpha}(\hat{A}^{\dagger}_{\alpha})$ are system operators encoding the nature and the strength of each dissipation channel with a rate γ_{α}. It is instructive to mention that the validity of the Lindblad equation is based on the Born-Markov approximation with the system-surroundings interaction in rotating-wave approximation, which in quantum optics is an excellent approximation, for the system frequencies are much larger than the decay rates [52].

Gauge Transformation

An interesting aspect of the generator of the QDS is its invariance in terms of unitary transformation of the Lindblad operators A_{α} and inhomogeneous transformations. In other words, the Lindblad operators and the system Hamiltonian are not uniquely determined by a given generator L [52]. More specifically, any other similarity transformation

$$\sqrt{\gamma_{\alpha}} \hat{A}_{\alpha} \rightarrow \sqrt{\gamma'_{\alpha}} \hat{A}'_{\alpha} = \sum_{\beta} U_{\alpha\beta} \sqrt{\gamma_{\beta}} \hat{A}_{\beta}, \tag{3.45}$$

with $U_{\alpha\beta}$ being an unitary matrix, will yield a different non-diagonal version of the Lindblad equation, Eq. (3.41) which still encodes the same information. Concerning the inhomogeneous transformations, by performing the following substitution, the Lindblad equation remains the same

$$\begin{aligned} \hat{A}_\alpha \to \hat{A}'_\alpha &= \hat{A}_\alpha + \eta_\alpha \hat{\mathbb{1}}, \\ \hat{H} \to \hat{H}' &= \hat{H} + \frac{1}{2\mathrm{i}} \sum_\alpha \left(\eta^*_\alpha \hat{A}_\alpha - \eta_\alpha \hat{A}^\dagger_\alpha \right) + \lambda \hat{\mathbb{1}}, \end{aligned} \tag{3.46}$$

whereby the η_α are complex numbers and λ a real number. The inhomogeneous transformation invariance turns out to be an important property, as it allows to use traceless Lindblad operators [52].

We close this chapter by pointing out that a microscopic derivation of the generator of the quantum dynamical semigroup L may also be achieved by resorting to the *Born approximation*. Moreover, it is worthwhile mentioning that thermal equilibrium is not necessarily obtainable in the QDS framework. However, if needed, it can be incorporated [57].

4 Light-Matter Interaction in Semiconductor Quantum Dots

The purpose of this chapter is to elaborate on the light matter interaction in semiconductor quantum dots. After a brief outline of the physics of the single particle states being the basis of many-body physics, we discuss the system Hamiltonian. More specifically, we focus on the carrier Hamiltonian in the two-band approximation and treat the light field quantum mechanically. In the framework of the dipole and rotating wave approximation, we then discuss the coupling of the carriers to the continuum of empty modes of the open radiation field. Given the size of the system under consideration in this thesis, we describe the equation of motion (EoM) approach. It is based on the expectation value, which is often convenient for the numerical simulations of the dynamics of many particles systems. The equation of motion formalism is intimately related to an hierarchy problem, which can be tackled by the cluster expansion tool. Finally, to illustrate the EoM scheme, we derive the semiconductor luminescence equations which constitute the starting point of the semiconductor quantum dots laser theory in Chapter 5.

4.1 Model System

4.1.1 Single-Particle States

It is reasonable to begin this chapter by reviewing the concept of the single-particle states and some of their properties in semiconductor nanostructures, as they are the foundation of many-body physics.

Self-assembled semiconductor quantum dots are routinely grown in the *Stranski-Krastanov* growth mode. In this layer-by-layer process leading to the formation of self-assembly of islands of atoms because of lattice-constant mismatch and surface energy minimization, a thin film of a few nanometer thickness termed *wetting layer* (WL) is formed between the quantum dots (QDs) and the substrate. The energy level diagram of the obtained structure, as depicted in Fig. 4.1, consists of localized states of the quantum dot lying energetically below a quasi-continuum of delocalized states belonging to the WL.

From the mathematical point of view, the single-particle wave functions pertaining to the

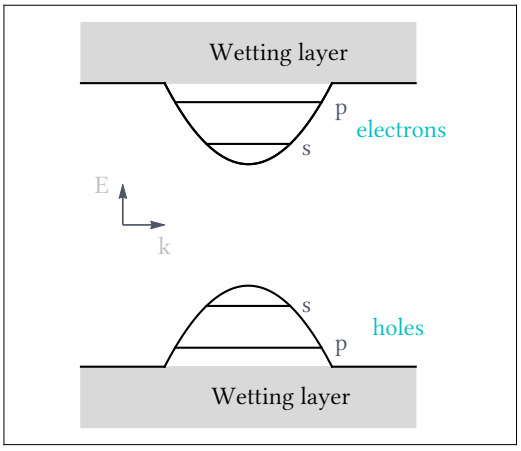

Figure 4.1 | Cartoon of the coupled quantum dot and wetting layer system. For the electrons in the conduction band and the holes in the valence band two confined shells are considered respectively. They are referred to as the s-shell and p-shell due to the in-plane symmetry of the quantum dot. Both shell lie energetically below a quasi-continuum of delocalized states belonging to the wetting layer.

coupled QD-WL system are obtained from the Schrödinger equation which reads

$$\left\{-\frac{\hbar^2}{2m}\nabla^2 + u(r)\right\}\varphi_\alpha = \varepsilon_\alpha\varphi_\alpha, \tag{4.1}$$

where φ_α denotes the single-particle wave function, and $u(r)$ encodes the effective single-particle potential. When it comes to solving the single-particle Schrödinger equation, several judicious methods may be used. On one hand, semi-empirical models may be used. These include the effective-mass approach [58, 59] and the $\boldsymbol{k}\cdot\boldsymbol{p}$-model [60]. Despite their success in emulating the band structures of semiconductor quantum dots [61, 62], these continuum approaches fail to include any information pertaining to the atomistic structure and symmetry of the quantum dots. To account for the full atomistic structure of the QDs and the symmetry of the crystal, appropriate methods, such as tight-binding models [63, 64], and pseudo-potential can be used.

Figure 4.2 displays the band structures, obtained from tight-banding approach, of three Zinc-blende material systems, GaAs, AlAs, and InAs. The existence of a direct band gap at Γ, which allows a recombination of carriers between the conduction and the valence bands by radiating or absorbing photons makes these structures a viable source for device application. In the vicinity of the Γ point, three bands may distinguished, see Fig. 4.3: the degenerate heavy- and light-hole band , and the split-off band resulting from the spin-orbit interaction.

An idiosyncrasy of self-assembled Stranski–Krastanov semiconductor QDs is their lens-shaped geometry allowing for a description in the framework of the effective-mass approximation, wherein a free carrier dispersion with effective masses for electrons and holes [1] is assumed.

[1] The concept of electron and hole has been introduced to describe an elementary excitation in semiconductor nanostructures. The electron corresponds to an excitation of charge carrier in conduction, while the vacancy leaves in the valence band is referred to as the hole. The hole is a quasi-particle of opposite charge and opposite spin with respect to the excited electron. A single electron-hole pair with Coulomb interaction is commonly termed *exciton*.

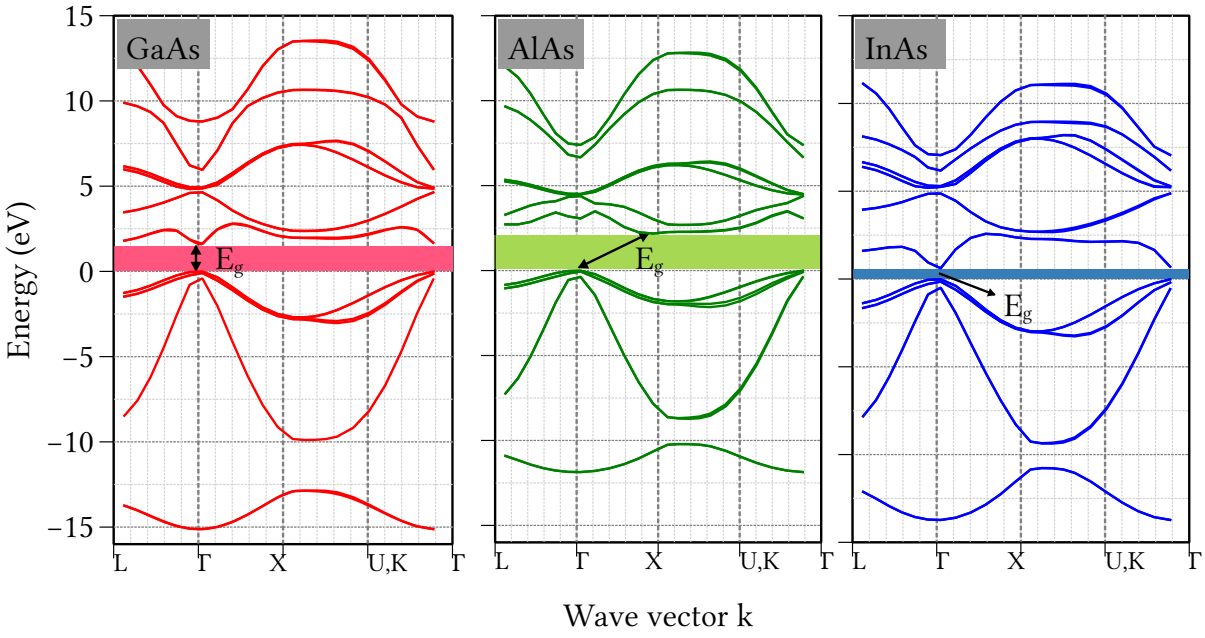

Figure 4.2 | Series of band structures. Band structures for GaAs, InAs, and AlAs. They are obtained from the tight-binding calculations. The data are kindly provided by C. Carmesin. At the so-termed high-symmetry point Γ, in all three band structures, a direct band gap of energy difference E_g appears, where AlAs shows the highest energy gap and InAs the lowest energy gap (0.4 eV). In band structure of AlAs an indirect band gap between the Γ-point at the valence band and a minimum near the X-point at the conduction band of about 3.0 eV exists. The direct band gap of GaAs amounts to 1.5 eV

By resorting to the envelope wave function approach, the single-particle state wave function may be split into a product of two functions depending on growth direction and in-plane coordinates, z and ρ, respectively:

$$\varphi_\alpha^\lambda(\boldsymbol{r}) = \xi_\alpha^\lambda(z)\phi_\alpha^\lambda(\rho)f_{k=0}^\lambda(r). \tag{4.2}$$

Here $f_{k=0}^\lambda(r)$ is the Bloch function encoding the information about the lattice structure. This disentanglement of the wave function allows for reducing the problem to that of an one-dimensional potential well in the growth direction. For lens-shaped quantum dots, the in-plane part $\phi_\alpha^\lambda(\rho)$ are well approximated by the eigenfunctions of the two-dimensional harmonic oscillator [65–68]. Given the in-plane symmetry, the first two confined shells for both electrons and holes are denoted by s and p, see Fig. 4.3.

Disregarding the effect of the localized states on the continuum, the in-plane part of the wetting layer are well approximated by resorting to plane waves with wave vector $\boldsymbol{k}$. Nevertheless because different avenues have been used for the wave functions in the quantum dot and the wetting layer, the wetting layer states are not orthonormal on the quantum dot states. To restore the orthogonality, the orthogonalized plane wave approach can be used [69]. These single-particle

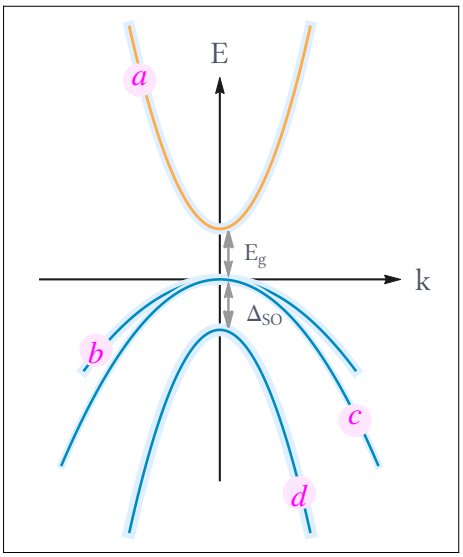

Figure 4.3 | Sketch of the band structure near Γ. Band structure of GaAs with direct band gap E_g in the vicinity of the Γ-point, including the lowest conduction band (a) and three valence bands (VBs): the heavy hole (b), light hole (c) and split-off hole (d). The latter is energetically lowered by the amount of spin-orbit coupling Δ_{SO}.

wave functions enter the definition of the Coulomb matrix elements, and the light-matter coupling strength, which will be discussed in the next section.

4.1.2 Model Hamiltonian

This section takes on the specification of the light matter Hamiltonian on which the semiconductor laser model is based. The Hamiltonian may be split in three parts, namely that of the charge carriers, the free quantized electromagnetic field, and the light matter interaction Hamiltonian.

The Carriers Hamiltonian

The matter Hamiltonian encoding the microscopic properties in semiconductor QDs may be divided in two parts. The free part, that describes a system of non-interacting carriers, contains information about the single-particle spectrum $\varepsilon_\alpha^{(c,v)}$. It is given by [70, 71]

$$H_0 = \sum_\alpha \left(\varepsilon_\alpha^c \hat{c}_\alpha^\dagger \hat{c}_\alpha + \varepsilon_\alpha^v \hat{v}_\alpha^\dagger \hat{v}_\alpha \right). \tag{4.3}$$

Here c_α ($c_\alpha^\dagger$) and v_α ($v_\alpha^\dagger$) are the fermionic field operators, which are responsible for the annihilation (creation) of an electron in the single-particle state $|\alpha\rangle$ of the conduction and valence band, respectively. The quantities ε^c and ε^v are the corresponding single-particle energies which must be obtained by resorting to one of the above aforementioned tools (e.g. Tight-binding approach or effective mass approximation). It is instructive to mention the straightforwardness in generalizing the free Hamiltonian in Eq. (4.3) to a multiband system [72].

The *Coulomb* interaction between the charge carriers is given by [70, 71]

$$H_C = \frac{1}{2}\sum_{\sigma\sigma'}\sum_{\alpha\alpha'}\left(V^{cc}_{\alpha\sigma,\sigma'\alpha'}\hat{c}^\dagger_\alpha\hat{c}^\dagger_\sigma\hat{c}_{\sigma'}\hat{c}_{\alpha'} + V^{vv}_{\alpha\sigma,\sigma'\alpha'}\hat{v}^\dagger_\alpha\hat{v}^\dagger_\sigma\hat{v}_{\sigma'}\hat{v}_{\alpha'} + 2V^{cv}_{\alpha\sigma,\sigma'\alpha'}\hat{c}^\dagger_\alpha\hat{v}^\dagger_\sigma\hat{v}_{\sigma'}\hat{c}_{\alpha'}\right), \quad (4.4)$$

where the *Coulomb* matrix elements, depending on the single-particle wave function $\langle \boldsymbol{x}|\alpha, i\rangle = \varphi^i_\alpha(\boldsymbol{x})$, are given by

$$V^{ii'}_{\alpha\sigma,\sigma'\alpha'} = \int d^3\boldsymbol{x}\int d^3\boldsymbol{x}'\varphi^{i*}_\alpha(\boldsymbol{x})\varphi^{i'*}_\sigma(\boldsymbol{x}')v(\boldsymbol{x}-\boldsymbol{x}')\varphi^{i'}_{\sigma'}(\boldsymbol{x}')\varphi^i_{\alpha'}(\boldsymbol{x}) \quad (4.5)$$

with $v(\boldsymbol{x}) = \dfrac{e^2}{4\pi\epsilon_0\epsilon_r}\dfrac{1}{x}$ being the Coulomb potential and $i \in \{c, v\}$ denoting the band index. In the Coulomb potential, ε_0 and ε_r stand for the vacuum and background dielectric constant, respectively. In Eq. (4.4), the first two terms account for the repulsive interaction between electrons within the same band (conduction or valence) while the last term controls the attractive interaction between electrons and holes in different bands.

The Light Field Hamiltonian

A prerequisite for an apposite description of light-matter interaction phenomena at the *quantum level* is the quantization of the electromagnetic field (EMF). From the perspective of quantum theory, information retrieval from the light field may be achieved in terms of photons for different modes of the EMF. As a consequence thereof, any interaction with the matter, for instance an absorption of photons, must result in the annihilation of photons from the field.

The traditional approach to quantize the EMF, being defined by the electric $\boldsymbol{E}(\boldsymbol{x}, t)$ and the magnetic $\boldsymbol{B}(\boldsymbol{x}, t)$ field, is to start from Maxwell's equations in free space [53, 73] which are given by

$$\boldsymbol{\nabla}\cdot\boldsymbol{E}(\boldsymbol{x}, t) = 0, \quad (4.6a)$$

$$\boldsymbol{\nabla}\cdot\boldsymbol{B}(\boldsymbol{x}, t) = 0, \quad (4.6b)$$

$$\boldsymbol{\nabla}\times\boldsymbol{E}(\boldsymbol{x}, t) = -\frac{\partial}{\partial t}\boldsymbol{B}(\boldsymbol{x}, t), \quad (4.6c)$$

$$\boldsymbol{\nabla}\times\boldsymbol{B}(\boldsymbol{x}, t) = \frac{1}{c^2}\frac{\partial}{\partial t}\boldsymbol{E}(\boldsymbol{x}, t). \quad (4.6d)$$

Here c denotes the speed of the light. The interesting aspect of Maxwell's equations for the EMF is that the fields may be written in terms of a scalar $\phi(\boldsymbol{x}, t)$ and a vector potential $\boldsymbol{A}(\boldsymbol{x}, t)$:

$$\begin{aligned}\boldsymbol{E}(\boldsymbol{x}, t) &= -\boldsymbol{\nabla}\phi(\boldsymbol{x}, t) - \frac{1}{c}\frac{\partial}{\partial t}\boldsymbol{A}(\boldsymbol{x}, t),\\ \boldsymbol{B}(\boldsymbol{x}, t) &= \boldsymbol{\nabla}\times\boldsymbol{A}(\boldsymbol{x}, t).\end{aligned} \quad (4.7)$$

Nevertheless, it should be noted that $\boldsymbol{A}$ and ϕ are not uniquely defined. More specifically, a gauge transformation

$$\boldsymbol{A} = \boldsymbol{A} + \boldsymbol{\nabla}\chi, \quad \phi' = \phi - \frac{\partial}{\partial t}\chi, \tag{4.8}$$

with $\chi = \chi(\boldsymbol{x}, t)$ being any scalar function of the position $\boldsymbol{x}$ and time t, leaves Eqs. (4.7) invariant. Suppose we choose

$$\boldsymbol{\nabla} \cdot \boldsymbol{A}(\boldsymbol{x}, t) = 0, \tag{4.9}$$

the so-called *Coulomb* or transverse gauge [53, 73], and $\phi(\boldsymbol{x}, t) = 0$, Eq. (4.7) reduces to

$$\begin{aligned} \boldsymbol{E}(\boldsymbol{x}, t) &= -\frac{1}{c}\frac{\partial}{\partial t}\boldsymbol{A}(\boldsymbol{x}, t), \\ \boldsymbol{B}(\boldsymbol{x}, t) &= \boldsymbol{\nabla} \times \boldsymbol{A}(\boldsymbol{x}, t), \end{aligned} \tag{4.10}$$

meaning the fields are solely described by the vector potential $\boldsymbol{A}(\boldsymbol{x}, t)$. Upon inserting Eq. (4.10) into Eq. (4.6c), the wave equation for the vector potential is obtained

$$\left(\boldsymbol{\nabla}^2 - \frac{1}{c^2}\frac{\partial^2}{\partial t^2}\right)\boldsymbol{A}(\boldsymbol{x}, t) = 0. \tag{4.11}$$

In order to solve the above wave equation, the vector potential is separated into positive and negative frequencies terms,

$$\boldsymbol{A}(\boldsymbol{x}, t) = \boldsymbol{A}^{(+)}(\boldsymbol{x}, t) + \boldsymbol{A}^{(-)}(\boldsymbol{x}, t), \tag{4.12}$$

where $\boldsymbol{A}^{(+)}(\boldsymbol{x}, t)$ involves only Fourier components with positive frequency, i.e only terms which vary as $e^{-\mathrm{i}\omega t}$ for $\omega > 0$, and $\boldsymbol{A}^{(-)}(\boldsymbol{x}, t)$ entails amplitudes which vary as $e^{\mathrm{i}\omega t}$. The positive and the negative frequency parts of the vector potential are then expanded in terms of the discrete set of orthogonal mode functions $\boldsymbol{u}_k(\boldsymbol{x})$ spanning the entire electromagnetic Hilbert space:

$$\boldsymbol{A}^{+}(\boldsymbol{x}, t) = \sum_k \frac{\mathcal{E}_k}{\omega_k}\xi_k \boldsymbol{u}_k(\boldsymbol{x})e^{-\mathrm{i}\omega_k t}, \quad \text{and} \quad \boldsymbol{A}^{-}(\boldsymbol{x}, t) = \sum_k \frac{\mathcal{E}_k}{\omega_k}\xi_k^* \boldsymbol{u}_k^*(\boldsymbol{x})e^{\mathrm{i}\omega_k t}, \tag{4.13}$$

where, $\mathcal{E}_k = \sqrt{\omega_k/2\epsilon_0 V}$ are the amplitude of the vacuum field in volume V, and the c-numbers ξ_k and ξ_k^* are the expansion coefficients. The set of mode function $u_k(\boldsymbol{x})$ pertaining to frequency ω_k fulfills the wave equation

$$\left(\nabla^2 - \omega_k^2/c^2\right)\boldsymbol{u}_k(\boldsymbol{x}) = 0, \tag{4.14}$$

where the frequency ω_k is connected to the wave vector $\boldsymbol{k}$ via $\omega_k = c|\boldsymbol{k}|$. By virtue of the transversality condition on the vector potential, Eq. (4.9), the mode functions should also obey the transversality condition, and form an orthonormal set:

$$\boldsymbol{\nabla} \cdot \boldsymbol{u}_k(\boldsymbol{x}) = 0, \quad \text{and} \quad \int_V \boldsymbol{u}_k^*(\boldsymbol{x}) \cdot \boldsymbol{u}_{k'}(\boldsymbol{x}) d^3\boldsymbol{x} = \delta_{kk'}. \tag{4.15}$$

Here, the spatial integration extends over the volume V, in which the field is to be considered. In case of cubic region of side $l = V^{1/3}$ with periodic boundary conditions, the spatial mode functions are the plane waves [53, 73]

$$\boldsymbol{u}_k(\boldsymbol{x}) \equiv \boldsymbol{u}_{\boldsymbol{k},\lambda}(\boldsymbol{x}) = \sqrt{\frac{1}{V}}\epsilon_\lambda(\boldsymbol{k})e^{\mathrm{i}\boldsymbol{k}\cdot\boldsymbol{x}}. \tag{4.16}$$

Here $\epsilon_\lambda(\boldsymbol{k})$ is referred to as the polarization vector which fulfills $\epsilon_\lambda(\boldsymbol{k}) \cdot \boldsymbol{k} = 0$. By upgrading ξ_α and ξ^*_α to the annihilation $\hat{b}_k$ and the creation operators $\hat{b}^\dagger_k$, respectively, the quantized version of the vector potential of a free field may be obtained [53, 73],

$$\hat{\boldsymbol{A}}(\boldsymbol{x}, t) = \sum_k \frac{\mathcal{E}_k}{\omega_k}\left\{\hat{b}_k \boldsymbol{u}_k(\boldsymbol{x})e^{-\mathrm{i}\omega_k t} + \hat{b}^\dagger_k \boldsymbol{u}^*_k(\boldsymbol{x})e^{\mathrm{i}\omega_k t}\right\}. \tag{4.17}$$

The creation $\hat{b}^\dagger_k$ and the annihilation $\hat{b}_k$ obey the commutation relation

$$[\hat{b}_k, \hat{b}^\dagger_{k'}] = \delta_{kk'}. \tag{4.18}$$

The Hamiltonian for the electromagnetic field is given by

$$H_{EMF} = \int \left(\frac{\varepsilon_0 \boldsymbol{E}^2}{2} + \frac{\boldsymbol{B}^2}{2\mu_0}\right) d^3\boldsymbol{x}. \tag{4.19}$$

Upon inserting the fields $\boldsymbol{E}$ and $\boldsymbol{B}$ into the above equation and by resorting to the conditions, Eqs (4.14) and (4.15), this Hamiltonian can be reduced to

$$H_{EMF} = \sum_k \hbar\omega_k \left(\hat{b}^\dagger_k \hat{b}_k + \frac{1}{2}\right). \tag{4.20}$$

The Light matter Interaction Hamiltonian

The coupling between light and matter are usually described by making use of the dipole approximation [53, 73–75]. More precisely, it is assumed that the spatial extent of the interaction region is small compared to the wave length of the quantized field. In this spirit, the light-matter interaction Hamiltonian reads as

$$\hat{H}_{int} = \mathrm{i}\sum_{\alpha\sigma}\sum_k \left(-g^k_{\alpha\sigma}\hat{b}_k\hat{c}^\dagger_\alpha\hat{v}_\sigma + g^{k*}_{\alpha\sigma}\hat{b}^\dagger_k\hat{v}^\dagger_\alpha\hat{c}_\sigma\right). \tag{4.21}$$

In writing down this Hamiltonian, we invoked the *rotating wave approximation* [53, 72–75] to erase the non-resonant part, as these terms entail phase factors leading to a rapidly oscillating dynamics. The first term in the above equation encodes the elementary process, whereby a photon is removed from the light field, and an electron is raised from the valence band to the conduction band. The second term accounts for the reverse process.

In Equation (4.21), the strength of the coupling between the quantized light field and the carrier transition between the single-particle states $|\alpha\rangle$ and $|\sigma\rangle$ is given by

$$g^k_{\alpha\sigma} = \mathcal{E}_k \int d^3\boldsymbol{x}\, \varphi^{c*}_\alpha(\boldsymbol{x})\, e\hat{\boldsymbol{x}}\, u_k(\boldsymbol{x})\varphi^v_\sigma(\boldsymbol{x}). \tag{4.22}$$

The avenue used for the computation of the coupling matrix elements, Eq (4.22), is the envelope-function approximation [72] that has been already discussed in Sect. 4.1.1 . The gist of this approximation consists in resolving the wave-functions $\varphi^c_\alpha(\boldsymbol{x})$ and $\varphi^v_\sigma(\boldsymbol{x})$ into a rapidly oscillating *Bloch*-factor $f_{k\approx 0}(\boldsymbol{x})$, and an envelope function that marginally changes over the unit cell, cf Sect. 4.1.1. Furthermore, by assuming an equal envelope for the conduction- and the valence-band electrons [72], Eq. (4.22) reduces to

$$g_{k,\alpha\sigma} = \mathcal{E}_k\, \boldsymbol{d}_{cv}\, \boldsymbol{u}_k(\boldsymbol{x}_0)\delta_{\alpha\sigma}, \tag{4.23}$$

where $\boldsymbol{x}_0$ represents the position of the matter, the semiconductor QD, and $\boldsymbol{d}_{cv}$ denote the interband matrix elements, which is the same for identical quantum dots. The expression of the light matter coupling strength in the envelope-function approximation implies that optical transitions take place only the *s–shells* or *p-shells* of electrons and holes may be observed.

By collecting all the contributions outlined above, the total Hamiltonian of the system under study is given by

$$H = H_0 + H_C + H_{EMF} + H_{int}. \tag{4.24}$$

Having set up the total Hamiltonian of the semiconductor QDs system, we now turn to the theoretical framework underlying the dynamics in these systems.

4.2 Dynamics in Semiconductor Quantum Dots Systems

The previous section was concerned with the Hamiltonian of a semiconductor QDs system. The aim of this section is to give a survey of the dynamical equations underlying the semiconductor laser model and the intimately related issue of infinite hierarchy.

4.2.1 Equation of Motion Approach

Expectation Value

For many-particle systems, solving the quantum Markovian master equation of Lindblad-type for the density matrix, cf. Sect. 3.2.4, both analytically and numerically turns out to be an elusive endeavor because of the exponential growth of the corresponding Hilbert spaces. One

way forward is to select the relevant expectation values (EV) of the system under consideration

$$\langle \hat{G} \rangle = \mathrm{Tr}[\hat{G}\hat{\rho}], \tag{4.25}$$

and directly derive their equations of motion (EoM). By virtue of the dynamics of the density matrix operator (cf. Sect. 3.2.4, Eq. (3.44)), the time derivative of the EV yields the generalized Ehrenfest EoMs which reads as [76]

$$\frac{d}{dt}\langle \hat{G} \rangle = -\mathrm{i}\langle [\hat{H}, \hat{G}] \rangle + \sum_{\alpha} \gamma_{\alpha} \left\{ \langle \hat{A}_{\alpha}^{\dagger} \hat{G} \hat{A}_{\alpha} \rangle - \frac{1}{2} \langle \hat{A}_{\alpha}^{\dagger} \hat{A}_{\alpha} \hat{G} \rangle - \frac{1}{2} \langle \hat{G} \hat{A}_{\alpha}^{\dagger} \hat{A}_{\alpha} \rangle \right\}. \tag{4.26}$$

Because of its ability to systematically incorporate many-body correlations into the dynamics of the system under study, the EoM approach has been extensively and successfully used in exploring ultra-cold Bose gases [77], exciton dynamics in quantum wells [70], cavity quantum electrodynamics [78], photoluminescence [79] and microcavity quantum dot lasers [80, 81]. An peculiarity of the EoM approach is its intimately related infinite hierarchy of differential equations, which can be rationalized by the interaction part of the Hamiltonian of the system under consideration. A prominent avenue which can be contemplated in truncating the unfolding hierarchy of EoM to obtain a closed set of equations of motion for the dynamical observables of interest, is the *cluster expansion* scheme. [82]

Cluster Expansion Scheme

Pioneered by *J. Fricke*, see Ref. [82], the cluster expansion scheme is a salient method allowing for a systematic dealing with the hierarchy problem in many-body physics. It has been successfully used in semiconductor physics, especially in describing the luminescence dynamics of quantum wells [79] and of quantum dots [71, 83]. The main idea of the cluster expansion method is to map every expectation value, say $\langle \hat{a}_1 \hat{a}_2 \dots \hat{a}_k \rangle$ onto its correlation function $\delta\langle \hat{a}_1 \hat{a}_2 \dots \hat{a}_k \rangle$. As result, equation of motion for the correlation function are obtained.

In order to systematically implement the cluster expansion, expectation values are classified as *singlet, doublets, quadruplets, quintuplets* and so on, depending on the number of particles they involve.

Definition 4.2.1. *The correlation function $\delta\langle \hat{a}^{\mathcal{I}} \rangle$ of an expectation value $\langle \hat{a}_1 \hat{a}_2 \dots \hat{a}_k \rangle$ is defined by*

$$\langle \hat{a}^{\mathcal{I}} \rangle = \delta\langle \hat{a}^{\mathcal{I}} \rangle + \delta\langle \hat{a}_F^{\mathcal{J}} \rangle = \sum_{P \in \mathcal{P}_{\mathcal{I}}} \prod_{\mathcal{J} \in P} \delta\langle \hat{a}^{\mathcal{J}} \rangle. \tag{4.27}$$

Here $\mathcal{I} = \{1, 2, \dots, k\}$ defines a set of indices and $\mathcal{P}$ is the corresponding partition being tantamount to a set family of disjoint nonempty subsets $\mathcal{J}$ of $\mathcal{I}$ with

$$\mathcal{I} = \cup_{\mathcal{J} \in \mathcal{P}} \mathcal{J}. \tag{4.28}$$

The quantity $\delta\langle \hat{a}_F^{\mathcal{J}} \rangle$ encodes all possible factorizations of the expectation value $\langle a^{\mathcal{I}} \rangle$ into correlations involving a smaller number of operators than the cardinality of the set $\mathcal{I}$.

To exemplify this, we collect the factorization of EV of a singlet, a doublet, and a triplet expectation value

$$\begin{aligned}
\langle \hat{a}_1 \rangle &= \delta\langle \hat{a}_1 \rangle, \\
\langle \hat{a}_1 \hat{a}_2 \rangle &= \delta\langle \hat{a}_1 \hat{a}_2 \rangle + \delta\langle \hat{a}_1 \rangle \delta\langle \hat{a}_2 \rangle, \\
\langle \hat{a}_1 \hat{a}_2 \hat{a}_3 \rangle &= \delta\langle \hat{a}_1 \hat{a}_2 \hat{a}_3 \rangle + \delta\langle \hat{a}_1 \hat{a}_2 \rangle \delta\langle \hat{a}_3 \rangle + \delta\langle \hat{a}_1 \hat{a}_3 \rangle \delta\langle \hat{a}_2 \rangle \\
&\quad + \delta\langle \hat{a}_2 \hat{a}_3 \rangle \delta\langle \hat{a}_1 \rangle + \delta\langle \hat{a}_1 \rangle \delta\langle \hat{a}_2 \rangle \delta\langle \hat{a}_3 \rangle.
\end{aligned} \tag{4.29}$$

It should be mentioned that the above definition for the correlation function holds only for bosonic systems. Notwithstanding, for fermionic operators a similar definition for the correlation function may be obtained by taking into account their antisymmetric property. Of a central importance in this thesis are EVs involving bosonic and fermionic particles which are referred to as mixed EV. An example of this kind of mean value is the so-called *photon-assisted polarization*, $\langle \hat{b}^\dagger \hat{v}^\dagger \hat{c} \rangle$, the equation of motion of which will be discussed in the next section. When classifying those EVs, one muss take into account that the excitation of one electron is immutably linked with the destruction of a valence band carrier and the creation of a conduction band carrier.

4.2.2 Semiconductor Luminescence Equations

Having dwelt on the expectation values and the powerful cluster expansion device to map them onto their corresponding correlation functions, we now turn our attention to the derivation of the semiconductor luminescence equations (SLEs) entailing the expectation values consistently up to the doublet level. On the ground of these SLEs being used to describe the spectrum and time-resolved photoluminescence of semiconductor nanostructures [71], we will set up the stripped down semiconductor quantum dots nanolasers theory, cf. Chap. 5.

We note that here the derivation of the SLEs assumes that the luminescence comes about in the incoherent regime, meaning that a coherent polarization is not expected to play a role, $\langle \hat{v}_\alpha^\dagger \hat{c}_\alpha \rangle = 0$, and $\langle \hat{b}_k \rangle = 0$. This is the case in scenarios, where carriers are incoherently or coherently generated in barrier, wetting layer or higher localized states with rapid dephasing and carrier relaxation resulting into a quasi-equilibrium distribution of the carriers at the lattice temperature. Nevertheless, in scenarios like resonance fluorescence [79, 84], all equations of motion must included these additional terms.

Furthermore, the derivation of these equations is based on the restriction of *s*- and *p*-shells for the localized states of the quantum dots, having zero and ± 1 angular momentum, respectively. Thereby, by virtue of the rotational symmetry of the system and the intimately related conservation of the angular momentum, all expectation value involving two carrier operators

are restricted to populations $\langle \hat{a}_\alpha^\dagger \hat{a}_{\alpha'} \rangle = f_\alpha^a \delta_{\alpha\alpha'}$, providing that initially all expectation values but for the population in the *s*- and *p*-shells are set to zero [71].

Carrier and Photon Numbers Dynamics

From the mathematical prescription outlined in Eq. (4.26), the time evolution of the photon number pertaining to one mode k of the light field reads as

$$\hbar \frac{d}{dt} \langle \hat{b}_k^\dagger \hat{b}_k \rangle = 2\mathrm{Re} \sum_\alpha |g_k|^2 \langle \hat{b}_k^\dagger \hat{v}_\alpha \hat{c}_\alpha \rangle. \tag{4.30}$$

In this equation, the term in the right-hand side, $\langle \hat{b}_k^\dagger \hat{v}_\alpha^\dagger \hat{c}_\alpha \rangle$, the so-called photon-assisted polarization amplitude has been scaled as $\langle \hat{b}_k^\dagger \hat{v}_\alpha \hat{c}_\alpha \rangle \to g_k^* \langle \hat{b}_k^\dagger \hat{v}_\alpha \hat{c}_\alpha \rangle$. Its dynamics is given by

$$\begin{aligned} \mathrm{i}\hbar \frac{d}{dt} \langle \hat{b}_k^\dagger \hat{v}_\alpha^\dagger \hat{c}_\alpha \rangle = \Omega_{k\alpha} \langle \hat{b}_k^\dagger \hat{v}_\alpha^\dagger \hat{c}_\alpha \rangle - \left(f_\alpha^c - f_\alpha^v \right) \sum_\sigma V_{\alpha\sigma\alpha\sigma} \langle \hat{b}_k^\dagger \hat{v}_\alpha^\dagger \hat{c}_\alpha \rangle \\ + \mathrm{i}|g_k|^2 f_\alpha^e f_\alpha^h + \mathrm{i} \sum_\sigma |g_k|^2 C^x_{\sigma\alpha\alpha\sigma}. \end{aligned} \tag{4.31}$$

In the above equation $\Omega_{k\alpha}$ reads as $\Omega_{k\alpha} = \tilde{\varepsilon}_\alpha^c - \tilde{\varepsilon}_\alpha^v - \hbar\omega_k - \mathrm{i}\gamma$ where $\tilde{\varepsilon}_\alpha^c$ and $\tilde{\varepsilon}_\alpha^v$ are the Coulomb-renormalized energies, which are given by

$$\tilde{\varepsilon}_\alpha^{c,v} = \varepsilon_\alpha^{c,v} - \sum_\sigma V_{\alpha\sigma\alpha\sigma} f_\sigma^{c,v}, \tag{4.32}$$

and ω_k is the resonance frequency of the optical mode k. In lieu of making use of the dissipator term appearing in Eq. (4.26), a phenomenological dephasing rate γ has been used to control the broadening of the spectral lines.

In semiconductor systems dephasing is the result of *Coulomb* scattering and scattering with acoustic or optical phonons. A microscopic description of this process may be achieved by augmenting the system Hamiltonian with an Hamiltonian encoding the carrier-phonon interaction [70, 85]. However, in this thesis a phenomenological dephasing rate is used to account for this process.

The second term in right-hand side of Eq. (4.31) is reminiscent of the quantum well case, where it is responsible for the excitonic photoluminescence below the band gap [79]. Here, however, it accounts for the corresponding excitonic resonances for the quantum dot states due to the interband Coulomb exchange interaction.

The quantum mechanical description of the light naturally gives rise to the source term of spontaneous emission $\langle \hat{c}_\sigma^\dagger \hat{v}_\sigma \hat{v}_\alpha^\dagger \hat{c}_\alpha \rangle$, the factorization $f_\alpha^e f_\alpha^h$ of which appears in the last line with the *electron-hole* correlation function $C^x_{\sigma\alpha\alpha\sigma} = \delta \langle \hat{c}_\sigma^\dagger \hat{v}_\alpha^\dagger \hat{c}_\alpha \hat{v}_\sigma \rangle$. Interestingly, unlike the atomic model, wherein the spontaneous emission source involved only electrons population, the formalism of the semiconductor QD entails two-particle expectation values consisting of electron,

and hole operators. It should be noted that the term encoding the stimulated emission or absorption process has been erased as we are considering a quantized open field.

The time evolution of the carrier population in the conduction band, $f_\alpha^c = \langle \hat{c}_\alpha^\dagger \hat{c}_\alpha \rangle$, reads as

$$\hbar \frac{d}{dt} f_\alpha^c = -2\,\mathrm{Re} \sum_k |g_k|^2 \langle \hat{b}_k^\dagger \hat{v}_\alpha^\dagger \hat{c}_\alpha \rangle + 2\,\mathrm{Im} \sum_{\sigma\sigma'\alpha'} V_{\alpha\sigma\sigma'\alpha} \left(C^c_{\alpha\sigma\sigma'\alpha'} - C^x_{\sigma\alpha\sigma'\alpha'} \right), \tag{4.33}$$

and that of the carrier population in the valence band, $f_\alpha^v = \langle \hat{v}_\alpha^\dagger \hat{v}_\alpha \rangle$, is given by

$$\hbar \frac{d}{dt} f_\alpha^v = 2\,\mathrm{Re} \sum_k |g_k|^2 \langle \hat{b}_k^\dagger \hat{v}_\alpha^\dagger \hat{c}_\alpha \rangle - 2\,\mathrm{Im} \sum_{\sigma\sigma'\alpha'} V_{\alpha\sigma\sigma'\alpha} \left(C^v_{\alpha\sigma\sigma'\alpha'} - C^x_{\sigma\alpha\sigma'\alpha'} \right). \tag{4.34}$$

In Eqs (4.33)-(4.34), two additional intraband correlation functions $C^c_{\alpha\sigma\sigma'\alpha'} = \delta \langle \hat{c}_\alpha^\dagger \hat{c}_\sigma^\dagger \hat{c}_{\sigma'} \hat{c}_{\alpha'} \rangle$ and $C^v_{\alpha\sigma\sigma'\alpha'} = \delta \langle \hat{v}_\alpha^\dagger \hat{v}_\sigma^\dagger \hat{v}_{\sigma'} \hat{v}_{\alpha'} \rangle$ arise.

Dynamics of Carrier Correlations

According to the cluster expansion scheme, the interband or electron-hole correlation is given by

$$C^x_{\alpha\sigma\sigma'\alpha'} = \langle \hat{c}_\alpha^\dagger \hat{v}_\sigma^\dagger \hat{c}_{\sigma'} \hat{v}_{\alpha'} \rangle + f_\alpha^c f_\sigma^v \delta_{\alpha\sigma'} \delta_{\sigma\alpha'}. \tag{4.35}$$

It encodes a process wherein synchronous transitions of a conduction-band-carrier from a state σ' to state α, and of valence-band-carrier from a state α' to a state σ occur. The term $\propto f_\alpha^c(1-f_\alpha^v)$ describes an uncorrelated electron-hole plasma for a given state α and is commonly referred to as the *Hartree-Fock factorization* in case of zero electron-hole correlation.

It might be instructive to mention that in deriving Eq. (4.31) we tacitly assume that the semiconductor nanostructure under consideration is devoid of any interemitter radiative coupling. However, if the quantum dots radiatively couple to each another, an effect being referred to as *superfluorescence* or *superradiance* [86–90], the source term of the spontaneous emission may be generalized to account for coupling of carrier transitions in different dots. This means correlation functions $\delta \langle \hat{c}_\alpha^\dagger \hat{v}_\sigma^\dagger \hat{c}_{\sigma'} \hat{v}_{\alpha'} \rangle = \delta \langle \hat{c}_{\alpha,x_1}^\dagger \hat{v}_{\sigma,x_2}^\dagger \hat{c}_{\sigma',x_2} \hat{v}_{\alpha',x_1} \rangle (1 - \delta_{x_1,x_2})$ involving two different quantum dots at different spatial position have to be included in Equation (4.31). It should be noted that for those correlation functions the contributions from the Coulomb interaction cancels, meaning that only the light matter interaction controls them.

The time evolution of the interband correlations reads as

$$
\begin{aligned}
\mathrm{i}\hbar\frac{d}{dt}C^{x}_{\alpha\sigma\sigma'\alpha'} &= \left(\tilde{\varepsilon}_{\sigma'} - \tilde{\varepsilon}^{c}_{\alpha} + \tilde{\varepsilon}_{\alpha'} - \tilde{\varepsilon}^{v}_{\sigma}\right) C^{x}_{\alpha\sigma\sigma'\alpha'} \\
&\quad + V_{\sigma'\alpha'\sigma\alpha}\left\{\left(1-f^{c}_{\sigma'}\right)\left(1-f^{v}_{\sigma}\right)f^{c}_{\alpha}f^{v}_{\alpha'} - \left(1-f^{c}_{\alpha}\right)\left(1-f^{v}_{\alpha'}\right)f^{c}_{\sigma'}f^{v}_{\sigma}\right\} \\
&\quad - \mathrm{i}\delta_{\alpha\alpha'}\delta_{\sigma\sigma'}\left\{\left(f^{v}_{\alpha}-f^{c}_{\alpha}\right)\sum_{k} g^{*}_{k}\langle\hat{b}^{\dagger}_{k}\hat{v}^{\dagger}_{\sigma}\hat{c}_{\sigma}\rangle + \left(f^{v}_{\sigma}-f^{c}_{\sigma}\right)\sum_{k} g_{k}\langle\hat{b}_{k}\hat{c}^{\dagger}_{\alpha}\hat{v}_{\alpha}\rangle\right\} \\
&\quad + \left(1-f^{v}_{\alpha'}-f^{c}_{\sigma'}\right)\sum_{\nu\nu'} V_{\sigma'\alpha'\nu\nu'}C^{x}_{\alpha\sigma\nu'\nu} - \left(1-f^{c}_{\alpha}-f^{v}_{\sigma}\right)\sum_{\nu\nu'} V_{\nu\nu'\sigma\alpha}C^{x}_{\nu'\nu\sigma'\alpha'} \\
&\quad + \left(f^{v}_{\sigma}-f^{v}_{\alpha'}\right)\sum_{\nu\nu'} V_{\nu\alpha'\sigma\nu'}C^{x+c}_{\alpha\nu\sigma'\nu'} + \left(f^{c}_{\alpha}-f^{c}_{\sigma'}\right)\sum_{\nu\nu'} V_{\sigma'\nu\nu'\alpha}C^{x}_{\nu\sigma\nu'\alpha'} \\
&\quad + \left(f^{c}_{\alpha}+f^{v}_{\alpha'}\right)\sum_{\nu\nu'} V_{\nu\alpha'\nu'\alpha}C^{x}_{\nu\sigma\sigma'\nu'} - \left(f^{c}_{\sigma'}+f^{v}_{\sigma'}\right)\sum_{\nu\nu'} V_{\sigma'\nu\sigma\nu'}C^{x}_{\alpha\nu\nu'\alpha'} \\
&\quad + \left(f^{c}_{\sigma'}-f^{c}_{\alpha}\right)\sum_{\nu\nu'} V_{\sigma'\nu\alpha\nu'}C^{x}_{\nu\sigma\nu'\alpha'} + \left(f^{v}_{\alpha'}-f^{v}_{\sigma}\right)\sum_{\nu\nu'} V_{\nu\alpha'\nu'\sigma}C^{x}_{\alpha\nu\sigma'\nu'},
\end{aligned}
\tag{4.36}
$$

where the following abbreviation has been introduced: $C^{x+c/v}_{\alpha\sigma\sigma'\alpha'} = C^{x}_{\alpha\sigma\sigma'\alpha'} + C^{c/v}_{\alpha\sigma\sigma'\alpha'}$. A restriction of the dynamics of the interband correlations C^{x}, Eq. (4.36) to the first lines is referred to as *singlet approximation*. The singlet approximation was used by *Jahnke et al* to investigate photoluminescence in quantum wells [79, 91], and by *Schwab et al* to describe photoluminescence in quantum dots [92]. The third line is the contribution arising from the light-matter Hamiltonian. The terms in the fourth account for the screening according to the *Lindhard* theory for the *Coulomb* interaction in the dynamics of the photon-assisted polarization. The scattering between all possible states gives rise to the Coulomb renormalization encoded by the last six terms.

In similar fashion the dynamics of the intra-band correlation $C^c_{\alpha\sigma\sigma'\alpha'} = \delta\langle \hat{c}^\dagger_\alpha \hat{c}^\dagger_\sigma \hat{c}_{\sigma'} \hat{c}_{\alpha'}\rangle$ may be obtained as

$$
\begin{aligned}
\mathrm{i}\hbar\frac{d}{dt}C^c_{\alpha\sigma\sigma\alpha'} = &-\left(\tilde{\varepsilon}_\alpha - \tilde{\varepsilon}^c_{\alpha'} - \tilde{\varepsilon}_\sigma + \tilde{\varepsilon}^c_{\sigma'}\right) C^c_{\alpha\sigma\sigma'\alpha'} \\
&- \left(V^*_{\alpha\sigma\sigma'\alpha'} - V_{\alpha\sigma\alpha'\sigma'}\right)\left[\left(1-f^c_\alpha\right)\left(1-f^c_\sigma\right)f^c_{\sigma'}f^c_{\alpha'} - \left(1-f^c_{\alpha'}\right)\left(1-f^c_{\sigma'}\right)f^c_\sigma f^v_\alpha\right] \\
&+ \left(f^c_{\sigma'} - f^c_\sigma\right)\sum_{\nu\nu'} V_{\sigma'\nu\nu'\sigma} C^{c+x}_{\alpha\nu\nu'\sigma} - \left(f^c_\alpha - f^c_{\alpha'}\right)\sum_{\nu\nu'} V_{\alpha'\nu\nu'\alpha} C^{c+x}_{\sigma\nu\sigma'\nu'} \\
&- \left(f^c_{\sigma'} - f^c_\alpha\right)\sum_{\nu\nu'} V_{\sigma'\nu\nu'\alpha} C^{c+x}_{\sigma\nu\nu'\alpha} + \left(f^c_\sigma - f^c_{\alpha'}\right)\sum_{\nu\nu'} V_{\alpha'\nu\nu'\sigma} C^{c+x}_{\alpha\nu\sigma'\nu'} \\
&+ \left(1 - f^c_{\alpha'} - f^v_{\sigma'}\right)\sum_{\nu\nu'} V_{\sigma'\alpha'\nu'\nu} C^c_{\alpha\sigma\nu\nu'} - \left(1 - f^c_\alpha - f^c_\sigma\right)\sum_{\nu\nu'} V_{\nu\nu'\sigma\alpha} C^c_{\nu\nu'\sigma'\alpha'} \\
&+ \left(f^c_\alpha - f^c_{\alpha'}\right)\sum_{\nu\nu'} V_{\alpha'\nu\alpha\nu'} C^c_{\nu\sigma\sigma'\nu'} - \left(f^c_{\sigma'} - f^c_\alpha\right)\sum_{\nu\nu'} V_{\nu\sigma'\nu'\alpha} C^c_{\nu\sigma\nu'\alpha'} \\
&+ \left(f^c_{\sigma'} - f^c_\sigma\right)\sum_{\nu\nu'} V_{\nu\sigma'\nu'\sigma} C^c_{\alpha\nu\nu'\alpha'} - \left(f^c_{\sigma'} - f^c_{\alpha'}\right)\sum_{\nu\nu'} V_{\alpha'\nu\sigma\nu'} C^c_{\alpha\nu\sigma'\nu'}.
\end{aligned}
\tag{4.37}
$$

By availing ourselves of the symmetry property of the Hamiltonian Eq.(4.24), the equation of motion for $C^v_{\alpha\sigma\sigma\alpha'} = \delta\langle \hat{v}^\dagger_\alpha \hat{v}^\dagger_\sigma \hat{v}_{\sigma'} \hat{v}_{\alpha'}\rangle$ can be derived. Interpreting the terms in the time evolution for the intraband correlation function can be achieved by following the same reasoning as in the case of the electron-hole correlation. Nevertheless, it should be noted that the contribution from the light-matter Hamiltonian vanish for $C^v_{\alpha\sigma\sigma\alpha'}$ and $C^c_{\alpha\sigma\sigma\alpha'}$. Note that an increase (decrease) of population in the conduction band amounts to the decrease (increase) of the total photon number,

$$
\frac{d}{dt}\left\{\sum_\alpha f^c_\alpha + \sum_k \langle \hat{b}^\dagger_k \hat{b}_k\rangle\right\} = 0, \tag{4.38}
$$

meaning that the Coulomb correlations only redistribute carriers without changing the total population $\mathrm{i}\frac{d}{dt}\Big|_{H_C}\left\{\sum_\alpha f^{c,v}_\alpha\right\} = 0$. It should also be noted that the dynamics of the carrier-carrier correlation functions remain undamped as no dephasing has been included in the derivation.

The set of coupled equations, Eqs. (4.30), (4.33), (4.34), (4.31), (4.36), and (4.37) constitute a solid apparatus for investigating the photoluminescence (PL) of semiconductor quantum dots, as they make allowances for interaction-induced effects, including a modification of the spontaneous emission source, and energy renormalizations. In the next section, we discuss the effect of carrier correlations in semiconductor quantum dots.

4.2.3 Effect of Carrier Correlations in Quantum Dots

Before closing this chapter, let us briefly address the role of carrier correlations in semiconductor quantum dots. In deriving the equation of motion for the so-termed photon assisted polarization, see Eq. (4.31), the light matter Hamiltonian gives rise to the source term of spontaneous emission $\sum_\alpha g_k \langle \hat{c}_\alpha \hat{v}_\alpha \hat{v}_\sigma \hat{c}_\sigma \rangle$. The corresponding cluster expansion is given by

$$\sum_\sigma g_k \langle \hat{c}_\sigma^\dagger \hat{v}_\sigma \hat{v}_\alpha^\dagger \hat{c}_\alpha \rangle = g_k f_\alpha^c \left(1 - f_\alpha^v\right) + g_k \sum_\sigma \delta \langle \hat{c}_\sigma^\dagger \hat{v}_\sigma \hat{v}_\alpha^\dagger \hat{c}_\alpha \rangle. \tag{4.39}$$

In the framework of the Hartree-Fock approximation which consists in neglecting the second term in the above relationship, the equation of motion for the photon assisted polarization can be solved in the adiabatic regime to obtain

$$\langle \hat{b}_k^\dagger \hat{v}_\alpha^\dagger \hat{c}_\alpha \rangle_{\text{stat}} = -\mathrm{i} \frac{g_k f_\alpha^c (1 - f_\alpha^v)}{\varepsilon_\alpha^c - \varepsilon_\alpha^v - \hbar\omega_k - \mathrm{i}\gamma}. \tag{4.40}$$

It should be noted that the above stationary solution being based on slowly varying populations neglects the Coulomb interaction. On Inserting this in equation of motion for the conduction band population, Eq. (4.33), one obtains

$$\left\{ \frac{d}{dt} + \frac{(1 - f_\alpha^v)}{\tau_\alpha^c} \right\} f_\alpha^c = 0, \quad \text{with} \quad \frac{1}{\tau_\alpha^c} = -\frac{2}{\hbar} \mathrm{Re} \sum_k \frac{\mathrm{i}|g_k|^2}{\varepsilon_\alpha^c - \varepsilon_\alpha^v - \hbar\omega_k - \mathrm{i}\gamma} \tag{4.41}$$

Here $1/\tau_\alpha^c$ is the Wigner-Weißkopf rate of spontaneous emission for conduction-band carriers in the limit $\gamma \to 0$ [53]. This relationship is interesting, as it reveals that in semiconductor quantum dots system, the decay of the population f_α^c is non-exponential, unless the valence band population f_α^v remains unchanged, for example through background doping. By virtue of Eq. (4.38), the dependence of the rate of decay, Eq. (4.41) on the carrier density, which is higher for larger population carries over to the PL. As consequence, any attempt to model the PL dynamics must steer clear of a simple decay rate, as semiconductor QD systems do not intrinsically show an exponential decay behavior known from two-level atom.

Another avenue which may be used in evaluating the spontaneous emission source term is the one-electron two-level approximation. The gist of this approximation consists in assuming that the relevant physics is determined by one confined shell for electrons and one for the holes. Thereby, the excited (unexcited) state for the two-level system amounts to the electron being the conduction (valence) band state. In the absence of Coulomb interaction, the two spin polarizations are uncorrelated meaning that the excitation processes entail only a single electron. As a result, the source for the spontaneous emission reduces to

$$\langle \hat{c}^\dagger \hat{v} \hat{v}^\dagger \hat{c} \rangle = f^c, \tag{4.42}$$

as a successive application of more than one annihilation or creation operator always amounts to zero. Carries indices are discarded, as only one confined electron and hole are considered. With Eq. (4.42), the population dynamics

$$\left\{ \frac{d}{dt} + \frac{1}{\tau} \right\} f^c = 0, \tag{4.43}$$

decays exponentially, which is now reminiscent of a two-level atom. Here, $1/\tau$ is the Wigner-Weißkopf rate for the considered two-level transition.

The exponential decay behavior obtained in the framework of the two-level approximation suggests that the excitation of a quantum dot conduction-band carrier is immutably connected to the absence of valance-band carrier. This is tantamount to a fully correlated electron-hole pair in the electron-hole picture. However, when dealing with semiconductor QD, wherein many carriers are present, an explicit calculation of their correlations being subject to scattering and dephasing processes must be considered.

4.3 Summary

In this chapter, we have set up the apparatus for adequately handling the light matter interaction in semiconductor quantum dots systems. Starting from the system Hamiltonian, we then discussed the equation of motion approach and its inherently related hierarchy problem. Having discussed the cluster expansion tool to prune the infinite hierarchy of equations of motion, we derived the SLEs constituting a consistent framework for investigating photoluminescence of semiconductor quantum dots into free space. By inspecting the SLEs, a non-exponential and excitation-density dependent decay was shown to arise from the semiconductor nature of quantum dots. In the next chapter, upon introducing a cavity system that will modify the photonic local density state seeing by the semiconductor quantum dots, a semiconductor laser theory will be introduced.

5 Semiconductor Quantum Dots Nanolasers Theory

Owing to their discrete interband optical spectrum with almost homogeneously broadened transitions and shell filling effects, semiconductor quantum dots (QDs) have emerged as strong candidates for implementing novel photonic sources for quantum information processing. When they are used as gain medium for optical microresonators, such as micropillars [11, 12], microdisks [13, 14] and photonic crystals [15, 16] being designed for a three-dimensional (3D) confinement of light and thereby a discretization of the mode spectrum, single-mode light source with a spontaneous emission factor β approaching unity can realized [17, 18, 35, 36].

This chapter aims at introducing a semiconductor laser theory, which forms a solid framework for investigating the light output and the intensity correlation function of microcavity lasers with quantum dots as the active material. In contrast to the approaches based on atomic two- or multi-level systems, resulting either in a set of rate equations [93, 94], or a master equation for the reduced density matrix [95–97], to model semiconductor QD-based laser devices, the laser theory in this chapter makes allowances for inherent semiconductor effects, such as a modified source term of spontaneous emission and Coulomb effects[71]. It complements the general semiconductor laser model based on a microscopic Hamiltonian, which has been formulated to investigate lasing without inversion [98], the influence of carrier dynamics and many-body effects [99, 100], and noise spectra [101], by providing the apparatus for accessing the photon statistics, which is of crucial importance for devices characterization.

Having its basis on the semiconductor luminescence equations (SLEs) that have been derived in the previous chapter, Sect. 5.1 reviews the SLEs by making allowances for the effects of embedding QDs inside a microcavity. We then outline the prerequisites at the bottom of the semiconductor quantum dots formalism in section 5.2.1. On their basis, we will derive the equations of motion allowing for monitoring the dynamics of the mean photon in the lasing mode of the cavity, see Sect. 5.2. In section 5.3, we proceed further to show how the semiconductor laser theory can be upgraded with the dynamics of photon-photon correlation, which allows for a quantum-optical characterization of the operating regimes of state-of-the-art nanolasers.

5.1 Semiconductor Laser Equations

A derivation of semiconductor QD laser theory from the semiconductor luminescence equations requires some modifications of the equations of motion, as an introduction of a cavity gives rise to some effects, such the *stimulated emission* or *absorption*, that have been disregarded in case of open field. On introducing a cavity, the dynamic of photon number is given by

$$\hbar\frac{d}{dt}\langle\hat{b}_k^\dagger\hat{b}_k\rangle = -2\kappa\langle\hat{b}_k^\dagger\hat{b}_k\rangle + 2\mathrm{Re}\sum_\alpha |g_k|^2\langle\hat{b}_k^\dagger\hat{v}_\alpha^\dagger\hat{c}_\alpha\rangle, \tag{5.1}$$

where $2\kappa_k$ controls the loss of photons from the cavity mode k. The loss rate is connected to the quality factor Q_k of the mode k via $Q_k = \hbar\omega_k/(2\kappa_k)$.

The dynamics of the carrier populations $f_\alpha^e = \langle\hat{c}_\alpha^\dagger\hat{c}_\alpha\rangle$, $f_\alpha^h = 1 - \langle\hat{v}_\alpha^\dagger\hat{v}_\alpha\rangle$ in respect to the light matter interaction H_{int} reads as

$$\hbar\frac{d}{dt}f_\alpha^{e,h} = -2\mathrm{Re}\sum_k |g_k|^2\langle\hat{b}_k^\dagger\hat{v}_\alpha^\dagger\hat{c}_\alpha\rangle. \tag{5.2}$$

The ability of the cavity mode to store photons for a time, $\tau_{cav}^k = Q_k/\omega_k$, in the proximity of the quantum dots gives rise to stimulated emission or absorption processes. These processes, commonly referred to as *cavity feedback* are controlled by the expectation values $\langle\hat{b}_k^\dagger\hat{b}_k\hat{c}_\alpha^\dagger\hat{c}_\alpha\rangle - \langle\hat{b}_k^\dagger\hat{b}_k\hat{v}_\alpha^\dagger\hat{v}_\alpha\rangle$, that modifies the dynamics of the photon-assisted polarization as

$$\begin{aligned}\left\{\hbar\frac{d}{dt} + \kappa_k + \gamma + \mathrm{i}\Delta_{\alpha k}\right\}\langle\hat{b}_k^\dagger\hat{v}_\alpha^\dagger\hat{c}_\alpha\rangle =& f_\alpha^e f_\alpha^h - \left(1 - f_\alpha^e - f_\alpha^h\right)\langle\hat{b}_k^\dagger\hat{b}_k\rangle + \sum_\sigma C_{\sigma\alpha\alpha\sigma}^x \\ &+ \mathrm{i}\left(1 - f_\alpha^e - f_\alpha^h\right)\sum_\sigma V_{\alpha\sigma\alpha\sigma}\langle\hat{b}_k^\dagger\hat{v}_\sigma^\dagger\hat{c}_\sigma\rangle \\ &+ \delta\langle\hat{b}_k^\dagger\hat{b}_k\hat{c}_\alpha^\dagger\hat{c}_\alpha\rangle - \delta\langle\hat{b}_k^\dagger\hat{b}_k\hat{v}_\alpha^\dagger\hat{v}_\alpha\rangle.\end{aligned} \tag{5.3}$$

As in the semiconductor luminescence equations, the time evolution of the photon-assisted polarization is determined by the detuning of the quantum dot transition from the optical modes $\Delta_{\alpha k} = \tilde{\varepsilon}_\alpha^e + \tilde{\varepsilon}_\alpha^h - \hbar\omega_k$. The renormalized energies $\tilde{\varepsilon}_\alpha^{e,h}$ arise from Hartree-Fock contributions of the Coulomb interaction with the Coulomb matrix element $V_{\alpha\sigma\alpha\sigma}$, which as well give rise to interband exchange contribution that couples the photon-assisted polarizations of different states σ. The first and third terms are the Hartree-Fock factorization of four carrier operators $\langle\hat{c}_\alpha^\dagger\hat{v}_\alpha\hat{v}_\sigma^\dagger\hat{c}_\sigma\rangle$ that describes the source term of the spontaneous emission.

The second term in the right hand side of Eq. (5.3) that is proportional to the photon number $\langle\hat{b}_k^\dagger\hat{b}_k\rangle$ in the mode k is the singlet-doublet factorization of the expectation value $\langle\hat{b}_k^\dagger\hat{b}_k\hat{c}_\alpha^\dagger\hat{c}_\alpha\rangle - \langle\hat{b}_k^\dagger\hat{b}_k\hat{v}_\alpha^\dagger\hat{v}_\alpha\rangle$, which accounts for the stimulated emission or absorption and therefore provides feedback due the photon population in the cavity. The correlations emerging from this factorization are triplet-level correlation between carriers and photons, which appear in the last line.

The dynamics is damped by the photon dissipation rate κ_k, and carrier-carrier as well as carrier-phonon interaction-induced dephasing, that is modeled by a phenomenological damping constant γ.

5.2 Mean Photon Number in Semiconductor Quantum Dots Laser Theory

5.2.1 Prerequisites

The intent of this section is to outline the assumptions on the ground of which the semiconductor laser theory is developed. It should be noted that these assumptions should not be deemed as limitations of the model. On the other hand, corroborated by corresponding experimental conditions, they are used for the sake of convenient formulation and can be lifted at the cost of a more involved analytical and numerical formulation [102].

The laser model considers high-Q microcavities with one long-lived mode being in resonance with the quantum dots *s*-shell emission, see Fig. 5.1. In micropillar and photonic crystal cavities this long-lived possibly degenerate mode is usually the so-termed fundamental mode energetically lowest in the spectrum [18]. In microdisks the higher-excited whispering gallery modes are the long-lived modes. The resonant cavity mode is assumed to be energetically well separated from higher cavity modes. These higher cavity modes, as well as a continuum of leaky modes are treated as the non-lasing modes, which function as a dissipation channel for the coupled QD-cavity system. In order to make the laser model numerically less demanding and at the same time reproduce the experimental data, the following assumptions are made:

- *δ-broadened sample quantum dots:* On the ground of the results obtained in Ref. [92], it is assumed that the fundamental mode of the cavity is predominantly feed by the resonant quantum dots. The calculations in Ref. [92] revealed that the calculated photoluminescence of an ensemble of quantum dots with inhomogeneous broadening and that of identical QDs coincide, when the light-matter coupling strength of the latter is chosen as the maximum value in the inhomogeneously broadened quantum dot ensemble. Therefore, only those emitters in resonance with the lasing mode are considered.

- *s-shell lasing*: Only the *s-shell* transitions take part in optical processes involving the lasing mode (stimulated and spontaneous emission as well as photon reabsorption). As result thereof, higher shells and the wetting layer contribute only to the carrier dynamics.

- *Marginal p-shell carries and photons correlations:* In the light of the aforementioned prerequisite, it goes without saying that the correlations between *p-shell* carriers and photons

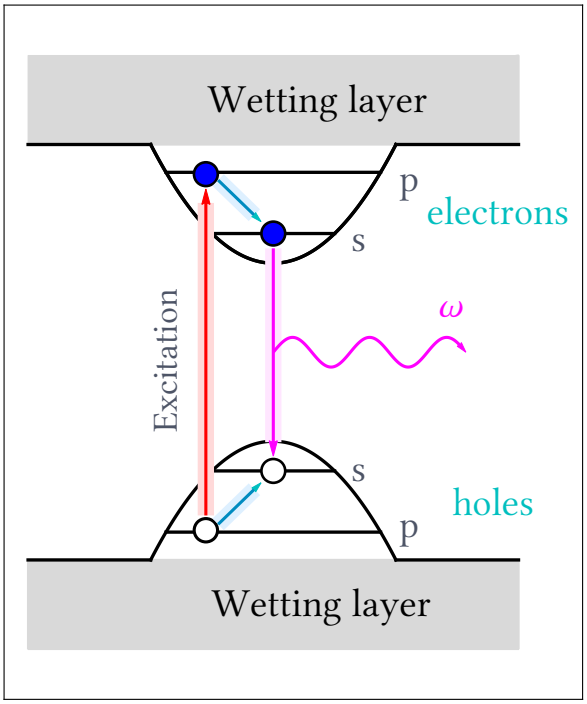

Figure 5.1 | Cartoon of the semiconductor QD laser model. A graphical representation of the semiconductor QD laser model. Carriers are generated in the *p*-shells. They then relaxed into the *s*-shells. The laser transition is defined by a recombination between *s*-shells electrons and holes.

in the lasing mode, resulting from the light-matter interaction, are marginal.

- *Relaxation time approximation*: Given the ultrafast carrier-scattering processes involved in carrier-carrier [69] and carrier-phonon interaction [85] in quantum dots, it is assumed that the carrier system is close to equilibrium. Consequently, scattering processes can be accounted for by resorting to the relaxation-time approximation [69]. Furthermore, it is assumed that for the coupled QD-cavity considered the temperature is low that up-scattering into energetically higher levels is negligible.

- *Marginal non-lasing modes feedback*. Stimulated emission and reabsorption of photons involving non-lasing are neglected, because photons spontaneously emitted into these non-lasing modes rapidly leave the cavity.

- *p-shell carriers generation via wetting layer:* From experimental point of view, carrier generation in the QD can be achieved by resonant optical pumping or by injecting carrier into the delocalized wetting layer or bulk states. Via scattering processes, the carrier then relaxes towards the *s*-shell. In the framework of the laser model, the *p*-shell is used to model the excitation process, wherein carriers are generated in it at a given rate P, see Fig. 5.1.

Having outlined the conditions underlying the semiconductor laser model, we now turn to the derivation of the relevant equations of motions suitable to capture a wide range of effect in semiconductor nanolasers. The starting point will be the semiconductor luminescence equations (SLE). Nevertheless, in deriving the laser equations the focus will be on the lasing regime where the stimulated emission dominates. In this regime, the influence of the carrier correlations $C^{x}_{\alpha\sigma\sigma\alpha}$ being linked with the Hartree-Fock source term of the spontaneous emission $f^{e}_{\alpha}f^{h}_{\alpha}$ is weak and can therefore be neglected. Moreover, the Hartree-like Coulomb effects between the quantum-dot carriers leading to intra- and interband interaction effects will be summarized in an effective transition energy and oscillator strength for the coupling to the laser mode.

5.2.2 Laser Equations

The formulation of a laser theory usually distinguishes between the rate of spontaneous emission into lasing $\frac{1}{\tau_l}$ and non-lasing modes $\frac{1}{\tau_{nl}}$, the sum of which yields the total spontaneous emission rate

$$\frac{1}{\tau_{sp}} = \frac{1}{\tau_l} + \frac{1}{\tau_{nl}}. \tag{5.4}$$

This distinction suggests to solve separately the time evolution of the photon-assisted polarization for the lasing mode, which for the s-shell transition reads as

$$\left\{\hbar\frac{d}{dt} + \kappa + \gamma\right\}\langle\hat{b}^{\dagger}\hat{v}^{\dagger}_{s}\hat{c}_{s}\rangle = f^{e}_{s}f^{h}_{s} - (1 - f^{e}_{s} - f^{h}_{s})\langle\hat{b}^{\dagger}\hat{b}\rangle + \delta\langle\hat{b}^{\dagger}\hat{b}\hat{c}^{\dagger}_{s}\hat{c}_{s}\rangle - \delta\langle\hat{b}^{\dagger}\hat{b}\hat{v}^{\dagger}_{s}\hat{v}_{s}\rangle, \tag{5.5}$$

where the index $k = k_l$ denoting the lasing mode has been omitted. Note that the detuning cancels out, as only resonant quantum dots are assumed to feed the lasing mode. In the framework of the semiconductor laser theory, the dynamics of the photon-assisted polarization for the non-lasing modes,

$$\left\{\hbar\frac{d}{dt} + \kappa_k + \gamma + \mathrm{i}\left(\tilde{\varepsilon}^{e}_{s} + \tilde{\varepsilon}^{v}_{s} - \hbar\omega_k\right)\right\}\langle\hat{b}^{\dagger}_{k}\hat{v}^{\dagger}_{s}\hat{c}_{s}\rangle\Big|_{k\neq k_l} = f^{e}_{s}f^{h}_{s}, \tag{5.6}$$

is adiabatically eliminated to introduce a time constant for the spontaneous emission into non-lasing modes according to the Weißkopf-Wigner theory [53]

$$\frac{1}{\tau_{nl}} = \frac{2}{\hbar}\sum_{k\neq k_l}\frac{|g_k|^2}{\kappa_k + \gamma + \mathrm{i}\left(\tilde{\varepsilon}^{e}_{s} + \tilde{\varepsilon}^{h}_{s} - \hbar\omega_k\right)}. \tag{5.7}$$

Note that, owing to the marginal photon population and the short lifetime of the non-lasing modes, the feedback term and carrier-photon correlation have been discarded in Eq. (5.6). The

time constant, Eq. (5.7) is related to the spontaneous emission coupling factor β, which has been introduced in Chap. 2, via

$$\frac{1}{\tau_{nl}} = \frac{1-\beta}{\tau_{sp}}, \tag{5.8}$$

where $1/\tau_{sp}$ is the total spontaneous emission rate.

By virtue of Eqs. (5.5), (5.6), and (5.8), the dynamics for the population dynamics in the s-shell takes the form

$$\frac{d}{dt}f_s^{e,h} = -2\frac{|g|^2}{\hbar}\mathrm{Re}\langle b^\dagger v_s^\dagger c_s\rangle + \mathcal{R}_{nl} + \mathcal{R}_{p\to s}^{e,h}. \tag{5.9}$$

Here $\mathcal{R}_{p\to s}^{e,h}$ controls the transition rate of carriers from the p- to the s-shell. It is given in the relaxation time approximation by

$$\mathcal{R}_{p\to s}^{e,h} = \left(1-f_s^{e,h}\right) f_p^{e,h}/\tau_{\mathrm{r}}^{e,h}, \tag{5.10}$$

where the blocking factor $1-f_s^{e,h}$ ensures that the populations cannot exceed unity. Note that only downwards directed scattering is included in $\mathcal{R}_{p\to s}^{e,h}$ which is well-suited for low-temperature situations. The first term on the right hand side of Eq. (5.9) encodes the carrier dynamics resulting from the interaction with the laser mode. The loss of carriers due to the recombination into non-lasing modes is given by $\mathcal{R}_{nl}$ which

$$\mathcal{R}_{nl} = -\sum_{k\neq k_l}|g_k|^2\langle \hat{b}_k^\dagger \hat{v}_s^\dagger \hat{c}_s\rangle = -\frac{f_s^e f_s^h}{\tau_{nl}}. \tag{5.11}$$

5.2.3 Carrier Generation Model

In the semiconductor quantum dot laser theory, the carrier dynamics for the p-shell, being used for the carrier generation, is given by

$$\frac{d}{dt}f_p^{e,h} = P\left(1-f_p^e-f_p^h\right) - \frac{f_p^e f_p^h}{\tau_{\mathrm{sp}}^p} - \mathcal{R}_{p\to s}^{e,h}. \tag{5.12}$$

In this Equation, the first term in the right hand side encodes the carrier generation scheme in the p-shell of each QD, wherein $\left(1-f_p^e-f_p^h\right)$ is the *Pauli-blocking factor*. It should be noted that P is to be interpreted as a *pump rate per emitter*, as the carrier generation comes about in the p-shell of each QD. The modeling of the spontaneous recombination of p-shell carriers into non-lasing modes is given by the second term. The last term is the aforementioned scattering term $\mathcal{R}_{p\to s}^{e,h}$ for transferring carriers only from the p- to the s-shell.

5.3 Photon Statistics in Semiconductor Quantum Dots Laser Theory

The most appealing aspect of the semiconductor quantum dot laser theory is its ability to grant access to the statistical properties of a quantum light field source in terms of the second-order correlation function. In the present section, we first review the classification of light with respect to photon statistics and proceed further to elaborate on their verification in terms of the second-order correlation function in the framework of the semiconductor quantum dot laser formalism.

5.3.1 Classification of Light

The most stable type of light that one can imagine is a perfectly *coherent light* beam which has constant angular frequency, phase and amplitude [28]. A paradigmatic example of such a light field is light emitted by an ideal single-mode laser operating well above threshold. From a mathematical point of view, coherent light is conveniently describable in terms of coherent states or *Glauber* states [103], which are an infinite superposition of *number* or *Fock states* $|n\rangle$, and which are eigenstates of the annihilation operator $\hat{b}$ of the quantum light field:

$$|\alpha\rangle = e^{-\frac{|\alpha|^2}{2}} \sum_n \frac{\alpha^n}{\sqrt{n!}} |n\rangle, \quad \text{and} \quad \hat{b}|\alpha\rangle = \alpha|\alpha\rangle. \tag{5.13}$$

For a coherent light beam, the probability distribution of the photon number can be expressed in terms of the mean photon number $\langle n\rangle$, and is given by the *Poisson distribution* [28]

$$\mathcal{P}_{\text{coh}}(n) = \frac{\langle n\rangle^n}{n!} e^{-\langle n\rangle}, \tag{5.14}$$

for which it holds $(\Delta n)^2 = \langle n\rangle$, where $(\Delta n)^2 = \langle n^2\rangle + \langle n\rangle$ is the photon number variance of the distribution.

Super-Poissonian or *thermal light* is the term used to refer to light, the distribution of which is broader than for Poissonian $\left[(\Delta n)^2 > \langle n\rangle\right]$. Its probability distribution is given by the *Bose-Einstein distribution* [28]

$$\mathcal{P}_{\text{th}}(n) = \frac{1}{\langle n\rangle + 1} \left(\frac{\langle n\rangle}{\langle n\rangle + 1} \right)^2, \tag{5.15}$$

having its largest value for $n = 0$ and decreases exponentially for increasing n.

A pure quantum state, the so-called number or Fock state $|n\rangle$ being the eigenstate of the photon number operator,

$$\hat{b}^\dagger \hat{b}|n\rangle = n|n\rangle. \tag{5.16}$$

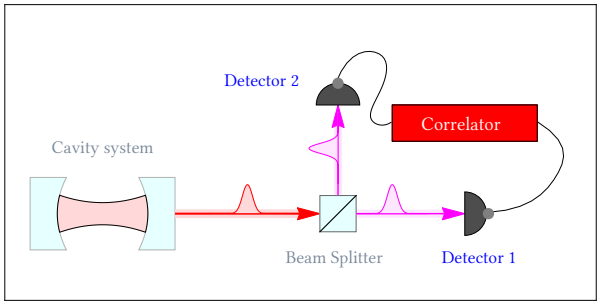

Figure 5.2 | Illustration of the Hanbury-Brown-Twiss (HBT) set up. A stream of photon is send through a 50/50 beam splitter which divided it equally between the two output ports. Photons in each output port of the BS are captured by photoelectrons, e. g avalanche photodiodes. The photocurrents of each detector are then multiplied and are integrated to yield the second-order correlation function.

is a genuine nonclassical light state. Its distribution is narrower than that of the coherent light field. A quantitative mapping out of the statistical properties of light sources is commonly achieved in terms of the second-order correlation function that will discussed in the next section.

5.3.2 Second-Order Photon Correlation Function

In the laboratory, the second-order photon correlation function allowing to characterize and verify the different states of light, is commonly measured by a *Hanbury Brown-Twiss* (HBT) setup as illustrated in Fig. 5.2. In this experimental arrangement, a stream of photons impinges on 50/50 beam splitter (BS). Photons in each output port of the BS are captured by detectors. On equipping one of the output channels with a variable delay τ, correlation of the light at different times can be monitored.

In his seminal paper [103], *Glauber* pointed out that the joint probability $P_2(t, t+\tau)\Delta t\Delta\tau$ to detect a photon both in the time interval Δt at t and in the time interval $\Delta\tau$ at $t+\tau$ is expressible in terms of normally ordered expectation values of the field amplitude,

$$G^{(2)}(t,\tau) = \langle \hat{b}^\dagger(t)\hat{b}^\dagger(t+\tau)\hat{b}(t+\tau)\hat{b}(t)\rangle. \tag{5.17}$$

For practical use, it is convenient to normalize the joint probability to the single time probabilities for photon detection $P_1(t)\Delta t$ and $P_1(t+\tau)\Delta\tau$:

$$g^{(2)}(t,\tau) = \frac{\langle \hat{b}^\dagger(t)\hat{b}^\dagger(t+\tau)\hat{b}(t+\tau)\hat{b}(t)\rangle}{\langle \hat{b}^\dagger(t)\hat{b}(t)\rangle\langle \hat{b}^\dagger(t+\tau)\hat{b}(t+\tau)\rangle}. \tag{5.18}$$

The zero-delay second-order photon correlation function $g^{(2)}(0)$ can be expressed in terms of the probability $p(n) = \langle n|\hat{\rho}|n\rangle$ of a given state to be found with a given occupancy number n:

$$g^{(2)}(0) = \frac{\sum_{n=0}^{\infty} n(n-1)p(n)}{\left[\sum_{n=0}^{\infty} np(n)\right]^2}, \tag{5.19}$$

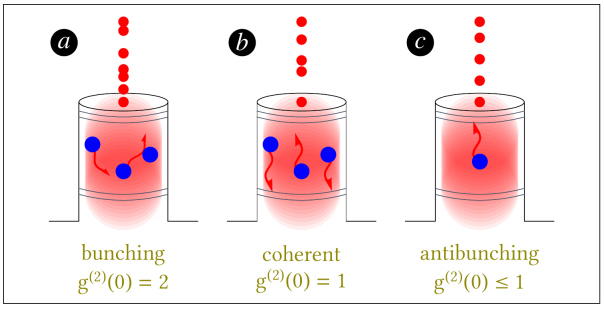

Figure 5.3 | Specification of a light source in terms of second-order correlation function. A pictorial comparison of bunched light (a), coherent light (b), and antibunched light (c). For bunched and antibunched light, the second-order correlation function takes the value of $g^{(2)}(0) = 2$, and $g^{(2)}(0) \leq 1$ respectively. A random time between the photon emission is observed in the case of coherent light source with $g^{(2)}(0) = 1$. Adapted from [104].

where $\hat{\rho}$ is the density matrix. Therefore, it captures the statistics of the state

For coherent light sources, one obtains

$$g^{(2)}(\tau = 0) = \frac{\langle\alpha|\hat{b}^\dagger\hat{b}^\dagger\hat{b}\hat{b}|\alpha\rangle}{\langle\alpha|\hat{b}^\dagger\hat{b}|\alpha\rangle^2} = 1. \tag{5.20}$$

In case of pure photon number states $|n\rangle$, the second-order correlation functions reads as

$$g^{(2)}(\tau = 0) = \frac{\langle n|\hat{b}^\dagger\hat{b}^\dagger\hat{b}\hat{b}|n\rangle}{\langle n|\hat{b}^\dagger\hat{b}|n\rangle^2} = 1 - \frac{1}{n}. \tag{5.21}$$

Here, for $n = 1$ we get $g^{(2)}(0) = 0$ for a genuine single-photon source. A nonclassical result is obtained for $n > 1$, $g^{(2)}(0) < 1$.

For thermal light, a tendency of the photons to arrive at the two detectors simultaneously is observed, as the zero-delay second-order correlation function reads as

$$g^{(2)}(0) = 1 + \frac{\langle(\hat{b}^\dagger\hat{b})^2\rangle - \langle\hat{b}^\dagger\hat{b}\rangle}{\langle\hat{b}^\dagger\hat{b}\rangle^2} = 2. \tag{5.22}$$

This phenomenon is commonly referred to as *photon bunching*, as opposed to *photon antibunching*, $g^{(2)}(0) \leq 1$. Note that for thermal and number-state field, the second order correlation function $g^{(2)}(\tau)$ tends to unity as the delay τ approaches the infinity [53]. Figure 5.3 gives a pictorial representation of the detection events of the three aforementioned cases. Note how in the case of antibunched light, Fig. 5.3 c), the emission events are well-spaced. Between two contiguous counting events, there is a time gap approximately equal to the radiative lifetime of transition of the emitter.

Extension of the Laser Equations

In order for the second-order correlation function to be incorporate into the semiconductor laser model, the set of laser equations has to be consistently extended up to the quadruplet level. By

deriving the equations, we assume that only photons stemming from the lasing mode contribute to the build up of correlations.

From the system Hamiltonian (4.24), the time derivative of the four-particle expectation value $\langle \hat{b}^\dagger \hat{b}^\dagger \hat{b}\hat{b} \rangle$ is given by

$$\hbar \frac{d}{dt} \langle \hat{b}^\dagger \hat{b}^\dagger \hat{b}\hat{b} \rangle = -4\kappa \langle \hat{b}^\dagger \hat{b}^\dagger \hat{b}\hat{b} \rangle + 4|g|^2 \mathrm{Re} \sum_\alpha \langle \hat{b}^\dagger \hat{b}^\dagger \hat{b} \hat{v}_\alpha^\dagger \hat{c}_\alpha \rangle. \tag{5.23}$$

In this equation, the index α runs over all resonant laser transitions from various quantum dots and the quantity $\langle \hat{b}^\dagger \hat{b}^\dagger \hat{b} \hat{v}_\alpha^\dagger \hat{c}_\alpha \rangle$ on its right hand side, which has been scaled as $\langle \hat{b}^\dagger \hat{b}^\dagger \hat{b} \hat{v}_\alpha^\dagger \hat{c}_\alpha \rangle \rightarrow g \langle \hat{b}^\dagger \hat{b}^\dagger \hat{b} \hat{v}_\alpha^\dagger \hat{c}_\alpha \rangle$, encode the correlation between the photon-assisted polarization and the photon number. According to the cluster expansion scheme, the correlation functions of the two expectation values, appearing in the above equation, read

$$\begin{aligned} \delta \langle \hat{b}^\dagger \hat{b}^\dagger \hat{b}\hat{b} \rangle &= \langle \hat{b}^\dagger \hat{b}^\dagger \hat{b}\hat{b} \rangle - 2 \langle \hat{b}^\dagger \hat{b} \rangle, \\ \delta \langle \hat{b}^\dagger \hat{b}^\dagger \hat{b} \hat{v}_\alpha^\dagger \hat{c}_\alpha \rangle &= \langle \hat{b}^\dagger \hat{b}^\dagger \hat{b} \hat{v}_\alpha^\dagger \hat{c}_\alpha \rangle - 2 \langle \hat{b} \hat{v}_\alpha^\dagger \hat{c}_\alpha \rangle \langle \hat{b}^\dagger \hat{b} \rangle. \end{aligned} \tag{5.24}$$

Note that the factor of two arises from the two realizations for the factorization.

On inserting Equation (5.24) into Equation (5.25) and using the time derivative of mean photon value, one obtains

$$\left(\frac{d}{dt} + 4\kappa \right) \delta \langle \hat{b}^\dagger \hat{b}^\dagger \hat{b}\hat{b} \rangle = 4|g|^2 \mathrm{Re} \sum_\alpha \delta \langle \hat{b}^\dagger \hat{b}^\dagger \hat{b} \hat{v}_\alpha^\dagger \hat{c}_\alpha \rangle. \tag{5.25}$$

The dynamics of the correlation function $\delta \langle \hat{b}^\dagger \hat{b}^\dagger \hat{b} \hat{v}_\alpha^\dagger \hat{c}_\alpha \rangle$ is given by

$$\begin{aligned} \left(\hbar \frac{d}{dt} + 3\kappa + \gamma \right) \delta \langle \hat{b}^\dagger \hat{b}^\dagger \hat{b} \hat{v}_\alpha^\dagger \hat{c}_\alpha \rangle = & -2|g|^2 \langle \hat{b}^\dagger \hat{v}_\alpha^\dagger \hat{c}_\alpha \rangle^2 + \left(f_\alpha^e + f_\alpha^h - 1 \right) \delta \langle \hat{b}^\dagger \hat{b}^\dagger \hat{b}\hat{b} \rangle \\ & + 2 f_\alpha^h \delta \langle \hat{b}^\dagger \hat{b} \hat{c}_\alpha^\dagger \hat{c}_\alpha \rangle - 2 f_\alpha^e \delta \langle \hat{b}^\dagger \hat{b} \hat{v}_\alpha^\dagger \hat{v}_\alpha \rangle \\ & + \left\{ \delta \langle \hat{b}^\dagger \hat{b} \hat{c}_\alpha^\dagger \hat{c}_\alpha \rangle - \delta \langle \hat{b}^\dagger \hat{b} \hat{v}_\alpha^\dagger \hat{v}_\alpha \rangle \right\} \langle \hat{b}^\dagger \hat{b} \rangle \\ & - 2\delta \langle \hat{b}^\dagger \hat{b} \hat{c}_\sigma^\dagger \hat{v}_\alpha^\dagger \hat{c}_\alpha \hat{v}_\sigma \rangle + \sum_\sigma \delta \langle \hat{b}^\dagger \hat{b}^\dagger \hat{v}_\sigma^\dagger \hat{v}_\alpha^\dagger \hat{c}_\alpha \hat{c}_\sigma \rangle. \end{aligned} \tag{5.26}$$

It should be note that the free evolution energy terms $\tilde{\varepsilon}_s^e + \tilde{\varepsilon}_s^h - \hbar\omega$ cancels out as only quantum dots being in resonance with fundamental cavity mode are taking int account. Furthermore, in accordance with the assumptions outlined in Sect. 5.1, we discarded the contribution of the Coulomb interaction

$$\begin{aligned} \mathrm{i}\hbar \frac{d}{dt} \delta \langle \hat{b}^\dagger \hat{b}^\dagger \hat{b} \hat{v}_\alpha^\dagger \hat{c}_\alpha \rangle \Big|_C = -2 \sum_\sigma \Big\{ & \left(1 - f_\alpha^e - f_\alpha^h \right) V_{\alpha\sigma\alpha\sigma} \delta \langle \hat{b}^\dagger \hat{b}^\dagger \hat{b} \hat{v}_\sigma^\dagger \hat{c}_\sigma \rangle \\ & - 2 \left(f_\alpha^e + f_\alpha^h \right) V_{\alpha\sigma\alpha\sigma} \delta \langle \hat{b}^\dagger \hat{b}^\dagger \hat{b} \hat{v}_\alpha^\dagger \hat{c}_\alpha \rangle \Big\} \end{aligned} \tag{5.27}$$

to Equation (5.26). The right hand side of Eq. (5.27) is reminiscent of the Hartree-Fock Coulomb terms in the Equation of motion for the photon-assisted polarization and therefore can be interpreted as renormalization of the single-particles energies and as interband exchange interaction, leading to additional renormalizations of the transitions energies as well as a redistribution of oscillator strength between different quantum dot transitions.

The dynamics of the triplet carrier-photon correlation $\delta\langle\hat{b}^\dagger\hat{b}\hat{c}_\alpha^\dagger\hat{c}_\alpha\rangle$, appearing in the right hand side of Eq. (5.26) and in the EoM of the photo-assisted polarization is given by

$$\begin{aligned}\left\{\hbar\frac{d}{dt}+2\kappa\right\}\delta\langle\hat{b}^\dagger\hat{b}\hat{c}_\alpha^\dagger\hat{c}_\alpha\rangle = -2|g|^2\mathrm{Re}\left\{\delta\langle\hat{b}^\dagger\hat{b}^\dagger\hat{b}\hat{v}_\alpha^\dagger\hat{c}_\alpha\rangle+\left(\langle\hat{b}^\dagger\hat{b}\rangle+f_\alpha^h\right)\langle\hat{b}^\dagger\hat{v}_\alpha^\dagger\hat{c}_\alpha\rangle\right\}\\ -2|g|^2\mathrm{Re}\sum_\sigma\delta\langle\hat{b}^\dagger\hat{v}_\sigma^\dagger\hat{c}_\alpha^\dagger\hat{c}_\sigma\hat{c}_\alpha\rangle\end{aligned} \tag{5.28}$$

and that of $\delta\langle\hat{b}^\dagger\hat{b}\hat{v}_\alpha^\dagger\hat{v}_\alpha\rangle$ reads as

$$\begin{aligned}\left\{\hbar\frac{d}{dt}+2\kappa\right\}\delta\langle\hat{b}^\dagger\hat{b}\hat{v}_\alpha^\dagger\hat{v}_\alpha\rangle = 2|g|^2\mathrm{Re}\left\{\delta\langle\hat{b}^\dagger\hat{b}^\dagger\hat{b}\hat{v}_\alpha^\dagger\hat{c}_\alpha\rangle+\left(\langle\hat{b}^\dagger\hat{b}\rangle+f_\alpha^e\right)\langle\hat{b}^\dagger\hat{v}_\alpha^\dagger\hat{c}_\alpha\rangle\right\}\\ +2|g|^2\mathrm{Re}\sum_\sigma\delta\langle\hat{b}\hat{c}_\sigma^\dagger\hat{v}_\alpha^\dagger\hat{v}_\sigma\hat{v}_\alpha\rangle.\end{aligned} \tag{5.29}$$

The correlation functions $\delta\langle\hat{b}\hat{c}_\sigma^\dagger\hat{v}_\alpha^\dagger\hat{v}_\sigma\hat{v}_\alpha\rangle$, $\delta\langle\hat{b}^\dagger\hat{v}_\sigma^\dagger\hat{c}_\alpha^\dagger\hat{c}_\sigma\hat{c}_\alpha\rangle$, and $\delta\langle\hat{b}^\dagger\hat{b}^\dagger\hat{v}_\sigma^\dagger\hat{v}_\alpha^\dagger\hat{c}_\alpha\hat{c}_\sigma\rangle$ describe a paradigmatic effect in cavity quantum electrodynamic, commonly known as *superradiance*. The phenomenon of superradiant coupling has been extensively investigated both theoretically [86–88] and experimentally [89, 104]. Nevertheless, in this thesis, we neglect these correlation functions in all calculations, as no indications of superradiance are seen in the experiments we intend to model with our theory. Moreover, for the sake of consistency, the correlation function $\delta\langle\hat{b}^\dagger\hat{b}\hat{c}_\sigma^\dagger\hat{v}_\alpha^\dagger\hat{c}_\alpha\hat{v}_\sigma\rangle$ will be discarded in all calculations, as it is a variation of the carrier correlation function $\delta\langle\hat{c}_\alpha^\dagger\hat{v}_\sigma^\dagger\hat{v}_\sigma\hat{c}_\alpha\rangle$, which has been omitted.

5.4 Summary

In this chapter, starting from the semiconductor luminescence equations, we have set up the formalism for dealing with semiconductor QDs micro- or nanolasers. Upon considering correlations functions up to the quadruplet level, the semiconductor laser model grants access to the second-order function which is of crucial importance when the threshold region can not be inferred from the input/output characteristics. The developed semiconductor QDs laser theory will be used in the subsequent chapters to investigate Non-Markovian delay in the formation of coherence in quantum-dot nanolasers operating in the cavity-QED regime, cf. Chap. 6, and the influence of background emitters on lasing in quantum dot micropillars, see Chap. 7.

Part

III

Nanolasers with Quantum Dot Emitters

6 Non-Markovianity of Lasing Dynamics

The ability in manufacturing semiconductor optical microcavities with dimensions down to the diffraction limit of the laser light provides a unique experimental paradigm for investigating cavity quantum electrodynamics effects. One of such nanocavities are the photonic-crystal cavities (PhC) that combine a small mode volume with a long photon storage time. Since their inception, PhC based nanolasers have witnessed a huge amount of interest because of their ultra-low lasing threshold [17, 20] , energy-efficiency, and fast signal modulation [7]. The impetus to this steadily growing interest is device applications such as optical communication, and quantum information processing. However, the small mode volume restraints the amount of gain material that can be brought into spatial overlap with the lasing mode. The reduction in the gain material is compensated by the Purcell effect [1, 7] that enhances the spontaneous emission and pushes the concept of lasing into a cavity-QED regime governed by photonic and electronic correlation, and fluctuations effects [20, 102, 104–107]

Mapping out the impact of correlations on lasing is mostly achieved in time-resolved experiment. In a recent time-resolved emission dynamics of InAsP/InP QDs PhC nanolaser, wherein a complete two-time map of the second-order photon correlation function is amenable, *Dr. Galan Moody* at the *National Institute of Standards and Technology, Colorado, USA* and our group [1] observed that coherent emission is not fully reached at the maximum intensity of the emitted pulse. Instead, it is delayed by up to 250 ps so that the emission entails a large thermal component above the lasing threshold, a result that is at odds with the previously reported experiment in Ref. [108] and questions the traditional lasing picture in which coherent emission is intimately linked with the presence of stimulated emission.

The aim of this chapter is to provide a sound explanation and understanding for this oddity observed in the lasing dynamics of the investigated device. To this end, a sophisticated theoretical basis is the semiconductor QDs laser theory, that has been introduced in Chapter 5. Nevertheless, being a single time model, it only allows for calculating single-time dynamical quantities. To bypass this obstacle, the theory has been upgraded with the *quantum regression theorem* [74, 109], which grants access to multitime expectation value dynamics, and therefore allows for calculating the two-time second-order photon correlation function.

[1] Dr. Galan Moody performed the experiment, I did the theoretical calculations

6.1 Nanolaser Characteristics

In this section, the characterization and the properties of the sample used in the two-photon correlation spectroscopy (TPCS) are presented. Moreover, the experimental realization and results including the input-output characteristics and the two-time second-order photon correlation dynamics are reviewed.

6.1.1 Sample Properties

Metal organic vapor phase epitaxy (MOVPE) is the technology used to grow the nanolaser gain medium consisting of a single layer of InAsP quantum dots nucleated at the center of a 320 nm thick InP buffer layer deposited on an exactly (001)-oriented InP substrate [110, 111]. It is instructive to mention that MOVPE, in contrast to the other growth techniques, such as molecular beam epitaxy, suppresses the spontaneous formation of strongly elongated nanostructures (quantum wires or quantum dashes) [112, 113]. The obtained QD density is on the order of $10^{10}\,\mathrm{cm}^{-2}$. A hexagonal PhC structure with a lattice constant of $a_m = 410\,\mathrm{nm}$ and an air-hole radius of $r = 0.293\,a_m$ has been fabricated by resorting to electron-beam lithography, a plasma-etching process to form the PhC, and wet etching to suspend the InP membrane. By leaving out three holes, the so-called $L3$-type defect cavity, a high-Q nanocavity with an effective mode volume of $1.3(\lambda/n)^3$ containing a few tens of QDs, is obtained. To further enhance the cavity quality factor Q, the position of the two holes forming the end mirrors of the cavity have been shifted outward by $0.18a_m$. Photoluminescence measurements, see Fig. 6.1 a) yield a cavity linewidth of $\gamma_c = 0.03\,\mathrm{nm}$, corresponding to a quality factor of $Q = 50000$, which defines the resolution limit of the spectrometer. The QD spontaneous-emission lifetime measured in an unpatterned region of the device under investigation amounts to $\tau_Q = 1.4\,\mathrm{ns}$ between 5 K and 100 K [114]. Within the PhC nanocavity, the interplay of the low cavity mode volume and high-Q factor leads to a significant Purcell enhancement of around five at 300 K.

6.1.2 Hypothesis of Temperature Tuning of the Emitter Number

An appealing aspect of the device under study is the ability to control its emission and photon correlation statistics by using the temperature as the turnstile to select the number of QDs that couple to the cavity mode. In Figure 6.1 a), from 5K to 300K, a shift of the center of the QD spontaneous emission from 1540 to 1580nm can be observed. This is accompanied by a broadening of the line width from $\sim$ 20nm to $\sim$ 100 nm. At low temperature, the large inhomogeneous line width of the QDs spectra is mainly caused by height dispersion of the dots [111]. The center of the inhomogeneous ensemble is strongly detuned from the cavity and only a few resonant emitters feed into the cavity mode. At room temperature, a strong overlap of the emitter ensemble

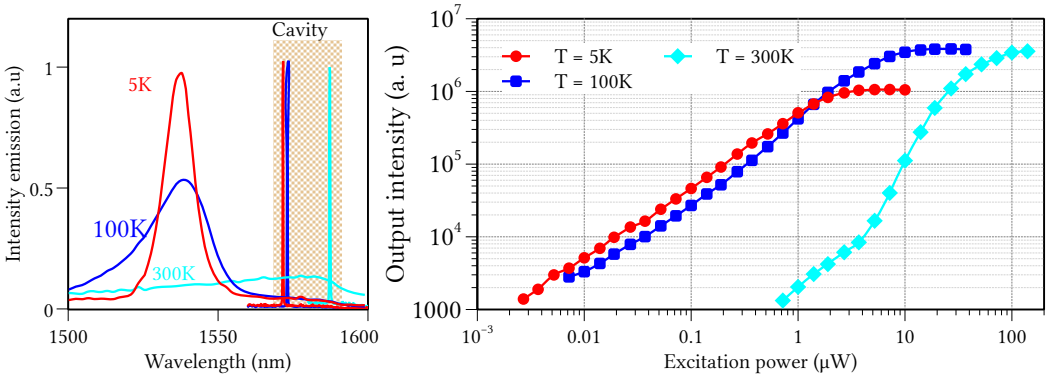

Figure 6.1 | Emission intensity of the cavity and the QDs for three different temperatures. a) Temperature dependence of the InAsP/InP QD spontaneous emission and cavity mode emission. The measured cavity linewidth at all temperature are limited by the spectrometer resolution, placing a lower bound on the cavity quality factor $Q > 50000$. b) Nanolaser output intensity versus input optical power for non-resonant pulsed excitation at three different temperatures 5K, 100K, and 300K.

with the lasing mode is observed.

6.1.3 Experimental Results

Input-Output Characteristics

To measure the input-output characteristics, the device is held in vacuum in a closed-cycle cryostat with a variable temperature from 4 K to 300 K. A Ti:sapphire laser emitting 1 ps pulses centered at 805nm at an 82MHz repetition rate has been used for the optical excitation. A 0.5 numerical-aperture objective is used to focus and collect infrared light from the device. To get rid of spurious light, the emitted light is spectrally filtered with 2nm bandwidth centered at the cavity resonance, and then dispatched into a single mode optical fiber. Figure 6.1 b) displays the input-output device characteristics for different temperatures, with the horizontal axis corresponding to the excitation pulse area and the vertical axis to the integrated emission intensity. Interestingly, there is a correlation between the shape of the input-output intensity and temperature. At room temperature, 300K, the typical *S*-shaped curve is indicative of a clear transition from primarily spontaneous emission (LED operation) to lasing, separated by a threshold region covering nearly one order of magnitude in excitation power. Such smeared-out threshold behavior is characteristic of cavity-enhanced high β-factor devices, wherein a large fraction of the spontaneous emission is funneled into the lasing mode [18]. Nevertheless, the integrated output intensity saturates at highest excitation powers suggesting that the nanolaser is fed by a limited number of saturable emitters. By lowering the temperature, the attainable gain is reduced by QDs being tuned out of resonance with the laser mode. At 100K, a saturation of the emis-

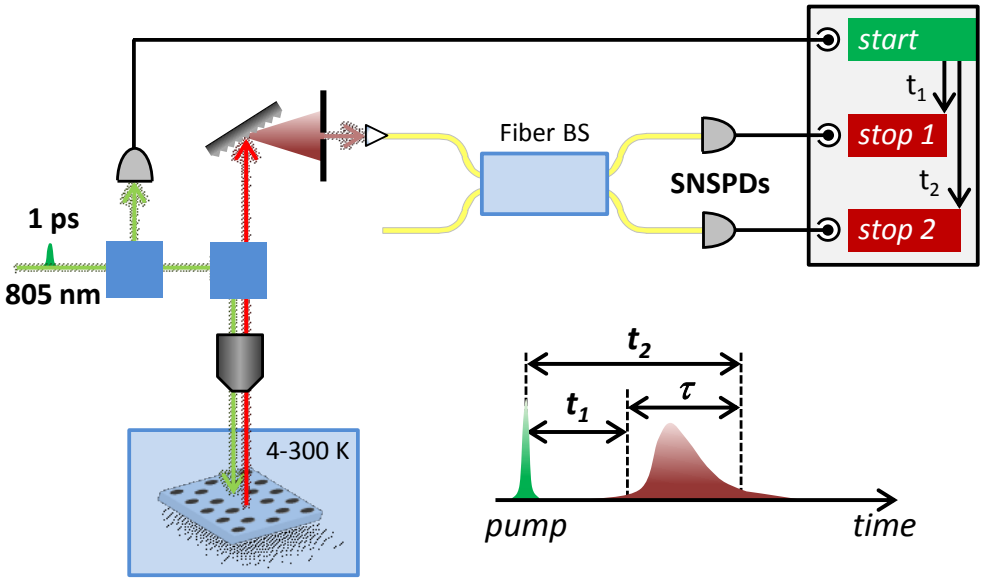

Figure 6.2 | Cartoon of the Hanbury Brown and Twiss setup. Illustration of the Hanbury Brown and Twiss setup with fiber-coupled superconducting nanowire single photon detectors (SNSPDS) for recording the dynamics of the second-order photon correlation function $g^{(2)}(t_1, t_2)$.

sion intensity already occurs at the point of the threshold and the data of 5K is thresholdless. Here, gain saturates completely before a sufficient number of intra-cavity photons are present to initiate lasing.

Photon Correlation Dynamics

A modified Hanbury Brown Twiss (HBT) interferometer has been used to record the full two-time photon correlation function. This approach is reminiscent of a previous study examining single-photon purity from a single QD [115]. In this experimental setup, see Fig. 6.2, the light emitted by the device is spectrally filtered, split using a fiber-based 50/50 beam splitter (BS), and then measured with WSi superconducting nanowire single-photon detectors (SNSPDs) with a timing jitter of $\approx$ 75 ps full-width at half-maximum. Photon arrival times t_1 and t_2 at the two SNSPDs are recorded relative to the Ti:sapphire excitation pulse. The time-tagged data are post-processed to construct dual start-stop correlation histograms that provide a complete mapping in t_1 and t_2 of the second-order photon correlation function,

$$g^{(2)}_{\mathrm{HBT}}(t_1, t_2) = \frac{\langle \hat{b}^\dagger(t_1)\hat{b}^\dagger(t_2)\hat{b}(t_2)\hat{b}(t_1)\rangle}{\langle \hat{b}^\dagger(t_1)\hat{b}(t_1)\rangle \langle \hat{b}^\dagger(t_2)\hat{b}(t_2)\rangle}, \quad t_2 \geq t_1. \tag{6.1}$$

Its numerator encodes the joint probability of detecting two photons at times t_1 and t_2, while the denominator describes the probability of detecting two uncorrelated photons at t_1 and t_2. It is instructive to mention that because the excitation source is pulsed, the temporal dynamics of

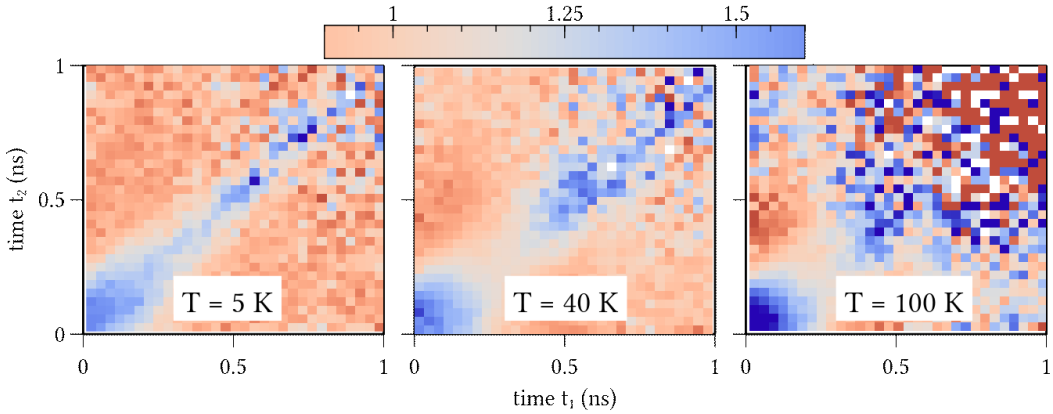

Figure 6.3 | Gallery of the two-time second-order photon correlation function. The measured two-time second-order photon correlation function at three different temperatures: T = 5 K, 40 K, and 100 K.

the $g^{(2)}(t_1, t_2)$ do not reduce to a simple single-time dependence on $\tau = t_2 - t_1$, as they would be for stationary excitation source [116]. The experimental data for different temperatures are displayed in Fig. 6.3. As an example, at 100K: If one photon is detected at t_1 = 0.1 ns, then the likelihood of a second photon being detected at t_2 = 0.1 ns (0.5 ns) is higher (lower) than it would be for a coherent state with the same temporal intensity profile. More interesting are the data for the equal-time second-order photon correlation function $g^{(2)}(t_1, \tau = 0)$, which corresponds to slices along the diagonal of the two-time map $g^{(2)}(t_1, t_2)$ for $\tau = 0$, and allows for monitoring the build up and the break down of the second-order coherence during the entire excitation pulse. It takes the value of 2 in the spontaneous emission regime and reaches 1 in the regime of coherent emission. The data are graphed together with the emission intensity for two different temperatures in Fig. 6.4. A closer examination of the data reveals a significant temporal delay δt between the maximum of the emission peak and the formation of coherent emission expressed by the minimum in the autocorrelation function $g^{(2)}(t_1, 0)$. The delay δt increases from $\sim$ 150 ps to $\sim$ 300 ps with temperature, leading to the high-intensity portion of the pulse being largely thermal despite the system operating in the regime of stimulated emission. These dynamics are in marked contrast to a previous study of a QD micropillar laser with $Q \approx 5000$ in which the onset of coherent emission coincides with the onset of stimulated emission at the pulse intensity maximum [108].

From these observations, the question which immediately arises is: *What is the origin of the observed delay?* It is the objective of this chapter to provide unequivocal answers to this question.

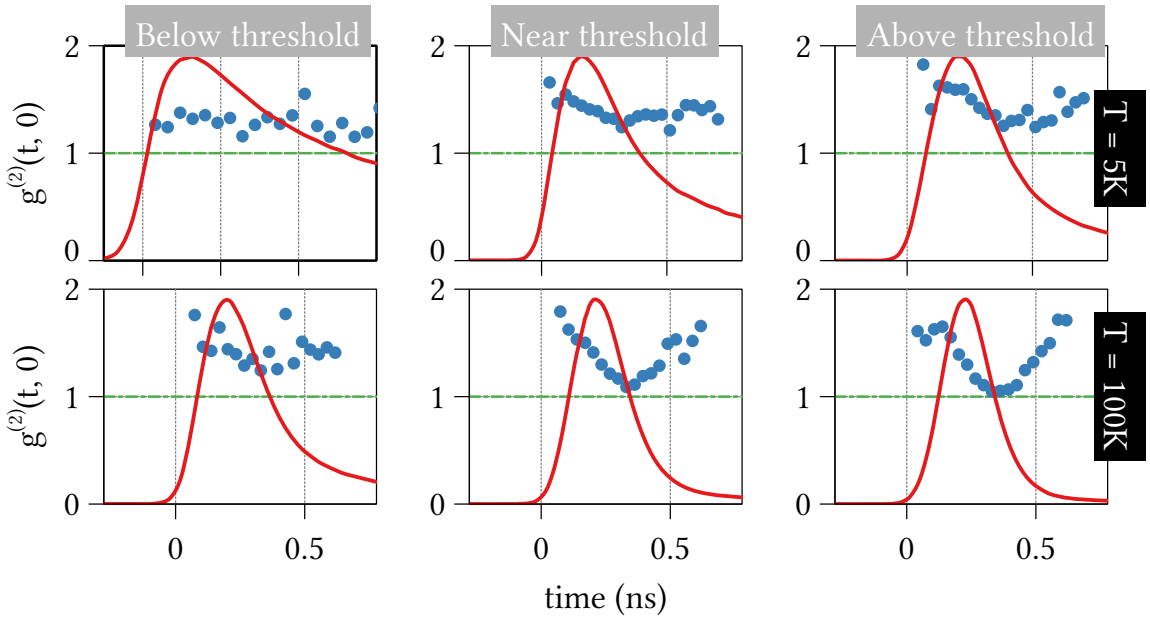

Figure 6.4 | Time-resolved zero-delay second-order photon autocorrelation function. In the LED regime at 5K $g^{(2)}(t_1, t_1) > 1$ as expected for incoherent thermal radiation. These dynamics are in marked contrast to 100 K for which the equal-time correlation function reaches unity during the emission.

6.2 Theoretical Model

In Chap. 3, we have derived the quantum Markovian master equation for the reduced density operator of any quantum system coupling to its surrounding. In the subsequent chapters, we make use of that formalism to derive the semiconductor laser equations, through which the dynamics of single-time quantities, such as the intracavity photon, and the second-order correlation function, can be obtained. The purpose of this section is to elaborate on a formalism combining the semiconductor laser theory, see Chap. 5 with the concept of quantum regression theorem (QRT) [74, 109] to calculate the two-time second-order photon correlation function. To that end, after discussing the multime averages, we then outline the formalism of the QRT. We proceed further to discuss how the semiconductor QDs laser theory can be upgraded with the QRT.

6.2.1 Multitime Averages

To formulate the multitime mean value, let us consider, for the sake of simplicity, two operators $\hat{F}$ and $\hat{G}$ of a given open quantum system. Then, the two-time correlation function is expressible as [74]

$$\langle \hat{F}(t+\tau)\hat{G}(t)\rangle = \mathrm{Tr}_s\mathrm{Tr}_e\left\{\hat{F}(t+\tau)\hat{G}(t)\hat{\rho}_s\otimes\hat{\rho}_e\right\}, \quad \tau > 0 \tag{6.2}$$

where $\hat{\rho}_s$ and $\hat{\rho}_e$ denote the density operator of the open quantum system and its surrounding, respectively. In the Heisenberg picture, the time dependence of the system operators are generated by the combined Hamiltonian H, see Eq. (3.17):

$$\begin{aligned} \hat{F}(t+\tau) &= \hat{U}^\dagger(t+\tau)\hat{F}\hat{U}(t+\tau), \\ \hat{G}(t) &= \hat{U}^\dagger(t)\hat{G}\hat{U}^\dagger(t) \end{aligned} \tag{6.3}$$

with $\hat{U}(t) = e^{-\mathrm{i}\hat{H}t}$. By inserting the above relationships into Eq. (6.2) and availing ourselves of the cyclic property of the trace operation, Eq. (6.2) can be rewritten as

$$\langle \hat{F}(t+\tau)\hat{G}(t)\rangle = \mathrm{Tr}_s\left\{\hat{F}\,\mathrm{Tr}_e\hat{Z}(\tau,t)\right\} \tag{6.4}$$

where the operator $\hat{Z}(\tau,t)$ has been introduced,

$$\hat{Z}(\tau,t) = \hat{U}^\dagger(\tau)\hat{G}\hat{\rho}_{\mathrm{tot}}(t)\hat{U}(\tau), \quad \text{with} \quad \hat{\rho}_{\mathrm{tot}}(t) = \hat{U}(t)\hat{\rho}_s \otimes \hat{\rho}_e\hat{U}^\dagger(t). \tag{6.5}$$

It is straightforward to see that the equation of motion for $\hat{Z}(\tau,t)$ in terms of τ reads as

$$\frac{\partial}{\partial\tau}\hat{Z}(\tau,t) = -\mathrm{i}[\hat{H},\hat{Z}(\tau,t)], \tag{6.6}$$

which is reminiscent of the von Neumann equation of motion for the density operator. This suggests that the equation of motion for $\mathrm{Tr}_e[\hat{Z}(\tau,t)]$ will be the same master equation for the reduced density operator that has been derived in Chap. 3, when assuming the Markovianity of the dynamics, Eq. (6.6) and the factorization of the total density operator at any time t as $\hat{\rho}_{\mathrm{tot}}(t) = \hat{\rho}_s(t)\otimes\hat{\rho}_e$. In other words, the dynamics of the auxiliary operator $\mathrm{Tr}_e[\hat{Z}(\tau,t)]$ can be described in terms of the evolution map $V(t,s)$ introduced in Chapter 3,

$$\mathrm{Tr}_e[\hat{Z}(\tau,t)] = V(t+\tau,t)\mathrm{Tr}_e[\hat{Z}(0,t)] = V(t+\tau,t)\hat{G}\hat{\rho}_s(t). \tag{6.7}$$

By inserting this expression into Equation (6.4), the two-time correlation function can therefore be written as an expectation value of $\hat{F}$ in respect of a modified initial reduced density operator $\hat{p}(t) = \hat{G}\hat{\rho}_s(t)$:

$$\langle \hat{F}(t+\tau)\hat{G}(t)\rangle = \mathrm{Tr}_s\left\{\hat{F}V(t+\tau,t)\hat{p}(t)\right\}. \tag{6.8}$$

It is instructive to note this formalism can straightforwardly be extend to obtain general time ordered correlation function of the form [74]

$$\langle \hat{F}_0(s_0)\hat{F}_1(s_1)\ldots\hat{F}_m(s_m)\hat{G}_n(t_n)\hat{G}_{n-1}(t_{n-1})\ldots\hat{G}_0(t_0)\rangle \tag{6.9}$$

which can be contemplated in quantum measurements. Here the terms are ordered as

$$t_n \geq t_{n-1} \geq \ldots t_0, \quad s_m \geq s_{m-1} \geq \ldots s_0. \tag{6.10}$$

We close this section by pointing out that the modified density operator $\hat{p}(t)$ is not required to be a faithful density operator i.e. hermitian, and positive definite.

6.2.2 Quantum Regression Theorem

As already mentioned in Sect. 4.2.1, the expectation value approach requires to compute the dynamics of the reduced density operator, and is limited to small size systems. For practical applications involving many-particle systems, the derivation of the equations of motion for the relevant set of observables is the convenient avenue. The time derivative in respect to τ of the two point correlation function $\langle \hat{F}(t+\tau)\hat{G}(t)\rangle$ is referred to as the quantum regression theorem and was firstly derived by M. Lax [109].

More formally, let us consider a set of operators $\hat{F}_\alpha$ for which the single-time expectation value equation, Eq. (4.26), cf. Sect. 4.2.1, can be written as [74]

$$\frac{d}{dt}\langle \hat{F}_\alpha(t)\rangle = \sum_\sigma f_{\alpha\sigma}(t)\langle \hat{F}_\sigma(t)\rangle, \tag{6.11}$$

where $f_{\alpha\sigma}(t)$ are some numerical coefficients. It should be noted that Eq. (4.26) is in general not a closed equation as already seen in the previous chapters. In the previous section, it has been demonstrated that two point correlation functions $\langle \hat{F}_\alpha(t+\tau)\hat{F}_\sigma(t)\rangle$ can be interpreted as single-time expectation values with respect to a modified initial density operator $\hat{p}_\sigma(t) = \hat{F}_\sigma\hat{\rho}(t)$. Because the assumptions leading to this interpretation are the same the hypothesis underlying the derivation of Eq. (6.11) it is legitimate to say that $\langle \hat{F}_\alpha(t+\tau)\hat{F}_\sigma(t)\rangle$ is solution of the expectation value equation, Eq. (6.11) with the modified system density operator $\hat{p}(t)$:

$$\frac{d}{d\tau}\langle \hat{F}_\alpha(t+\tau)\hat{F}_\sigma(t)\rangle = \sum_\lambda f_{\alpha\lambda}(t+\tau)\langle \hat{F}_\lambda(t+\tau)\hat{F}_\sigma(t)\rangle, \quad \tau > 0. \tag{6.12}$$

This is the celebrated quantum regression theorem, the initial condition of which is given by $\langle \hat{F}_\alpha(t+\tau)\hat{F}_\sigma(t)\rangle_{\tau=0} = \langle \hat{F}_\alpha(t)\hat{F}_\sigma(t)\rangle$ which follows from the single time dynamics, Eq. (6.11). It can be straightforwardly generalized as [74]

$$\frac{d}{d\tau}\langle \hat{F}_\alpha(t)\hat{F}_\alpha(t+\tau)\hat{F}_\sigma(t)\rangle = \sum_\lambda f_{\alpha\lambda}(t+\tau)\langle \hat{F}_\alpha(t)\hat{F}_\lambda(t+\tau)\hat{F}_\sigma(t)\rangle, \quad \tau > 0. \tag{6.13}$$

6.2.3 Two-time Photon Correlation Dynamics

Let us now proceed further by applying the quantum regression theorem to compute the two-time photon correlation function under pulsed excitation in the framework of the semiconductor laser model. It is instructive to mention that for continuous wave excitation, the delay-time dependent $g^{(2)}(\tau = t_2 - t_1)$ has been calculated in [116] by adapting the quantum regression theorem to the non-linear coupled laser equations. In this thesis at hand, however, the technique is applied to a pulsed excitation scheme, which requires the calculation of the full two-time quantity.

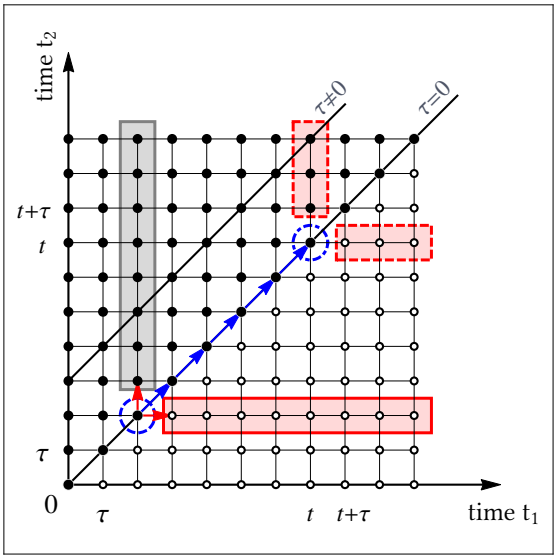

Figure 6.5 | Schematic representation of the calculation of the two-time photon correlation function A cartoon of the computation of the two-time photon correlation function $g^{(2)}(t_1, t_2)$. The blue dashed circles correspond to the values of the equal-time second-order photon correlation function $g^{(2)}(t_1, t_1)$. The gray rectangle represents the calculation of $g^{(2)}(t_1, \tau = t_2 - t_1)$, while the red rectangle results from the symmetry consideration.

The main goal in having recourse to the quantum regression theorem consists in mapping the two-time calculation of $g^{(2)}(t_1, t_2)$ onto a series of single-time calculations that are performed successively. To that end, at each time t_1 a modified density operator has to be introduced as

$$\hat{p}(t_1) = \frac{\hat{b}(t_1)\hat{\rho}\hat{b}^\dagger(t_1)}{\langle \hat{b}^\dagger(t_1)\hat{b}(t_1)\rangle}. \tag{6.14}$$

It is straightforward to see that $\mathrm{Tr}\{\hat{p}(t_1)\} = 1$. Even though this modified density operator is not a genuine density operator as it is not *Hermitian*, $\hat{p}(t_1) \neq \hat{p}^\dagger(t_1)$, it will be used to determine the initial conditions of all expectation values in the semiconductor laser model for the time evolution with respect to the second time argument t_2. Expectation values with respect to $\hat{p}(t_1)$ are written as $\langle\langle \cdots \rangle\rangle$.

Interestingly, the above mathematical prescription leading to the modified density operator changes the order of expectation values that are calculated with respect to $\hat{p}(t_1)$ due to the multiplication with two photon operators in the numerator. For example, the mean value of four photon operators $\langle \hat{b}^\dagger(t_1)\hat{b}^\dagger(t_2)\hat{b}(t_2)\hat{b}(t_1)\rangle$, and the carrier-photon correlator $\langle \hat{b}^\dagger(t_1)\hat{b}(t)\hat{c}^\dagger(t_1)\hat{c}(t_1)\rangle$ become respectively the mean photon number and the carrier population with the modified density operator:

$$\langle\langle \hat{b}^\dagger(t_2)\hat{b}(t_2)\rangle\rangle = \frac{\langle \hat{b}^\dagger(t_1)\hat{b}^\dagger(t_2)\hat{b}(t_2)\hat{b}(t_1)\rangle}{\langle \hat{b}^\dagger(t_1)\hat{b}(t_1)\rangle}, \tag{6.15a}$$

$$\langle\langle \hat{c}^\dagger(t_2)\hat{c}(t_2)\rangle\rangle = \frac{\langle \hat{b}^\dagger(t_1)\hat{b}(t)\hat{c}^\dagger(t_1)\hat{c}(t_1)\rangle}{\langle \hat{b}^\dagger(t_1)\hat{b}(t_1)\rangle}. \tag{6.15b}$$

Within the cluster expansion scheme, both the t_1-time and t_2-time evolutions must be performed at the same level of approximation. While the t_1-time evolution includes expectation values up to

the quadruplet level, the t_2-time evolution must be restricted to the doublet level. Consequently, the second-order correlation function may be rewritten as

$$g^{(2)}_{\mathrm{HBT}}(t_1, t_2) = \frac{\langle\langle \hat{b}^\dagger(t_2)\hat{b}(t_2)\rangle\rangle}{\langle \hat{b}^\dagger(t_2)\hat{b}(t_2)\rangle_{\mathrm{D}}}, \tag{6.16}$$

leading to the following initial condition for the t_2-dynamics

$$\begin{aligned}\langle\langle \hat{b}^\dagger(t_2)\hat{b}(t_2)\rangle\rangle\Big|_{t_2=t_1} &= g^{(2)}(t_1, t_1)\langle \hat{b}^\dagger(t_1)\hat{b}(t_1)\rangle_{\mathrm{D}} \\ &= \frac{\langle \hat{b}^\dagger(t_1)\hat{b}^\dagger(t_1)\hat{b}(t_1)\hat{b}(t_1)\rangle.\langle \hat{b}^\dagger(t_1)\hat{b}(t_1)\rangle_{\mathrm{D}}}{\langle \hat{b}^\dagger(t_1)\hat{b}(t_1)\rangle^2_{\mathrm{Q}}}.\end{aligned} \tag{6.17}$$

The subscripts D and Q stand for the doublet and quadruplet respectively.

To perform the numerical simulation of the two time photon correlation function we proceed as follows. At time $t = 0$, we take the observables vector

$$\boldsymbol{u} = \left(\langle \hat{b}^\dagger\hat{b}\rangle, \langle \hat{b}^\dagger\hat{v}^\dagger\hat{c}\rangle, f_s^e, f_s^h, \langle \hat{b}^\dagger\hat{b}^\dagger\hat{b}\hat{b}\rangle, \langle \hat{b}^\dagger\hat{b}^\dagger\hat{b}\hat{v}^\dagger\hat{c}\rangle, \langle \hat{b}^\dagger\hat{b}\hat{c}^\dagger\hat{c}\rangle, \langle \hat{b}^\dagger\hat{b}\hat{v}^\dagger\hat{v}\rangle\right) \equiv 0 \tag{6.18}$$

and propagate it with the stripped-down semiconductor laser equation. At time $t = t_1$ the time evolution is interrupted by a removal of a photon from the system. The value of $\boldsymbol{u}(t_1)$ is saved and subsequently used to defined the initial condition

$$\tilde{\boldsymbol{u}}(t_1, \tau = 0) = \left(\langle\langle \hat{b}^\dagger\hat{b}\rangle\rangle, \langle\langle \hat{b}^\dagger\hat{v}^\dagger\hat{c}\rangle\rangle, \langle\langle \hat{c}^\dagger\hat{c}\rangle\rangle, \langle\langle \hat{v}^\dagger\hat{v}\rangle\rangle\right) \neq 0 \tag{6.19}$$

according to Eqs. (6.15a)-(6.15b), for the τ-dynamics at doublet level. Figure 6.5 displays the procedure. The point in the blue dashed circle correspond to the values of $\boldsymbol{u}(t_1)$, whereas the points in the gray rectangle represent the values of $\tilde{\boldsymbol{u}}(t_1, \tau)$. The points in the red rectangle are obtained by using the symmetry properties of the two time photon correlation function.

6.3 Numerical Simulations

6.3.1 Parameters Acquisition

In order to make qualitative and quantitative comparisons between experimental and theory, some parameters involved in the semiconductor laser model have to be calibrated. The commonly used strategy for determining these parameters is to match the measured input-output to the theoretical one.

To accommodate the hypothesis of the temperature tuning of the optical gain in the stripped-down semiconductor laser model, the involved emitting dipole number is changed from 240(300 K) to 10(5 K). The β-factor is used to quantify the jump in the emission intensity at the threshold.

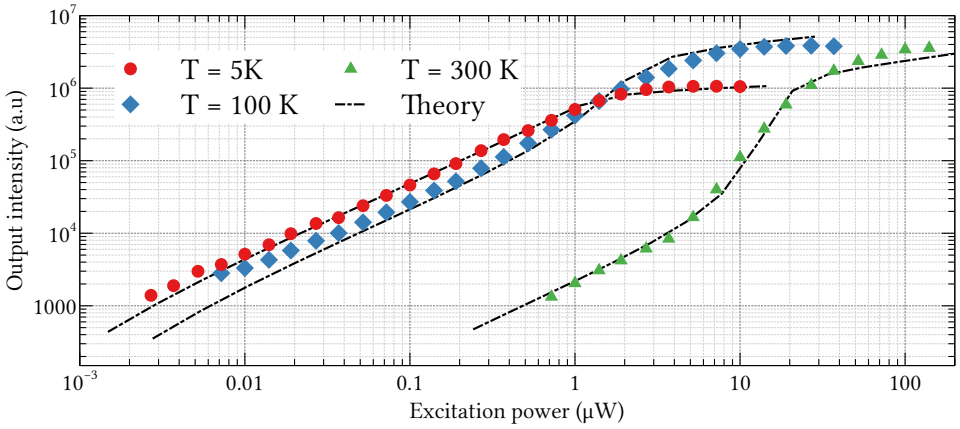

Figure 6.6 | Theoretical reproduction of the experimental input-output curves. Input-output curves for three different temperatures: $T = 5\text{K}, 100\text{K}$, and 300K. The dashed black lines are the numerical calculations based on the stripped-down semiconductor QD laser model, see Chap. 5.

At first glance, it might be tempting to use different values for the parameter β at different temperatures, in other words, making the β-factor temperature dependent. Still, the reduction of jump observed when lowering the temperature from 300 K to 100 K is due to the onset of the saturation before the threshold is fully developed [117]. Being determined by the ratio of the spontaneous emission channels, the β factor is not expected to change much with the temperature. For the simulation, a β factor of 0.04 corresponding to $\sqrt{\beta^{-1}} \approx 5$ photons in the cavity at the lasing threshold, has been used. A large β factor for nanolasers is in contrast to macroscopic ($\beta \lesssim 10^{-4}$) and mesoscale ($10^{-4} \lesssim \beta \lesssim 10^{-2}$) lasers with significantly more gain material and cavity photons at threshold [118]. Consequently, in nanolasers the emission and photon statistics are particularly sensitive to large relative fluctuations in the photon number, which scale as $\approx \beta^{1/4}$ and can be as large as 40% for our device [95]. In QD nanolasers with high β factors similar to that presented here, large fluctuations in the photon number are responsible for strong intensity and timing fluctuations that are correlated, leading to a departure from coherent and Poissonian statistics in the emission dynamics.

The experiment is well described by a quality factor of $Q = 140000$. The light-matter strength is assumed to be the same for all temperatures and amounts to $g = 5.5\,\mu\text{eV}$. As it can be seen in Fig. 6.6, an overall excellent agreement is achieved by using a dephasing rate of $\gamma = 0.5\,\text{meV}$ (only at 300 K, $\gamma = 0.7\text{meV}$). The spontaneous emission time is obtained by using the expression, cf Chap. 5

$$\tau_{\text{sp}} = \frac{(\kappa + \gamma)\,\beta}{2|g|^2} \tag{6.20}$$

and amounts to $\tau_{sp} = 305\,\text{ps}$ at 300 K, implying a Purcell factor of around five.

Before closing this section, we note that the Gaussian excitation pulse used in experiment is

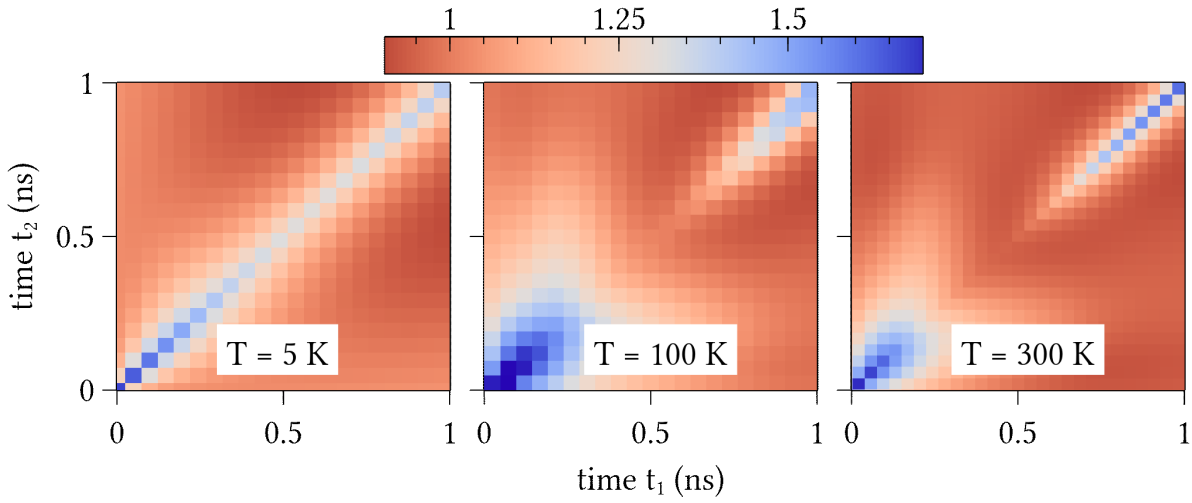

Figure 6.7 | Theoretical calculation of the two-time second-order correlation function. Numerical calculations of the two-time second-order photon correlation function under pulsed excitation for three different temperatures: T = 5K, 100K and 300K.

modeled by a time-dependent carrier-generation $P(t)$ being expressible as

$$P(t) = \frac{P_{\text{area}}}{\sqrt{2\pi}\sigma} \exp\left[-\frac{(t-t_0)^2}{2\sigma^2}\right]. \tag{6.21}$$

Here, P_{area} is the area of the excitation pulse and σ is a parameter being related to the full width at half maximum via FWHM = $2\sqrt{2\ln 10}\sigma$.

6.3.2 Photon Correlation Dynamics

Having calibrated the semiconductor laser model and equipped ourselves with the quantum regression theorem, we are now ready to simulate the full two-time photon correlation dynamics, Eq. (6.1), by availing ourselves of the procedure elaborated in section 6.2.3. To this end, for the device operating at 5 K and 100 K, we pick three values of the excitation area. In case of 100 K, these values correspond to below, at, and above the threshold. In Figure 6.7, the results of $g^{(2)}(t_1, t_2)$ for the highest excitation area are graphed. Slices along the diagonal for $\tau = 0$ are displayed together with the emission intensity for the LED, and lasing operational regimes of the device under consideration. Interestingly, the theory reproduces qualitatively the feature observed in the experiment. At 5 K , $g^{(2)}(t_1, t_1) > 1$ throughout the entire pulse and does not change significantly with excitation power, as is expected for a thermal light source. In contrast, at 100 K sufficient gain leads to the development of a threshold region in the input-output curve, cf. Fig. 6.8. This is well reflected by the autocorrelation calculation. Below threshold, $g^{(2)}(t_1, t_1) > 1$ at all times, whereas a value of one is reached during the emission pulse at higher

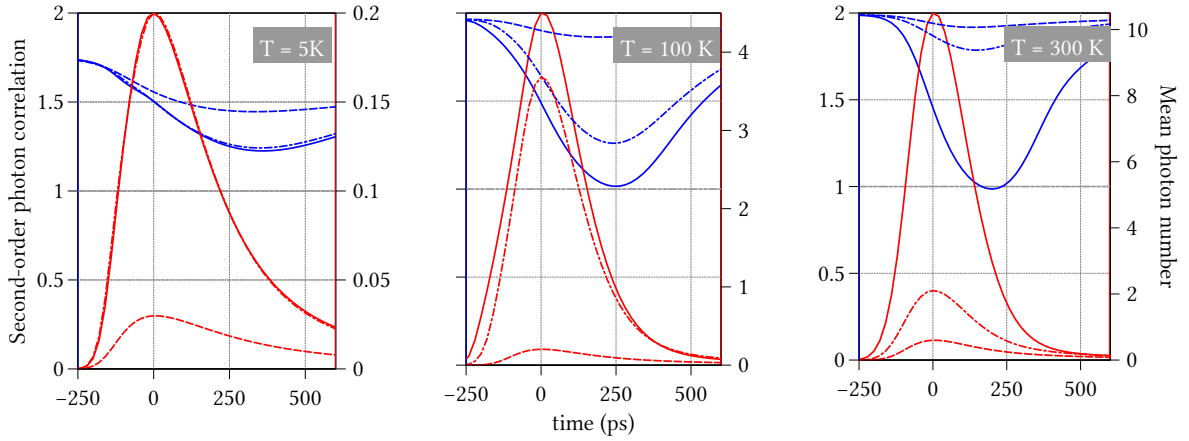

Figure 6.8 | Theoretical calculation of the equal-time second-order correlation function Numerical calculations of the equal-time second-order photon correlation function under pulsed excitation for three different temperatures: T = 5K, 100K and 300K.

excitation area confirming that the carrier density is high enough to drive coherent emission. It is noteworthy that under pulsed excitation, the emission pulse of a nanolaser undergoes various stages: After carriers have been created by the excitation pulse, the confined QD states that feed the laser transition are filled by carrier scattering on a timescale of the carrier relaxation time $\tau_r \approx 500\,\text{fs}$. Already during the relaxation process, spontaneous thermal emission begins as soon as carriers populate the lasing levels (rising edge of the emission pulse).

6.3.3 Adiabatic Elimination

Given the accuracy yielded by the coupled equations of motion of the microscopic laser model in simulating the observed delay in the build-up of the coherence, the theory can be instrumental in gaining more insights into the process at the bottom of the delayed coherence.

From the semiconductor QD laser theory, it is apparent that the photon production does not adiabatically follow its source, namely the spontaneous and stimulated emission, but is determined by the so-called the phtoton-assisted polarization having its own time evolution equation which reads

$$\frac{d}{dt}\langle \hat{b}^\dagger \hat{v}_s^\dagger \hat{c}_s \rangle = -(\kappa + \gamma)\langle \hat{b}^\dagger \hat{v}_s^\dagger \hat{c}_s \rangle + \left(1 - f_s^e - f_s^h\right)\langle \hat{b}^\dagger \hat{b} \rangle + \delta\langle \hat{b}^\dagger \hat{b} \hat{c}_s^\dagger \hat{v}_s \rangle - \delta\langle \hat{b}^\dagger \hat{b} \hat{c}_s^\dagger \hat{v}_s \rangle. \tag{6.22}$$

A similar relationship exists between the higher-order photon-correlation function $\delta\langle \hat{b}^\dagger \hat{b}^\dagger \hat{b} \hat{b} \rangle$ used to compute the equal-time second-order correlation function $g^{(2)}(t_1, t_1)$ and the higher-order photon-assisted polarization $\delta\langle \hat{b}^\dagger \hat{b}^\dagger \hat{b} \hat{v}_s^\dagger \hat{c}_s \rangle$ that describes interband recombination and the emission of a photon in the presence of an additional photon. The dynamics of this process is

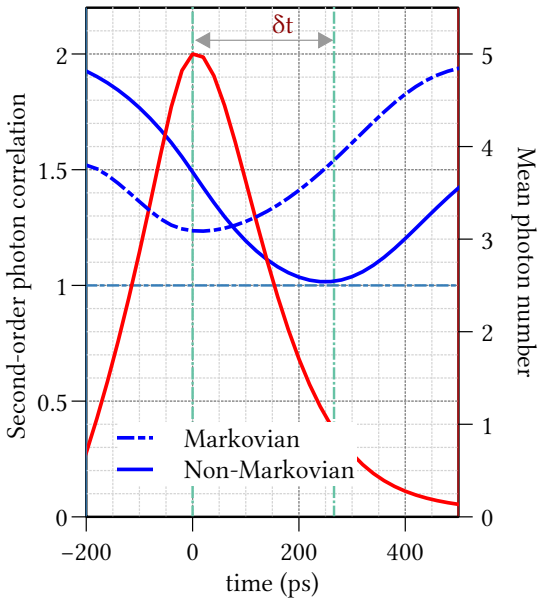

Figure 6.9 | Comparison of the Markovian and non-Markovian equal-time second-order correlation function. Comparison of the correlation dynamics from the full set of coupled laser equations (solid blue curve) and dynamics in which the correlations between carriers and photons are adiabatically eliminated (dashed blue curve). The disappearance of the delay δt in the formation of coherence in the latter case identifies the non-Markovian polarization dynamics as the origin of the observed effect.

expressible as

$$\begin{aligned}\left(\frac{d}{dt}+3\kappa+\gamma\right)\delta\langle\hat{b}^\dagger\hat{b}^\dagger\hat{b}\hat{v}_s^\dagger\hat{c}_s\rangle = 2|g|^2\langle\hat{b}^\dagger\hat{v}_s^\dagger\hat{c}_s\rangle^2 - \left(1-f_s^e-f_s^h\right)\delta\langle\hat{b}^\dagger\hat{b}^\dagger\hat{b}\hat{b}\rangle \\ + 2f_s^h\delta\langle\hat{b}^\dagger\hat{b}\hat{c}_s^\dagger\hat{c}_s\rangle - 2f_s^e\delta\langle\hat{b}^\dagger\hat{b}\hat{v}_s^\dagger\hat{v}_s\rangle \\ + \langle\hat{b}^\dagger\hat{b}\rangle\left(\delta\langle\hat{b}^\dagger\hat{b}\hat{c}_s^\dagger\hat{c}_s\rangle - \delta\langle\hat{b}^\dagger\hat{b}\hat{v}_s^\dagger\hat{v}_s\rangle\right).\end{aligned} \tag{6.23}$$

In order for the origin of delayed coherence formation to be comprehended, we identify the dominant contributions to the dynamics of both polarizations, (6.22) and (6.23), at the crossing of the threshold, given by the terms $\propto \langle b^\dagger b\rangle$. While the dynamics of the photon in the cavity mode is driven by the polarization via the carrier inversion term $\left(1-f_s^e-f_s^h\right)$, the evolution of the higher-order polarization is driven by *correlations* between carriers and photons $\left(\delta\langle b^\dagger b c_s^\dagger c_s\rangle - \delta\langle b^\dagger b v_s^\dagger v_s\rangle\right)$.

To pin down the responsible factor for the delay, we eliminate the dynamics of the carrier-photon correlations by solving (5.28) and (5.29), cf. Sect. 5.3.2, adiabatically:

$$\begin{pmatrix}\delta\langle\hat{b}^\dagger\hat{b}\hat{c}_s^\dagger\hat{c}_s\rangle\\ \delta\langle\hat{b}^\dagger\hat{b}\hat{v}_s^\dagger\hat{v}_s\rangle\end{pmatrix} = \frac{|g|^2}{\kappa}\mathrm{Re}\left[\delta\langle\hat{b}^\dagger\hat{b}^\dagger\hat{b}\hat{v}_s^\dagger\hat{c}_s\rangle\begin{pmatrix}-1\\1\end{pmatrix} + \langle\hat{b}^\dagger\hat{v}_s^\dagger\hat{c}_s\rangle\begin{pmatrix}\langle\hat{b}^\dagger\hat{b}\rangle+f_s^e\\ \langle\hat{b}^\dagger\hat{b}\rangle+f_s^h\end{pmatrix}\right]. \tag{6.24}$$

In Fig. 6.9 the dynamics of the remaining equations of motion (blue dashed curve) are compared to the full dynamics (blue solid curve). Evidently, when the correlation dynamics are eliminated in a Markovian sense, the delay disappears and the maximum of the emission peak coincides with the minimum of the autocorrelation function (blue dashed curve). Therefore, this confirms our initial assertion that the traditional lasing picture in which coherent emission is directly

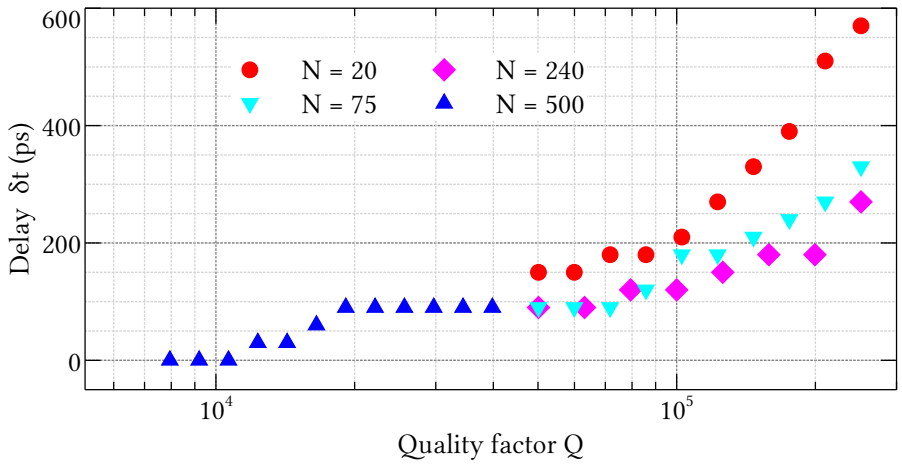

Figure 6.10 | Dependence of the delay on the cavity quality factor. Delay δt between emission intensity maximum and the minimum in the zero-delay second-order photon autocorrelation function as a function of the cavity-Q factor. A dephasing rate of γ= 0.5 meV (0.7 meV) is used for N = 20 and 75 (240 and 500). Note that a few-emitter gain material requires a sufficiently high cavity- Q factor to reach lasing. Below that, $g^{(2)}$ remains thermal and an offset δt can no longer be defined.

related to the presence of stimulated emission is too general. Instead, the photon number and its fluctuations respond to microscopic polarizations, and these develop on different timescales due to the presence of carrier-photon correlations, causing the observed effect. Finally, we identify the delay in coherence formation as a property of high-Q nanolasers that is generally absent in conventional laser devices. In Fig. 6.10 the delay δt is plotted against the cavity-Q factor for four different sets of parameters that are representative of typical laser systems, and in particular the number N of involved emitting dipoles. As a general trend, a delay begins to form for Q-factors above 10,000 and can, in principle, become as large as 0.5 ns in cavities with extreme Q factors, such as microsphere or whispering-gallery mode resonators [119]. Lower-Q cavities require a larger amount of gain material to cross the threshold, which is why the curves for 20, 75 and 240 emitters set in at a minimum Q-value. Below this value, stimulated emission is not reached, and the system operates as an LED. In the bad-cavity regime, lasing can be reached with sufficient gain material and the absence of a delay. Then, a Markovian description of the laser dynamics, in which coherence forms as an instantaneous response of the photonic field to stimulated emission, is justified.

6.4 Summary

In this chapter, a QD-PhC nanolaser has been theoretically and experimentally investigated. By resorting to the temperature as a turnstile for the amount of gain material that couples to the cavity mode, it can be shown that the device under study operates in two regimes: LED, and

laser emission regime. The delay between the time-resolved intensity emission and the build up the coherence, observed in experiment is qualitatively well reproduced by the semiconductor QD laser theory in conjunction with the quantum regression theorem. This non-instantaneous response of the photon-autocorrelation function to the onset of stimulated emission leads to the fact that the emitted pulse of the device under consideration is largely thermal and becomes coherent with a delay of 250 ps after the emission-pulse maximum. On the basis of the semiconductor laser theory, a systematic analysis ascribes this effect to the non-Markovian dynamics of the carrier-photon correlation amounting to the response of the gain material to the spontaneous and stimulated emission.

7 Gain Contribution of Background Emitters in Single Quantum Dot Nanolasers

Measuring and controlling the gain contribution of background emitters in micro- and nanolaser is of crucial importance for the understanding of the lasing transition, especially in single quantum dot (SQD) nanolaser. Experimental implementation of SQD nanolaser, wherein a single quantum dot solely modulate the optical gain is a demanding task. This is mainly due to the presently available technology in manufacturing quantum dot (QD) cavity systems, wherein a non-negligible gain contribution by non-resonant transitions is hard to avoid to overcome the laser threshold [20, 120, 121]. In current microlasers, the gain medium is based on self-assembled QDs, which nucleate randomly on the active area of the microlaser [20–22]. As a consequence, most of these QDs may feed the lasing mode in an uncontrolled way, and only a small fraction of them have suitable spectral positions so they can be tuned through the cavity mode by resorting to the temperature as a turnstile. In the long run, scenarios with only a SQD in spectral resonance and spatially matched with the cavity mode are possible. For such device to lase, it requires a high quality factor cavities and a strong light-matter rate that has to overcome the cavity loss rate at least by a factor of two, leading towards the coherent strong coupling regime [12, 121]. Consequently, even spectrally far off-resonant QDs may couple to lasing mode by the combination of different mechanisms including, inter alia Auger-like scattering processes [122–124], interaction of QD excitation with acoustic phonons [125], and Coulomb interaction with multi-exciton states [126], whereby off-resonant QDs can illuminate the cavity mode within a wide energy range of tens of milli-electron volts.

Towards grasping and controlling the impact of off-resonant emitters on the lasing behavior which will be imperative for the optimization of future micro- and nanolasers, a versatile two-color excitation protocol has been recently put forward by the group of Prof. *Stephan Reitzenstein* in Berlin. The very essence of the two-color excitation scheme is to disentangle the contribution of the off-resonant emitters from that of the resonant emitter by selectively exciting resonantly the spectrally narrow p-shell of a target QD, while the gain of the off-resonantly coupled QDs is controlled simultaneously by above-band excitation. Thereby, the gain contribu-

tion of the background emitters to the device output can be tailored by tuning the ratio between the two different excitation powers.

The present chapter aims at elaborating on the prerequisite formalism for the theoretical description of the experimental results in the framework of the two-color excitation concept. After presenting the microscopic laser model in section 7.1, the experimental data are compared to the numerical calculations in section 7.2. A short conclusion summarizes the findings.

7.1 Theoretical Model

The semiconductor QD laser model introduced in Chapter 5 assumes that the selected high-Q cavity mode is predominantly feed by those QDs in resonance and neglects the contribution of slightly detuned QDs. This assumption is underpinned by calculations, see Ref. [71] which showed that the photoluminescence of an inhomogeneously broadened QD ensemble coincides with that of an ensemble of identical QDs in resonance, with the light-matter coupling strength being chosen as the maximum value in the inhomogeneously broadened QD ensemble.

The intent of this present section is to show how to effectively account for off-resonant emitters in the framework of this stripped-down semiconductor laser model without having to consider explicitly an inhomogeneously broadened sample of QDs as done in Ref. [102].

7.1.1 Microscopic Laser Equations

To effectively account for off-resonant QDs, which via a combination of different mechanisms including Auger-like scattering processes [122–124], interaction of QD excitation with acoustic phonons [125], and Coulomb interaction with multi-exciton states [126] may couple to the cavity mode, we divide the gain medium into groups of QDs.

Let us consider M groups of QDs that couple to the selected cavity mode, thus resonantly or via the aforementioned channels. Each group contains N_ξ emitters. Then the dynamics of the intra-cavity photon is given by

$$\hbar \frac{d}{dt}\langle \hat{b}^\dagger \hat{b}\rangle = -2\kappa \langle \hat{b}^\dagger \hat{b}\rangle + \sum_{\xi=1}^{M} N_\xi |g_\xi|^2 \langle \hat{b}^\dagger \hat{v}_s^\dagger \hat{c}_s\rangle_\xi . \tag{7.1}$$

Here κ denotes the cavity loss rate, g_ξ encodes the effective light-matter coupling of each group, and the operators $c^\dagger$ (c), $v^\dagger$ (v) create (annihilate) a charge carrier in the resonant transition of each emitter, which is assumed to be the s-shell. The dynamics of carrier populations in the lasing transition is given by

$$\hbar \frac{d}{dt} f_{s,\xi}^{e,h} = -2|g_\xi|^2 \langle \hat{b}^\dagger \hat{v}_s^\dagger \hat{c}_s\rangle_\xi + \mathcal{R}_{\mathrm{nl}}(\beta_\xi) + \mathcal{R}_{p\to s,\xi}^{e,h}(\boldsymbol{P}). \tag{7.2}$$

As in Chapter 5, the rate $\mathcal{R}^{e,h}_{p\to s,\xi}$ encodes the generation of excited carriers in the resonant laser levels of the subsystem ξ via scattering that follows excitation from M pump sources with a respective pump powers $\boldsymbol{P} = (P_1, \ldots, P_M)$. The dependence of the rate $\mathcal{R}^{e,h}_{p\to s,\xi}$ on $\boldsymbol{P}$ suggests that the dynamics of the charge carries in one group may be modified by the excitation of the other groups. The spontaneous recombination of carriers into non-lasing modes is given by the rate $\mathcal{R}_{\mathrm{nl}}$ that depends on the β-factor of each subsystem of the gain medium. The time evolution of Eqs. (7.1)-(7.2) is determined by a balance of these interaction processes with the environment and the light-matter interaction of each group via photon-assisted polarizations

$$\hbar\frac{d}{dt}\langle\hat{b}^\dagger\hat{v}_s^\dagger\hat{c}_s\rangle_\xi = -\left(\kappa+\gamma_\xi\right)\langle\hat{b}^\dagger\hat{v}_s^\dagger\hat{c}_s\rangle_\xi + f^e_{s,\xi}f^h_{s,\xi} - \left(f^e_{s,\xi}+f^h_{s,\xi}-1\right)\langle b^\dagger b\rangle \tag{7.3}$$

with the dephasing rate γ_ξ associated with the QD transitions resonant with the laser mode. This equation contains the spontaneous-emission contribution $f^e_{s,\xi}f^h_{s,\xi}$ and the stimulated emission or absorption terms proportional to the intra-cavity mean photon number that also appears in rate–equation theories. It is instructive to mention that all subsystems of the gain medium are coupled via the common light field of the cavity in our multipartite gain medium laser model. As a consequence thereof, one subsystem of the gain medium may in fact be indirectly excited by others by reabsorbing the cavity photons emitted by them and vice-versa.

By augmenting the dynamics of Eqs. (7.1)-(7.3) with that of additional carrier-photon correlation functions $\delta\langle\hat{b}^\dagger\hat{b}^\dagger\hat{b}\hat{v}_s^\dagger\hat{c}_s\rangle_\xi$, $\delta\langle\hat{b}^\dagger\hat{b}\hat{c}_s^\dagger\hat{c}_s\rangle_\xi$ and $\delta\langle\hat{b}^\dagger\hat{b}\hat{v}_s^\dagger\hat{v}_s\rangle_\xi$ for each subsystem, access to the second-order correlation function $g^{(2)}(0) = 2 + \delta\langle\hat{b}^\dagger\hat{b}^\dagger\hat{b}\hat{b}\rangle/\langle\hat{b}^\dagger\hat{b}\rangle^2$ is amenable in the framework of our multipartite gain medium laser model. Similar to the mean photon number, we modify the dynamics of the photon-photon correlation as

$$\hbar\frac{d}{dt}\delta\langle\hat{b}^\dagger\hat{b}^\dagger\hat{b}\hat{b}\rangle = -4\kappa\delta\langle\hat{b}^\dagger\hat{b}^\dagger\hat{b}\hat{b}\rangle + \sum_{\xi=1}^{M} N_\xi|g_\xi|^2\delta\langle\hat{b}^\dagger\hat{b}^\dagger\hat{b}\hat{v}_s^\dagger\hat{c}_s\rangle_\xi. \tag{7.4}$$

7.1.2 Effective Spontaneous Emission Factor

In chapter 2, the spontaneous emission factor β has been introduced to parametrize the fraction of the total spontaneous emission that is funneled into the lasing mode, i.e.,

$$\beta = \frac{\Gamma_l}{\Gamma_{nl}+\Gamma_l}. \tag{7.5}$$

Here Γ_l and Γ_{nl} are the rate of spontaneous emission into the lasing and nonlasing modes, respectively. Because the spontaneous emission rate can be added up, an effective β-factor for

the multipartite gain medium may be introduced as

$$\begin{aligned}\beta_{\text{eff}} &= \frac{\sum_{\xi=1}^{M} \Gamma_{l,\xi}}{\sum_{\xi=1}^{M} \left(\Gamma_{l,\xi} + \Gamma_{nl,\xi}\right)}, \\ &= \frac{\Gamma_{l,1}}{\sum_{\xi=1}^{M} \left(\Gamma_{l,\xi} + \Gamma_{nl,\xi}\right)} + \ldots + \frac{\Gamma_{l,M}}{\sum_{\xi=1}^{M} \left(\Gamma_{l,\xi} + \Gamma_{nl,\xi}\right)},\end{aligned} \tag{7.6}$$

where $\Gamma_{l,\xi}$ and $\Gamma_{nl,\xi}$ are the rate of spontaneous emission of ξ-th group into the lasing and nonlasing modes, respectively. In the steady state, the spontaneous emission rate from each subsystem into the lasing mode is given by

$$\Gamma_{l,\xi} = 2N_\xi |g_\xi|^2 \langle \hat{b}^\dagger \hat{v}_s^\dagger \hat{c}_s \rangle_\xi, \tag{7.7}$$

which depends on the photon-assisted polarization $\langle \hat{b}^\dagger \hat{v}_s^\dagger \hat{c}_s \rangle_\xi$, the value of which can be obtained by solving the corresponding equation of motion in the steady state

$$-(\kappa + \gamma_\xi)\langle \hat{b}^\dagger \hat{v}_s^\dagger \hat{c}_s \rangle_\xi + f_{s,\xi}^e f_{s,\xi}^h = 0. \tag{7.8}$$

It should be noted that we have omitted the stimulated emission channel, as only photons stemming from spontaneous emission enter the definition and the calculation of the β-factor. The loss into the nonlasing modes can be read from the populations dynamics in the s-shell (cf. Chap. 5) and is given by

$$\Gamma_{nl}^{\xi} = N_\xi (1 - \beta_\xi) \frac{f_\xi^e f_\xi^h}{\tau_{\text{sp}}^{\xi}}. \tag{7.9}$$

By combining the above equations and using the definition of the light-matter coupling in terms of the spontaneous emission time, cf. Chap. 5

$$g_\xi^2 = \frac{\hbar \beta_\xi (\kappa + \Gamma_\xi)}{2\tau_{\text{sp}}^{\xi}}, \tag{7.10}$$

one obtains the expression for the effective β-factor

$$\beta_{\text{eff}} = \beta_1 \left(1 + \frac{N_2}{\lambda_2 N_1} \frac{\langle \hat{b}^\dagger \hat{v}_s^\dagger \hat{c}_s \rangle_2}{\langle \hat{b}^\dagger \hat{v}_s^\dagger \hat{c}_s \rangle_1}\right)^{-1} + \beta_2 \left(1 + \frac{N_1}{\lambda_1 N_2} \frac{\langle \hat{b}^\dagger \hat{v}_s^\dagger \hat{c}_s \rangle_2}{\langle \hat{b}^\dagger \hat{v}_s^\dagger \hat{c}_s \rangle_1}\right)^{-1}, \quad \text{with} \quad \lambda = \frac{\beta_2}{\beta_1} \frac{|g_1|^2}{|g_2|^2} \tag{7.11}$$

for $M = 2$. Here β_ξ is the spontaneous emission factor of each group. The value of this effective β-factor implicitly depends on the excitation rates of each subsystem of the gain medium and can, thereby, be tuned as will be discussed later. Note that more intricate many-body effects can already lead to deviations from a constant β-factor of each subsystem, see Refs. [127, 128].

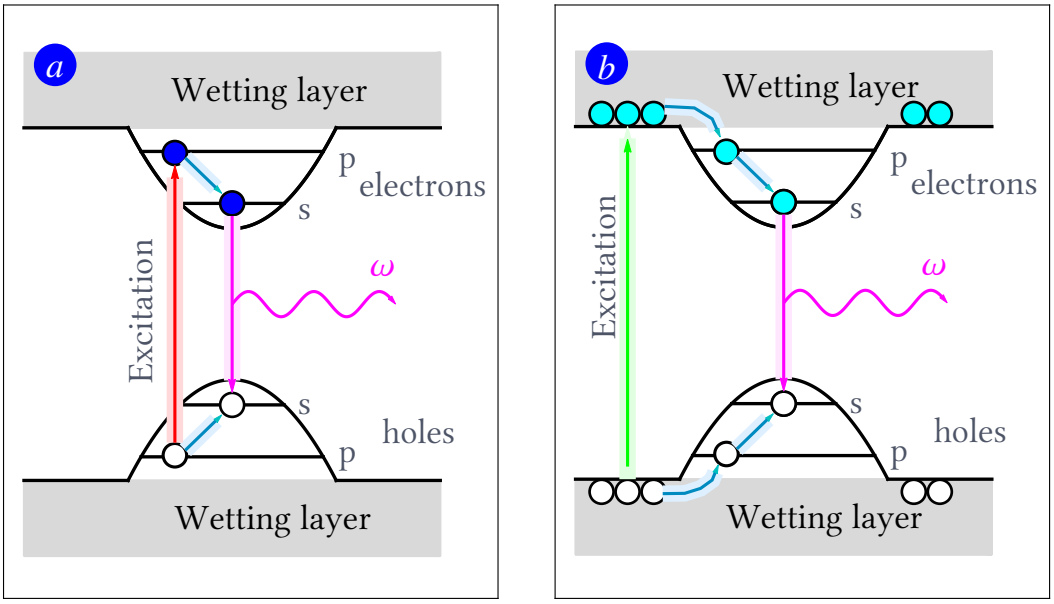

Figure 7.1 | Comparison of the two excitation schemes used in the two-color excitation protocol. a) *In the p-shell excitation scheme*, the target QD is selected via excited electronic state by using infrared source. b) *In the above-band excitation*, carriers are non-resonantly generated in the continuum of barrier states by the green laser. This is followed by a non-radiative relaxation into the QD s-shell via excited states.

7.2 Simulation and Experimental Results

The present section is devoted to the theoretical and experimental results that are obtained in collaboration with the group of Prof. *Stephan Reitzenstein* in Berlin. In the framework of this collaboration, the effect of background emitters on the lasing behavior of SQD microlasers has been analyzed by applying an advanced two-color excitation concept where the background gain contribution of off-resonant QDs can be continuously tuned by precisely balancing the relative excitation power of two lasers emitting at different wavelengths. High-quality low-mode volume GaAs-based QD-micropillar structure containing a single layer of self-assembled InGaAs QDs as gain medium has been used for the study. For more details regarding the growth and the experimental set up, see Ref. [129].

7.2.1 Model Calibration

The parameters of the background emitters (BG) and the resonant single quantum dot (QD) involved in the multipartite laser model are determined by comparing the theoretical and experimental results using green and infrared excitation separately. More specifically, the calculated input-output characteristics have been matched to the measured one.

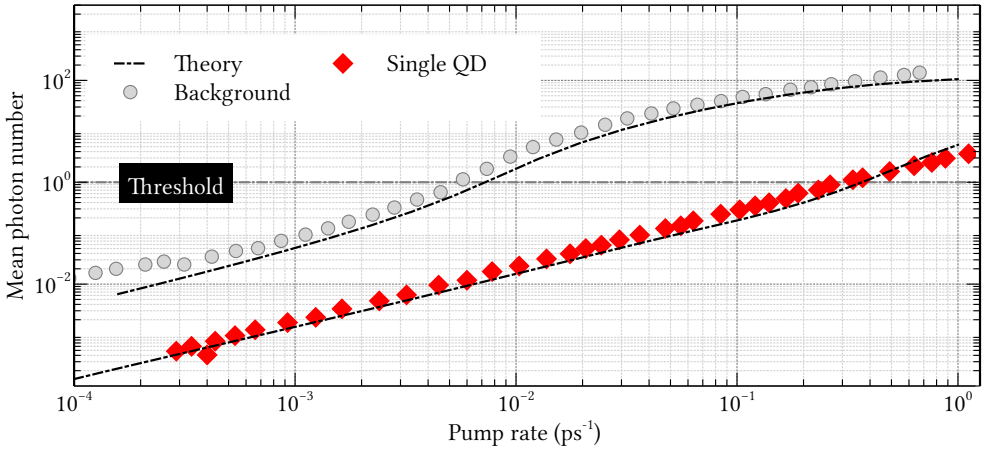

Figure 7.2 | Theoretical and experimental input-output characteristics. The gray circle corresponds to the input-output characteristics for only exciting above-band, and the red diamond for only exciting the p-shell of the target quantum dot (IR), cf. 7.1. The dot-dashed black line are the numerical calculations. For the SQD, a light-matter constant of $g_{\mathrm{QD}} = 50\,\mu\mathrm{eV}$ has been used. A β-factor of $\beta_{\mathrm{QD}} = 0.9$ and a dephasing rate of $\gamma_{\mathrm{QD}} = 1.36\,\mu\mathrm{eV}$ was sufficient to reproduce the experimental data. For the off-resonant QDs, the following parameters set have been used: $[N_{\mathrm{BG}}, g_{\mathrm{BG}}, \gamma_{\mathrm{BG}}, \beta_{\mathrm{BG}}] = [160, 20\,\mu\mathrm{eV}, 80\,\mu\mathrm{eV}, 0.25]$. The horizontal gray dashed line marks the lasing transition.

A graphical representation of the two-color excitation scheme is shown in Fig. 7.1. Non-resonant carrier excitation is modeled by charge carrier creation into the higher QD p-states, either via direct excitation in a case of the infrared excitation at rate P_{IR}, or via in-scattering of carriers that are excited into the energetically higher-lying states of the barrier material by green laser excitation at rate P_{G}:

$$\frac{d}{dt} f^{e,h}_{p,\mathrm{BG}} = (P_G + \Delta P_{\mathrm{IR}}) \left(1 - f^{e}_{p,\mathrm{BG}} - f^{h}_{p,\mathrm{BG}}\right) - \mathcal{R}^{e,h}_{p\to s,\mathrm{BG}}(P_{\mathrm{G}}, P_{\mathrm{IR}}), \tag{7.12a}$$

$$\frac{d}{dt} f^{e,h}_{p,\mathrm{QD}} = P_{\mathrm{IR}} \left(1 - f^{e}_{p,\mathrm{QD}} - f^{h}_{p,\mathrm{QD}}\right) - \mathcal{R}^{e,h}_{p\to s,\mathrm{QD}}(P_{\mathrm{G}}). \tag{7.12b}$$

The dependence of the rate $\mathcal{R}^{e,h}_{p\to s,\mathrm{BG}}$ in Eq. (7.12a) on P_{IR} and P_{G} is motivated by the fact that a small fraction of the infrared laser used to select the resonant quantum dot is captured by the background emitters.

By matching the height of the jump between experimental and numerical results a β-factor of the resonant QD $\beta_{\mathrm{QD}} = 0.9$, and of the background emitters $\beta_{\mathrm{BG}} = 0.25$ have been extracted, see Fig. 7.2. For the lasing mode, a quality factor of $Q = 15000$ as determined in the experiment has been used in the calculations. Regarding the light-matter coupling constant, an estimate of $g_{\mathrm{QD}} = 50\,\mu\mathrm{eV}$ for the resonant QD is known from experiment. This value has been used as upper bound for the coupling constant of the BG emitters, for which we use $g_{\mathrm{QD}} = 20\,\mu\mathrm{eV}$. For the damping of the inter-band transition in the respective subsystems, the following values have been used: $\gamma_{\mathrm{QD}} = 1.36\,\mu\mathrm{eV}$, $\gamma_{\mathrm{BG}} = 80\,\mu\mathrm{eV}$. Noteworthy, small variations of the dephasing rates

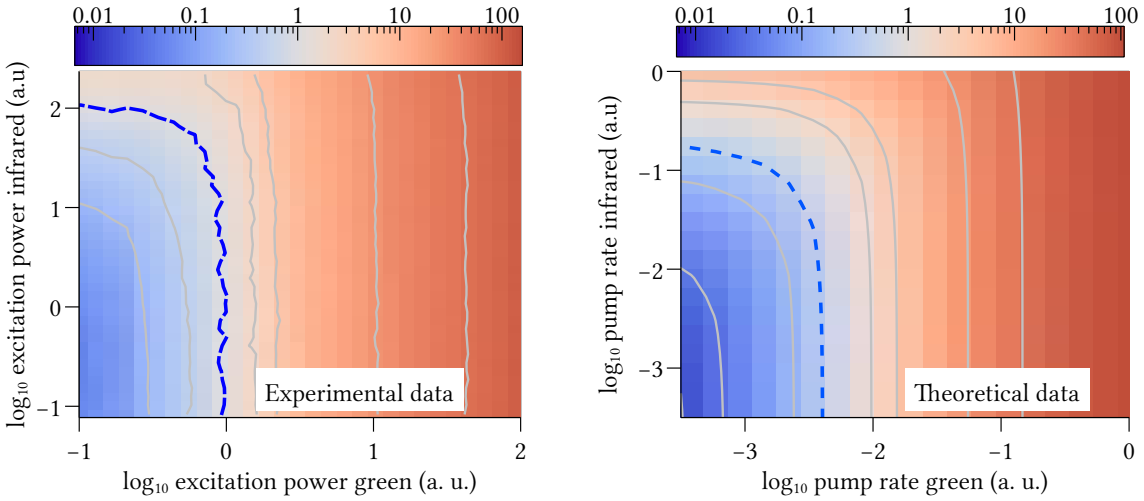

Figure 7.3 | Input-output map in the two-color excitation scheme. The left panel shows the experimental dependence of the emission intensity on the excitation conditions in the two-color excitation scheme. The right panel displays the theoretical calculation. The parameters set for the resonant quantum dot and the background emitters are the same as in Fig. 7.2. The blue dashed line in both panels represents the lasing threshold according to the usual definition $\langle \hat{b}^\dagger \hat{b} \rangle = 1$ for microlasers.

result in qualitatively the same behavior.

A number of $N_{\mathrm{BG}} = 160$ of BG emitters that are distributed over a spectral range of tens of milli-electron volts have been used. In principle, depending on the individual detuning situation, cavity-feeding rates differ for all emitters, especially due to the differences in the efficiency of the underlying coupling mechanism. Since the exact spectral position are not known, and in order to avoid microscopic computations of phonon- or Auger-assisted feeding rates [123, 124, 130] their contributions have to be thought of as an ensemble average. This means that g_{BG} and β_{BG} are effective values that apply equally for all background emitters in the model.

7.2.2 Two-Color Excitation Map

Having determined the parameters involved in our laser model by matching the input-output curves of the two limiting cases of either exciting dominantly the single target QD or all QDs in the micropillar, we now turn our attention to the study of the transition between them by gradually unbalancing between the two different pumping rates.

Input-Output Excitation Map

Figure 7.3 displays the contour plot of the input-output curve obtained from the experiment, see the left panel, and the theoretical model, see right panel. The vertical axis represents the

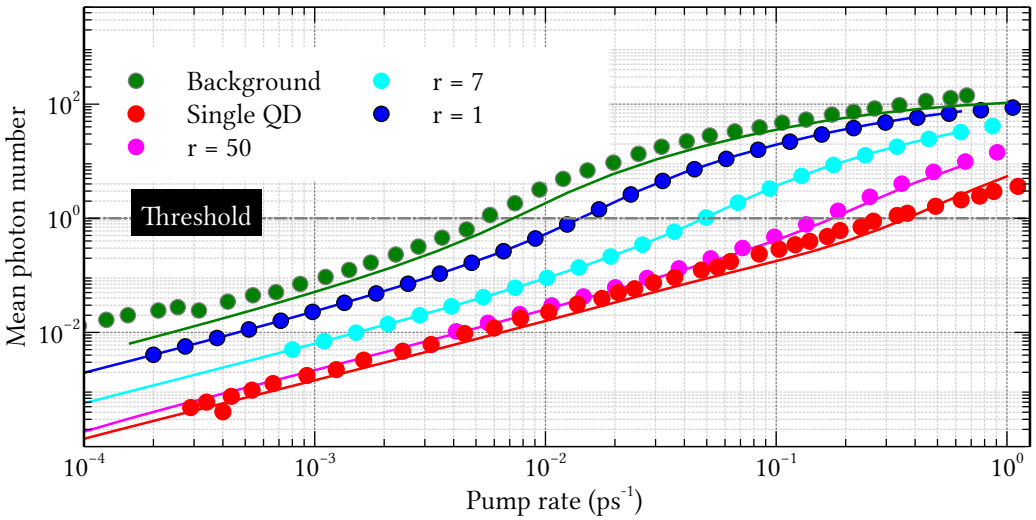

.

Figure 7.4 | Diagonal cross-sections through the 2D excitation map. Diagonal cross-sections through the 2D excitation map for five different green to infrared excitation power ratios $r \in \{0, 1, 7, 50, \infty\}$. The ratio corresponds to constant relative contribution of the off-resonant emitters to the gain medium. The case $r = 0$ and $r = \infty$ correspond to the p-shell excitation of the SQD and the above-band excitation of the background emitters, respectively. The gray dashed line indicates the lasing threshold ($\langle \hat{b}^\dagger \hat{b} \rangle = 1$). The horizontal axis corresponds to the sum of both excitation power: $P = P_{\mathrm{IR}}(1 + r)$.

p-shell excitation of the target single QD, whereas the horizontal axis encodes the strength of the above-band excitation. An increase in the corresponding pump rate of the latter leads to an increased excitation of the background emitters in the micropillar. The threshold power ($\langle \hat{b}^\dagger \hat{b} \rangle = 1$), obtained from the numerical calculations by matching the calculated input-output characteristics to the experimentally measured one, is shown in the left panel by the blue dashed line. Noteworthy, the qualitative agreement between the experimental and the theory maps is very high. Moreover, it is clear from the maps that the difference between input-output curves for the limiting cases is not linked with different scaling factors for the excitation power but indeed with the difficulty in achieving lasing conditions with a single quantum dot gain.

Cross Section Cut

By performing a diagonal cross cut through the 2D excitation map, a visualization of the change in the shape of the input-output characteristic is amenable. Figure 7.4 shows the diagonal cross-section pertaining to the input-output curve a fixed ratios $r \in \{1, 7, 50\}$ between both excitation powers, i.e., constant contribution-percentage of the off-resonant emitters. The upper- and lower- most input-output curves correspond to the two limiting cases, see Fig. 7.2. The solid lines are the complementary simulated curves. It should be noted that the curves in Fig. 7.4

are plotted against the sum of both pump rates. From these curves, one observes that the jump in the transition regime is correlated with the increase of the background emitters contribution. In other words, the higher the off-resonant emitter-contribution, the more pronounced the s-shape in the transition regime. Thereby, the threshold position shifts toward lower total excitation powers.

Effective Spontaneous Emission Factor

For the coupled system consisting of resonant and background emitters, the effective β-factor, Eq. (7.11), reduces to

$$\beta_{\text{eff}} = \beta_{\text{QD}} \left(1 + \frac{N_{\text{BG}}}{\lambda} \frac{\langle \hat{b}^\dagger \hat{v}_s^\dagger \hat{c}_s \rangle_{\text{BG}}}{\langle \hat{b}^\dagger \hat{v}_s^\dagger \hat{c}_s \rangle_{\text{QD}}} \right)^{-1} + \beta_{\text{BG}} \left(1 + \frac{\lambda}{N_{\text{BG}}} \frac{\langle \hat{b}^\dagger \hat{v}_s^\dagger \hat{c}_s \rangle_{\text{QD}}}{\langle \hat{b}^\dagger \hat{v}_s^\dagger \hat{c}_s \rangle_{\text{BG}}} \right)^{-1} \tag{7.13}$$

with $\lambda = \dfrac{\beta_{\text{BG}}}{\beta_{\text{QD}}} \left| \dfrac{g_{\text{QD}}}{g_{\text{BG}}} \right|^2$. In the limit of vanishing contributions from the background subsystem, the effective β-factor takes on the high β_{QD} value of the resonant emitter, whereas as significantly lower $\beta_{\text{eff}} = \beta_{\text{BG}}$ is observed in the case of dominating background:

$$\beta_{\text{eff}} = \begin{cases} \beta_{\text{QD}} & \text{for} \quad N_{\text{BG}} \to 0 \\ \beta_{\text{BG}} & \text{for} \quad N_{\text{BG}} \to \infty \end{cases} \tag{7.14}$$

Figure 7.5 (middle panel) depicts the numerical calculation of the effective β-factor. In region of dominant contribution of the p-shell excitation, the effective β-factor reaches the maximal value of $\beta_{\text{eff}} = 0.37$ which is still two times smaller than the extracted value of $\beta_{\text{QD}} = 0.9$ for the target resonant QD. This points out that even weak above-band excitation with a pump rate as low as $10^{-4}\,\text{ps}^{-1}$ leads to a significant background emitter related occupation of the cavity mode. As a result, a degradation of the effective β-factor is observed. On the other hand, when using only above-band excitation of the system and in the strong excitation regime, a value close to $\beta_{\text{BG}} = 0.25$ is obtained for the effective β-factor. This is interesting in the sense that, it corroborates the dominant role of the background emitters in this range. Nevertheless, in the regime of intermediate infrared pumping rates, the single quantum gains a meaningful contribution. As a result, its fingerprint becomes apparent in the microlaser characteristics meaning that in this low excitation regime a SQD gain microlaser can be disentangled from a multi-QD laser.

Photon Statistics

In the framework of the multipartite gain medium laser model, more insights into the gain contribution of background emitters in SQD microlaser may be obtained by analyzing the second-

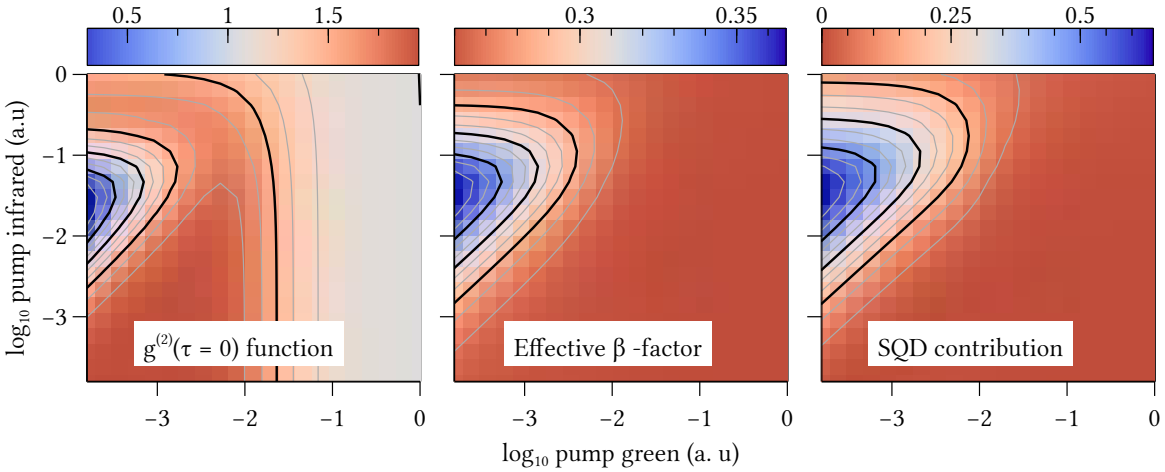

Figure 7.5 | Second-order photon correlation function, effective spontaneous emission factor, and single QD contribution excitation map. The left panel displays the excitation map of the second-order correlation function, Eq. (7.15), in the two-color excitation scheme, while the middle and the right panels show the effective spontaneous emission factor, Eq. (7.13), and the single QD contribution, Eq. (7.16) respectively. The set of parameters used for the simulations are the same as in Fig. 7.2.

order photon correlation function map

$$g^{(2)}(P_{\mathrm{G}}, P_{\mathrm{IR}}) = 2 + \frac{\delta\langle \hat{b}^\dagger \hat{b}^\dagger \hat{b}\hat{b}\rangle}{\langle \hat{b}^\dagger \hat{b}\rangle^2}, \tag{7.15}$$

the numerical calculation of which is displayed in Fig. 7.5 (left panel). Interestingly, as in the case of the effective spontaneous emission factor, similar regions and a non-monotonic behavior with P_{IR} can be observed. In the low excitation regime, the resonant SQD and the background emitters behave as a QD ensemble, as the emission is thermal ($g^{(2)}(\tau = 0) = 2$). This at first sight unexpected thermal character of the emitted light may be traced back to the fact that a small fraction of the infrared pump rate also drives the background emitters. It is instructive to note that the similar effect would be visible, even if there was no fraction of P_{IR} exciting the background subsystem, as both subsystems are coupled via the lasing mode, see Eq. (7.3). Nevertheless, with increasing carrier population, i.e high P_{IR} spontaneous emission becomes faster, as it is proportional to populations ($f^e f^h$), and at inversion, stimulated emission sets in for the SQD but not for the background emitters. As consequence thereof, the statistical properties of the emitted light is dominated by the SQD contribution, evidenced by non-classical behavior and anti-bunching. At high above-band excitation, coherent emission is reached at pump rates of about $10^{-1}\,\mathrm{ps}^{-1}$. Even though the SQD alone does not provide a sufficient gain to cross the laser threshold, coherent emission can be approached when P_{IR} is further increased as a small fraction of the p-shell excitation also drives the BG emitters.

Single QD Contribution

To put more flesh on the effective-β-factor and the second-order correlation function $g^{(2)}(0)$ dependences on the excitation power, we introduce an *asymmetry parameter* $\mathcal{C}_{\mathrm{SQD}}$,

$$\mathcal{C}_{\mathrm{SQD}} = 2\left|\frac{\mathcal{I}_T - \mathcal{I}_{\mathrm{BG}}}{\mathcal{I}_T + \mathcal{I}_{\mathrm{BG}}}\right| \tag{7.16}$$

which measures the relative contribution of the single QD to the emission of the microlaser. In this equation, $\mathcal{I}_T$ represents the total emission (BG emitters and the SQD) and the $\mathcal{I}_{\mathrm{BG}}$ stands for the background emission only, where the SQD is removed in the model. It is important to note that this asymmetry parameter is not amenable in experiment, as the presence of the SQD is noticeable even if it is not directly excited. The accessibility of this parameter in theory is actually quite interesting, because it reveals in how far the single emitter enhances the emission. In Figure 7.5 (right panel), it can be seen that in the blue region the emission enhancement reaches up to 70%. There is a slight non-linear behavior discernable that appears to come from the onset of stimulated emission of the single QD. It is reflected by the contour lines being more closely spaced between 10^{-3} ps and 10^{-2} ps in the vertical direction. All curves bending back at higher IR excitation power reflect that the single QD is actually a saturable absorber and cannot be driven to emit any more photons. The blue to red region one could interpret as the regime where the SQD contribution is enhanced by the background, whereas the red region is completely dominated by the background.

In their sum, the isolated contribution of the SQD and the effective β-factor provide important insight into the interplay of resonant and background contributions in a nanolaser that can operate close to the ideal regime of single-emitter lasing. This insight could not be obtained from the mean photon number alone, which is a more intricate quantity as it reflects the properties of the photons in the cavity, rather than their origin. At the same time, the autocorrelation function obtained from our microscopic model demonstrates that a single device can be operated in any regime of non-classical, coherent, or thermal emission by choosing the resonant (IR) and background (green) excitation to realize any point in the two-color maps. Due to the high relevance of the photon statistics to understand the nature of the micropillar emission, it will be interesting to address the autocorrelation function under two-color excitation in future experimental studies in order to confirm the predictions of figure 7.5 (left panel).

7.3 Summary

In this chapter, the relative gain contribution of the single resonant QD and background emitters that are off-resonant in the single QD nanolaser has been theoretically and experimentally

investigated by the judicious two-color excitation scheme. The gist of this more advanced excitation scheme consists in monitoring the contribution of the background emitters and the resonant QD by selectively exciting the latter via its *p*-shell and by resorting to the above-band excitation for the former. The remarkable feature of this excitation scheme is its ability to control the transition between a device having characteristics reminiscent to those of a macroscopic laser with QD ensemble gain, and microlaser operating in the cavity quantum electrodynamic regime. Such being the case, it makes allowances for shedding more light on the operation of high-quality microlasers close to the limiting case of the thresholdless single-emitter laser.

In contrast to the mainstream understanding of the β-factor to be constant for a given microcavity system, our investigation shows that a dominant single QD gain contribution results in a higher effective β-factor meaning the spontaneous emission factor depends on and may be tuned by the specific excitation conditions determining the effective gain. The study of the second-order photon correlation also endorses the role of the dominant single QD.

Part

IV

Coupled-Cavity Arrays

8 Collective Lasing in Disordered Coupled-Cavity Arrays

This chapter aims at investigating theoretically and numerically the collective lasing in disordered Jaynes-Cummings-Hubbard coupled-cavity arrays (CCAs). CCAs are quantum simulators for the physics of many-body systems. After reviewing the history of quantum simulators in section 8.1, the theoretical model is outlined in section 8.2. Here, we discuss the quantization of the light field in CCAs, and the Jaynes-Cummings-Hubbard model describing CCAs in which each cavity contains a two-level emitter interacting with the local mode. We proceed further by deriving the equations of motion (EoMs) for the correlation functions which are essential for obtaining all local quantities of interest. By introducing a diagonal average approximation (DAA), it will be shown that results for translation invariant coupled resonators, i.e homogeneous coupled cavities, can be extended for weak photonic disordered array of cavities. The results of the numerical simulations are presented in Sect. 8.3. A short conclusion summarizes the findings.

8.1 General Introduction

An idiosyncrasy of strongly-correlated many-particle systems being pervasive in solid-state materials is the shortness of the length- and timescales on which their dynamics play out. As consequence thereof, accessing their microscopic properties with the state-of-art experimental technology is a very convoluted task. The controllability of the state of individual constituents is even harder. Over the years, and motivated by *Feynman's* view [131] of using a *computer* having quantum mechanical primitive to emulate highly complex systems, artificial platforms, the so-termed *quantum simulators*, have been put forward to explore the rich physics of strongly-correlated many-body systems. Arguably, the first proposed architecture is an array of *Josephson junctions* [132, 133] with which the properties of interacting bosonic particles [134–136] have been successfully emulated. Another artificially designed platforms are ultra-cold atoms trapped in optical lattices [137]. They turned out to be outstanding quantum simulators of large variety of condensed-matter phenomena, including inter alia the superfluid-to-Mott-insulator quantum phase transition [138], and a Tonks-Girardeau gas [139]. In addition to emulating quantum

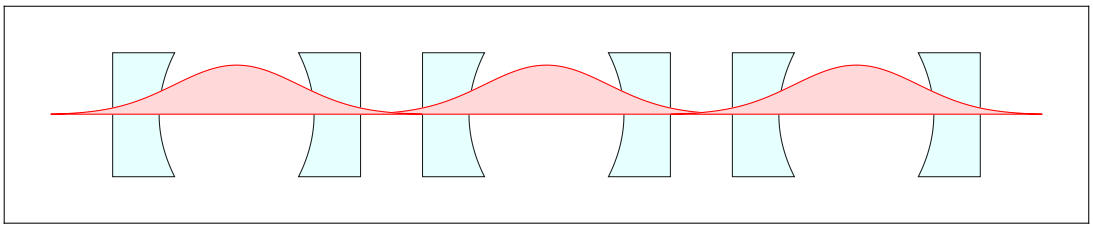

Figure 8.1 | **Cartoon of coupled-cavity arrays**. A graphical representation of an array of coupled cavities. Overlap of the light field modes of contiguous cavities gives rise to photon hopping.

many-particles phenomena, ultra-cold atoms in optical lattices also proved to be instrumental in the implementation of quantum information processing by entangling contiguous atoms via controlled collisions [140].

Implementation of quantum simulators based on coupled high-quality cavity arrays in photonic crystal cavities [141–143], in superconducting transmission lines [144–148], or toroidal microcavities [119, 149], constitute new appealing avenues for simulating strongly correlated many-body models. Unlike architectures based on Josephson junctions and optical lattices, CCAs allow for a high degree of control and addressability of single sites. The coupling between contiguous cavities naturally arises from the overlap between evanescent field modes, see Fig. 8.1.

In the Jaynes-Cummings-Hubbard version of the architecture, each cavity interacts with a two-level system (e.g. quantum dot, atom or Cooper pair box). The local light-matter interaction in strong coupling regime gives rise to optical nonlinearities and an effective photon-photon repulsion, resulting in Mott-insulator states of light, and a transition to superfluidity of photons when the photon hopping process overpowers the photon blockade effect [24, 25, 142]. The optical nonlinearities can also be realized when each cavity is filled with four-level atoms of a particular level structure, and an external laser is used to drive them in the same manner as in the electromagnetically induced transparency [25].

In addition to functioning as quantum simulators for quantum many-body phenomena, coupled-cavity arrays have witnessed huge amount of interest in implementing quantum information processing devices: quantum gates [150], the generation of entangled states such cluster state [26, 151–153], the generation of single photons in parallel [154], quantum states transfer [27], just to cite a few.

In Reference [155], the emergence of collective photonic modes in homogeneous coupled-cavity arrays has be demonstrated to give rise to lasing far out of resonance between emitter and cavity. In this chapter, we investigate the effect of disorder in the local photonic frequencies on this collective lasing behavior.

8.2 Theoretical Model

8.2.1 Light Field Hamiltonian in Coupled-Cavity Arrays

To derive the light field Hamiltonian in CCAs, see Fig. 8.1, we follow references [25, 156, 157] and describe the array of cavities by a real, periodic dielectric medium

$$\varepsilon(\boldsymbol{x}) = \varepsilon(\boldsymbol{x} + \boldsymbol{X}), \tag{8.1}$$

where $\boldsymbol{x}$ is a given three dimensional vector, and $\boldsymbol{X} = X\boldsymbol{l}$ for all tuples of integers $\boldsymbol{l} = (l_1, l_2, l_3)$.

As proceeded in Chap. 4, we start the quantization of the electromagnetic field (EMF) in the periodic coupled-cavity lattice from Maxwell's equations, which in the presence of a dielectric medium read as

$$\begin{aligned}
\boldsymbol{\nabla} \cdot \boldsymbol{B}(\boldsymbol{x}, t) &= 0, \\
\boldsymbol{\nabla} \cdot \boldsymbol{D}(\boldsymbol{x}, t) &= 0, \\
\boldsymbol{\nabla} \times \boldsymbol{E}(\boldsymbol{x}, t) &= -\frac{\partial}{\partial t}\boldsymbol{B}(\boldsymbol{x}, t), \\
\boldsymbol{\nabla} \times \boldsymbol{H}(\boldsymbol{x}, t) &= \frac{\partial}{\partial t}\boldsymbol{D}(\boldsymbol{x}, t).
\end{aligned} \tag{8.2}$$

Here, the electric $\boldsymbol{E}(\boldsymbol{x}, t)$ and the auxiliary field $\boldsymbol{D}(\boldsymbol{x}, t)$ are linearly related to each other via

$$\boldsymbol{D}(\boldsymbol{x}, t) = \varepsilon_0 \varepsilon(\boldsymbol{x}) \boldsymbol{E}(\boldsymbol{x}, t). \tag{8.3}$$

The Coulomb gauge which describes the EMF in terms of the vector potential $\boldsymbol{A}(\boldsymbol{x}, t)$ has to be generalized to make allowance for the dielectric medium [158]:

$$\boldsymbol{\nabla} \cdot [\varepsilon(\boldsymbol{x}) \boldsymbol{A}(\boldsymbol{x}, t)] = 0, \tag{8.4}$$

which fulfills automatically the transversality condition on the auxiliary field $\boldsymbol{D}(\boldsymbol{x}, t)$,

$$\boldsymbol{\nabla} \cdot \left\{ \varepsilon(\boldsymbol{x}) \frac{\partial}{\partial t} \boldsymbol{A}(\boldsymbol{x}, t) \right\} = 0. \tag{8.5}$$

In dielectric medium the wave equation for the vector potential, Eq. (4.11) becomes

$$\boldsymbol{\nabla} \times \boldsymbol{\nabla} \times \boldsymbol{A}(\boldsymbol{x}, t) + \frac{\varepsilon(\boldsymbol{x})}{c^2} \frac{\partial^2}{\partial t^2} \boldsymbol{A}(\boldsymbol{x}, t) = 0 \tag{8.6}$$

It is illuminating to mention the similarity between coupled-cavity lattice and the scenario in condensed-matter physics, wherein an itinerant electron feels an atomic potential sharing the periodicity of the crystal lattice. Here the individual cavities are the optical counterpart of the isolated atoms, and the spatial mode in the cavities corresponds to the atomic wave function.

This analogy suggests to use tight-binding approach for the vector potential, which satisfies the Bloch theorem [72],

$$\boldsymbol{A}(\boldsymbol{x}+\boldsymbol{X},t) = e^{\mathrm{i}\boldsymbol{k}\boldsymbol{X}}\boldsymbol{A}(\boldsymbol{x},t). \tag{8.7}$$

In the framework of the tight-binding approach, the vector potential is then expanded in terms of Wannier functions being used to describe the spatial part of one site cavity-mode:

$$\boldsymbol{A}(\boldsymbol{x},t) = \sum_l u(\boldsymbol{x}-\boldsymbol{X}_l)e^{\mathrm{i}(\boldsymbol{k}\boldsymbol{X}_l-\omega t)}, \quad \text{with} \quad \boldsymbol{X}_l = X\boldsymbol{l}. \tag{8.8}$$

The Wannier functions fulfill the eigenvalue equation

$$\frac{\omega_c^2}{c^2}\varepsilon_{\boldsymbol{X}}(\boldsymbol{x})u_{\boldsymbol{X}} - \nabla\times(\nabla\times u_{\boldsymbol{X}}) = 0 \tag{8.9}$$

and the normalization condition

$$\int d\boldsymbol{x}\, u^*_{\boldsymbol{X}}(\boldsymbol{x})u_{\boldsymbol{X}}(\boldsymbol{x}) = 1. \tag{8.10}$$

Here ω_c is the resonance frequency of the cavity and $\varepsilon_{\boldsymbol{X}}(\boldsymbol{x})$ accounts for the local dielectric function. Note that by virtue of the periodicity ω_c does not depend on $\boldsymbol{X}$.

By inserting Eq. (8.8) in the wave equation for the vector potential, Eq. (8.6), one obtains

$$\sum_l \left\{ \frac{\varepsilon(\boldsymbol{x})\omega^2}{c^2}u(\boldsymbol{x}-\boldsymbol{X}_l) - \nabla\times\nabla\times u_{\boldsymbol{X}}(\boldsymbol{x}-\boldsymbol{X}_l) \right\} e^{\mathrm{i}(\boldsymbol{k}\boldsymbol{X}_l-\omega t)} = 0 \tag{8.11}$$

By multiplying both sides of this equation with $u^*_{\boldsymbol{X}}(\boldsymbol{x})$ and performing a spatial integration, the dispersion relation for the coupled-cavity lattice arises

$$\omega^2 = \omega_c^2 \frac{1+\sum_{l\neq 0} e^{\mathrm{i}\boldsymbol{k}\boldsymbol{X}_l}\beta_l}{1+\Delta\alpha+\sum_{l\neq 0} e^{\mathrm{i}\boldsymbol{k}\boldsymbol{X}_l}\alpha_l}, \tag{8.12}$$

where for $l \neq 0$ α_l, β_l and Δ_α are defined as [156, 157]

$$\alpha_l = \int d\boldsymbol{x}\, u^*_{\boldsymbol{X}}(\boldsymbol{x})u_{\boldsymbol{X}}(\boldsymbol{x}-\boldsymbol{X}_l), \tag{8.13a}$$

$$\beta_l = \int d\boldsymbol{x}\, \varepsilon_{\boldsymbol{X}}(\boldsymbol{x}-\boldsymbol{X}_l)u^*_{\boldsymbol{X}}(\boldsymbol{x})u_{\boldsymbol{X}}(\boldsymbol{x}-\boldsymbol{X}_l), \tag{8.13b}$$

$$\Delta\alpha = \int d\boldsymbol{x}\, [\varepsilon(\boldsymbol{x}) - \varepsilon_{\boldsymbol{X}}(\boldsymbol{x})]\, u^*_{\boldsymbol{X}}(\boldsymbol{x})u_{\boldsymbol{X}}(\boldsymbol{x}), \tag{8.13c}$$

To evaluate the sum terms in Eq. (8.12), the coupling between the cavities is assumed to be sufficiently weak so that only the overlap between the Wannier functions pertaining to contiguous

cavities contribute [25, 156, 157]. This amounts to keeping only terms $\alpha_{\pm 1}$ and $\beta_{\pm 1}$, wherefrom Eq. (8.12) may be reduced to

$$\omega^2 = \omega_c^2 \frac{1 + 2\beta_1 \cos(kX)}{1 + \gamma + 2\alpha_1 \cos(kX)} \tag{8.14}$$

by resorting to symmetry considerations allowing to require that $\alpha_1 = \alpha_{-1}$ and $\beta_1 = \beta_{-1}$ [25, 156, 157]. We can simplify the above dispersion relation further by defining the coupling factor

$$\lambda = \int d\boldsymbol{x} \left[\varepsilon(\boldsymbol{x}) - \varepsilon_{\boldsymbol{X}}(\boldsymbol{x})\right] u^*_{\boldsymbol{X}}(\boldsymbol{x}) u_{\boldsymbol{X}}(\boldsymbol{x} - \boldsymbol{X}), \tag{8.15}$$

and by making use of the fact that $\Delta\alpha$ and α_1 are marginal quantities, i.e $\Delta\alpha \approx 0$, $\alpha_1 \approx 0$ [157] to obtain

$$\omega \approx \omega_c \left[1 + \lambda \cos(kX)\right]. \tag{8.16}$$

For $kX \approx 0$ which is tantamount to the large wave-length limit, one obtains

$$\omega \approx \omega_c + \omega_c \lambda. \tag{8.17}$$

By interpreting the first term as the on-site contribution and the second term as the correction resulting from the contiguous hopping process [157], the quantization of the light field in coupled-cavity array reads as

$$H_{EMF} = \omega_c \sum_{\alpha} \hat{b}^\dagger_\alpha \hat{b}_\alpha + \mathcal{J} \sum_{\langle \alpha, \beta \rangle} \left(\hat{b}^\dagger_\alpha \hat{b}_\beta + \hat{b}^\dagger_\beta \hat{b}_\alpha \right), \tag{8.18}$$

where $\sum_{\langle \alpha, \beta \rangle}$ stands for the sum of all pairs of cavities which are contiguous and $\mathcal{J} = \lambda \omega_c$.

8.2.2 Jaynes-Cummings-Hubbard Model

In the previous section, we have derived the light field Hamiltonian for coupled-cavity lattice by requiring that the building blocks have the same resonant frequency and the probability of the hopping process is the same for all cavity interactions. Needless to say that this model Hamiltonian does not echo practical situation wherein the lattice may entail some disorder leading to a fluctuation of the resonant frequency and the tunneling rate from cavity to cavity.

In this thesis, we are interested in disordered coupled-cavity systems with each cavity being coupled to a two-level emitter. Such a system is commonly described by the so-called *Jaynes-Cummings-Hubbard model* which is given by

$$H = \sum_{\alpha\beta} t_{\alpha\beta} \hat{b}^\dagger_\alpha \hat{b}_\beta + \sum_{\alpha} \varepsilon_\alpha \hat{\sigma}^\dagger_\alpha \hat{\sigma}_\alpha + \sum_{\alpha} \left(g_\alpha \hat{b}^\dagger_\alpha \hat{\sigma}_\alpha + g^*_\alpha \hat{b}_\alpha \hat{\sigma}^\dagger_\alpha \right). \tag{8.19}$$

The operators $\hat{\sigma}_\alpha^\dagger$ and $\hat{\sigma}_\alpha$ are the fermionic excitation and deexcitation operator in each site, respectively. The transition energy of the two-level system is given by ε_α. The operators $\hat{b}_\alpha^\dagger$ and $\hat{b}_\alpha$ describe the local photonic operator in each cavity, whose frequency is $t_{\alpha\beta} = \omega_\alpha \delta_{\alpha\beta}$. The coupling between cavities is ensured by the photonic hopping term $t_{\alpha\beta} = \mathcal{J}_{\alpha\beta}(1 - \delta_{\alpha\beta})$. Note that $t_{\alpha\beta}^* = t_{\beta\alpha}$. The last term is the pivotal Jaynes-Cummings Hamiltonian encapsulating the light-matter interaction with a coupling constant g_α.

8.2.3 Orthogonal Transformation

When dealing with coupled-cavity arrays, it is convenient to introduce collective modes (CMs) for the photons [23] as they allow one to diagonalize the photonic part the system Hamiltonian. These are defined by the following orthogonal transformation,

$$\hat{b}_k = \sum_\alpha S_{\alpha k} \hat{b}_\alpha, \quad \hat{b}_k^\dagger = \sum_\alpha S_{k\alpha} \hat{b}_\alpha^\dagger. \tag{8.20}$$

Here k denotes the photonic eigenmode or the collective mode of the coupled-cavity system and $S_{k\alpha} = \langle k|\alpha\rangle$ are the basis transformation coefficients whose complex conjugation reads $S_{k\alpha}^* = S_{\alpha k} = \langle \alpha|k\rangle$. In the basis of the CMs, the above Hamiltonian, Eq. (8.19) is expressible as

$$H = \sum_k \Omega_k \hat{b}_k^\dagger \hat{b}_k + \sum_\alpha \varepsilon_\alpha \hat{\sigma}_\alpha^\dagger \hat{\sigma}_\alpha + \sum_{k,\alpha} \left(g_{k\alpha} \hat{b}_k^\dagger \hat{\sigma}_\alpha + g_{k\alpha}^* b_k \hat{\sigma}_\alpha^\dagger \right), \tag{8.21}$$

where $g_{k\alpha} = S_{\alpha k} g_\alpha$ and $\Omega_k = \sum_{\alpha\beta} S_{k\alpha} t_{\alpha\beta} S_{\beta k}$ denotes the CMs frequencies of the coupled-cavity system. Note that the above transformation considers one-dimensional lattice site. For the case of one-dimensional homogeneous closed ring of coupled cavities, analytical expressions exist for the transformation coefficients and the modes frequencies. They are given by

$$\begin{cases} S_{k\alpha} &= \dfrac{1}{\sqrt{N}} e^{\mathrm{i}k\alpha}, \\ \Omega_k &= \omega_c + 2\mathcal{J}\cos(k) \end{cases} \tag{8.22}$$

where $k = 2\pi l/N$, $l = 1, \ldots, N$ with N being the number of sites in the array. The CMs are referred to as *Bloch modes*.

8.2.4 Notation

Before embarking on the derivation of the equations of motion for the calculation of the local quantities, we first denote the relevant quantities which are involved. At the mean photon level, only three coupled EoMs for three quantities are essential:

$$\begin{aligned} n_{\alpha\beta} &= \langle \hat{b}_\alpha^\dagger \hat{b}_\beta \rangle, \\ \psi_{\alpha\beta} &= -\mathrm{i}g_\beta \langle \hat{b}_\alpha^\dagger \hat{\sigma}_\beta \rangle, \\ f_{\alpha\beta} &= \langle \hat{\sigma}_\alpha^\dagger \hat{\sigma}_\beta \rangle. \end{aligned} \tag{8.23}$$

These c-number are two-cavity correlation functions, and $N \times N$ matrices, where N denotes the number of considered cavities. The $n_{\alpha\beta}$ encode the inter-cavity coherence. Its diagonal elements $n_{\alpha\beta} \equiv n_\alpha$ are the local mean photon number. The $\psi_{\alpha\beta}$ represent the inter-cavity photon-assisted polarization and describe an correlated event where a creation of a photon in the α-th cavity is connected to an interband transition in the β-th cavity. Its diagonal elements $\psi_{\alpha\alpha} \equiv \psi_\alpha$ are the on-site photon-assisted polarization. The last quantities, $f_{\alpha\beta}$, are the inter-cavity emitter-emitter correlation whose diagonal elements $f_{\alpha\beta} = \langle \hat{\sigma}_\alpha^\dagger \hat{\sigma}_\alpha \rangle \equiv f_\alpha$ give the number of emitters in the excited states.

8.2.5 Equations of Motion for the Correlation Functions

We proceed further to derive the equations of motion for the above correlation functions by resorting to the formalism outlined in Chap. 4,

$$\begin{aligned}\frac{d}{dt}\langle \hat{G} \rangle = -\mathrm{i}\langle [\hat{H}, \hat{G}] \rangle &+ \sum_\alpha P_\alpha \left\{ \langle \hat{\sigma}_\alpha \hat{G} \hat{\sigma}_\alpha^\dagger \rangle - \frac{1}{2}\langle \hat{\sigma}_\alpha \sigma_\alpha^\dagger \hat{G} \rangle - \frac{1}{2}\langle \hat{G} \hat{\sigma}_\alpha \sigma_\alpha^\dagger \rangle \right\} \\ &+ \sum_\alpha \gamma_\alpha \left\{ \langle \hat{\sigma}_\alpha^\dagger \hat{G} \hat{\sigma}_\alpha \rangle - \frac{1}{2}\langle \hat{\sigma}_\alpha^\dagger \sigma_\alpha \hat{G} \rangle - \frac{1}{2}\langle \hat{G} \hat{\sigma}_\alpha^\dagger \sigma_\alpha \rangle \right\} \\ &+ \sum_\alpha \kappa_\alpha \left\{ \langle \hat{b}_\alpha^\dagger \hat{G} \hat{b}_\alpha \rangle - \frac{1}{2}\langle \hat{b}_\alpha^\dagger b_\alpha \hat{G} \rangle - \frac{1}{2}\langle \hat{G} \hat{b}_\alpha^\dagger b_\alpha \rangle \right\},\end{aligned} \tag{8.24}$$

where P_α, γ_α and κ_α are the site-dependent pump, two-level decay, and cavity loss rates respectively. In the following, they will be assumed to be the same for all sites. A derivation of the equations of motion where all model parameters depend on the site indices is provided in the appendix.

We start the derivation of the EoMs with the mean value of the photonic quadratic product $n_{\alpha\beta}$, the time evolution of which is coupled to the inter-cavity photon-assisted polarization. Its dynamics in turn is coupled to higher-ranking correlators. To prune the unfolding hierachy of the equations of motion we avail ourselves with the cluster expansion technique. Thereby, we separate carrier numbers from photon-assisted polarizations and photon quadratic products as in the following

$$\begin{aligned}\langle \hat{b}_\alpha^\dagger \hat{b}_\beta \hat{\sigma}_\nu^\dagger \hat{\sigma}_\nu \rangle &\approx \langle \hat{b}_\alpha^\dagger \hat{b}_\beta \rangle \langle \hat{\sigma}_\nu^\dagger \hat{\sigma}_\nu \rangle = n_{\alpha\beta} f_\nu, \\ \langle \hat{b}_\alpha^\dagger \hat{\sigma}_\beta \hat{\sigma}_\nu^\dagger \hat{\sigma}_\nu \rangle &\approx \langle \hat{b}_\alpha^\dagger \hat{\sigma}_\beta \rangle \langle \hat{\sigma}_\nu^\dagger \hat{\sigma}_\nu \rangle = \psi_{\alpha\beta} f_\nu.\end{aligned} \tag{8.25}$$

Local Basis Representation

The expectation value of the photonic quadratic evolves as

$$\dot{n}_{\alpha\beta} = \mathrm{i} \sum_\nu \left(t_{\beta\nu}^* n_{\nu\alpha} - n_{\beta\nu} t_{\nu\alpha}^* \right) - \kappa n_{\alpha\beta} + \psi_{\alpha\beta} + \psi_{\beta\alpha}^*. \tag{8.26}$$

The dynamics of the c-number $\psi_{\alpha\beta}$ in the right hand side of this above equation is given by

$$\dot{\psi}_{\alpha\beta} = \mathrm{i}\sum_{\nu} \Delta^{*}_{\alpha\nu}\psi_{\nu\beta} - \frac{1}{2}(\kappa+\lambda)\,\psi_{\alpha\beta} + n_{\alpha\beta}|g|^2\left(2f_\beta - 1\right) + |g|^2 f_{\alpha\beta}. \tag{8.27}$$

Here $\Delta_{\alpha\nu} = t_{\alpha\nu} - \varepsilon\delta_{\alpha\nu}$. The notation $\lambda = \gamma + P$ has been introduced, and denotes the total dephasing rate of the inter-cavity photon-assisted polarization. Note that the light-matter coupling strength and the two-level transition energy are taken to be the same for all sites, $g_\alpha = g$, and $\varepsilon_\alpha = \varepsilon$. The correlation function appearing in the last term has its own dynamic which reads

$$\dot{f}_{\alpha\beta} = -\lambda f_{\alpha\beta} + (2f_\alpha - 1)\,\psi_{\alpha\beta} + \psi^{*}_{\beta\alpha}\left(2f_\beta - 1\right) + \left[P - 2f_\alpha\left(\psi_\alpha + \psi^{*}_{\alpha}\right)\right]\delta_{\alpha\beta}. \tag{8.28}$$

Eigenmode Basis Representation

The Equations (8.26)-(8.28) can be expressed in the photon eigenmode basis by fully or when convenient partially transforming the involved matrix as

$$\begin{aligned} n_{kq} &= \sum_{\alpha\beta} S^{*}_{k\alpha} n_{\alpha\beta} S^{*}_{\beta q}, \\ \psi_{k\beta} &= \sum_{\alpha} S^{*}_{k\alpha}\psi_{\alpha\beta}. \end{aligned} \tag{8.29}$$

By applying this transformation to the coupled EoMs Eqs. (8.26)-(8.28), we end up with the following equations of motion for the correlation functions

$$\dot{n}_{kq} = \left[\mathrm{i}\left(\Omega_k - \Omega_q\right) - \kappa\right] n_{kq} + A_{kq}, \tag{8.30a}$$

$$\dot{\psi}_{k\alpha} = -\frac{1}{2}(2\mathrm{i}\Delta_k + \gamma)\,\psi_{k\beta} + |g|^2 n_{k\beta}\left(2f_\beta - 1\right) + |g|^2 f_{k\beta}, \tag{8.30b}$$

$$\dot{f}_{\alpha\beta} = -\lambda f_{\alpha\beta} + (2f_\alpha - 1)\,\psi_{\alpha\beta} + \psi^{*}_{\beta\alpha}\left(2f_\beta - 1\right) + (P - 2f_\alpha A_k)\,\delta_{\alpha\beta}. \tag{8.30c}$$

Here $A_{kq} = \psi_{kq} + \psi^{*}_{qk}$, and $\Delta_k = \varepsilon - \Omega_k$ is the detuning of the k photonic mode.

8.2.6 Diagonal Average Approximation

The diagonal average approximation [1] (DAA) has been introduced to express the above equations in the same basis. Its consists in approximating some diagonal quantities by their average. Generally, for a given $N \times N$ matrix A, its average is expressed as its trace divided by its dimension:

$$\bar{A} = \frac{1}{N}\sum_{\alpha} A_{\alpha\alpha}. \tag{8.31}$$

[1] It has been proposed by Dr. Paul Gartner

Because for homogeneous systems, it is legitimate to write $\bar{A} = A_\alpha$, the approximations $f_\alpha \approx \bar{f}$ and $A_k \approx \bar{A}$ are deemed to be reasonable in case of a weak disorder. The parameter region for which the approximation will break down can be worked out by comparing results based on this approximation to that of the full solution of Eqs. (8.26)-(8.28).

In the framework of the DAA, one obtains from Eqs. (8.30a)-(8.30c) at the steady state a set of equations involving only collective mode-basis quantities

$$n_{kq} = \frac{A_{kq}}{\left[\kappa - \mathrm{i}\left(\Omega_k - \Omega_q\right)\right]}, \tag{8.32a}$$

$$\psi_{kq} = \frac{2|g|^2}{\Gamma + 2\mathrm{i}\Delta_k}\left[f_{kq} + n_{kq}\left(2\bar{f} - 1\right)\right], \tag{8.32b}$$

$$\lambda f_{kq} = \left(2\bar{f} - 1\right) A_{kq} + \left(P - 2\bar{f}\bar{A}\right)\delta_{kq}. \tag{8.32c}$$

In this approximation, the fact that the source $\delta_{kq}P$ is diagonal in the mode indices suggests that only the non-diagonal terms are zero. As a result, one obtains

$$\kappa n_k = A_k, \tag{8.33a}$$

$$A_k = F_k\left[f_k + 2\left(2\bar{f} - 1\right) n_k\right], \tag{8.33b}$$

$$(P + \gamma) f_k = P + 2\bar{f}\left(A_k - \bar{A}\right) - A_k, \tag{8.33c}$$

where $F_k = 4|g|^2\Gamma/((\Gamma^2 + 4\Delta_k^2)$ denotes the spontaneous emission of the two-level emitter into the collective mode k. From Eq. (8.33a) it follows that $A_k \geq 0$ for all k, as the photon populations n_k are positive quantities. By averaging Eq. (8.33c) one obtains

$$\bar{f} = \bar{f}_0 - \frac{\bar{A}}{P + \gamma} \quad \text{or} \quad \bar{A} = (f_0 - \bar{f})(P + \gamma), \tag{8.34}$$

where $\bar{f}_0 = P/(P + \gamma)$. For $\bar{A} = 0$, $\bar{f} = \bar{f}_0$, meaning that $\bar{f}_0$ is the average number of excited emitters in the absence of the carrier-photon interaction.

By eliminating in Eqs. (8.33a) and (8.33c) A_k by using (8.33b) and $\bar{A}$ via Eq. (8.34), one obtains two coupled algebraic equations for n_k and f_k

$$\kappa n_k = \left(2\bar{f} - 1\right) F_k n_k + F_k f_k, \tag{8.35a}$$

$$f_k = \left[\bar{f}_0 - 2\bar{f}\left(\bar{f}_0 - \bar{f}\right)\right] + \frac{\kappa}{P + \gamma}\left(2\bar{f} - 1\right) n_k. \tag{8.35b}$$

By inserting Eq. (8.35b) into Eq. (8.35a), one obtains for the population of the collective mode

$$\kappa n_k = \frac{|g|^2\Gamma\left[\bar{f}_0 - 2\bar{f}\left(\bar{f}_0 - \bar{f}\right)\right]}{\Delta_k^2 + \dfrac{2\Gamma^2|g|^2}{\kappa\,(P + \gamma)}\left(\bar{f}_1 - \bar{f}\right)}, \tag{8.36}$$

where the quantity $f_1 = \dfrac{1}{2} + \dfrac{\kappa\,(P + \gamma)}{8|g|^2}$ has been introduced. As the expression obtained for the photonic population n_k is reminiscent of the homogeneous case [155], where DAA is exact, we conclude that the DAA equation extends for weak disorder the translation-invariant results.

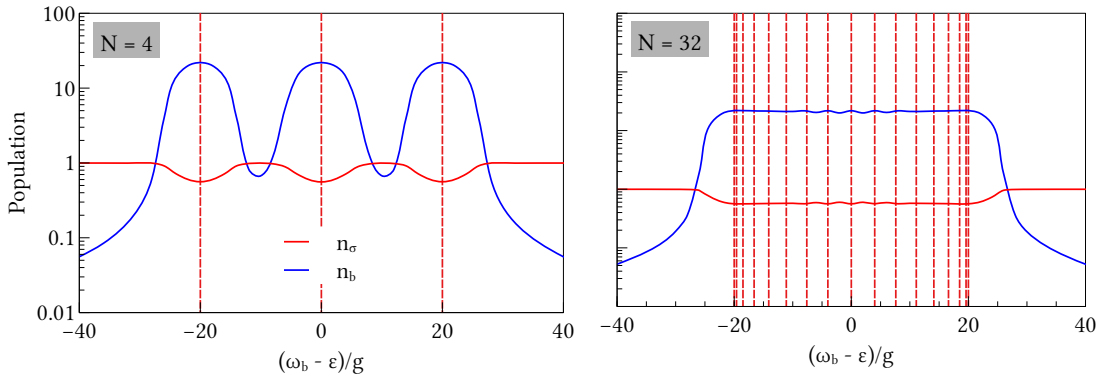

Figure 8.2 | Collective lasing in homogeneous closed ring of cavities. Local mean photon number (red line) and emitter population(blue line) as function of the emitter frequency ε. The vertical red dashed lines are the collective modes. At $\Omega_k = \varepsilon$ an increase in the local mean photon number is observed. The following parameters have been used: $N = 4$ (left panel), $N = 32$ (right panel), $\mathcal{J} = 10g$, $P_\sigma = 5g$, $\kappa = 0.1g$, and $\gamma = 0.01g$.

8.3 Numerical Simulations

In this section, the focus will be on the numerical analysis of the collective lasing in disordered CCAs. To this end, we start by reproducing the results that have been obtained for the one-dimensional homogeneous coupled-cavity arrays in Ref. [155]. After discussing the effect of the disorder on the collective lasing, we then investigate the extent of the parameter region for which the diagonal average approximation is applicable by checking against the full solution of Eqs. (8.26)-(8.28).

8.3.1 Collective Lasing

Homogeneous Coupled-Cavity Arrays

The investigations in Ref. [155] considers a one-dimensional closed ring of CCAs and are carried out in the strong coupling regime, meaning $\kappa, \gamma \ll g$. The parameters have been chosen so that each isolated building block operates in the lasing regime, the so-termed one-emitter laser. In this case, a half inversion of the emitter is observed, $n_\sigma = \langle \hat{\sigma}^\dagger \hat{\sigma} \rangle \approx n_\sigma^L = 0.5$, and the cavity is feed with a large number of photons $n_b \approx n_b^L = P_\sigma / 2\kappa$ [155]. For the investigated architecture, the collective modes are the Bloch modes that have been already introduced in Sect. 8.2.3,

$$\Omega_k = \Omega + 2\mathcal{J}cos(k), \quad k = \frac{2\pi l}{N}, \quad l = 1, \ldots, N, \tag{8.37}$$

where N is the number of cavities in the array. The modes form a band with their frequencies distributed across the interval $[\omega_b - 2\mathcal{J}, \omega_b + 2\mathcal{J}]$. For the parameters set that have been used in [155], we solve the coupled equations for n_k and f_k, Eqs. (8.35a)-(8.35b). In Fig. 8.2, we graph

the local mean photon number n_b, and the emitter population for arrays with $N = 4, 32$. As reported in [155], each collective mode is coupled to N emitters and enters its own lasing regime at $\Omega_k = \varepsilon$. This gives rise to an increase of the photon number in the local cavity despite the detuning between the emitter and the local cavity. The increase is accompanied by a decrease of the emitter population to $n_\sigma^L \approx 1/2$ from its saturation value 1. Note that because of the symmetry property of the cosine-function, the Bloch modes are degenerated. At resonance, the driven modes are equally feed by the emitters, $n_{k=0,\pi} = N n_b^L$ at the edges, and $n_{\pm k} = N n_b^L/2$ for the other central modes. The height and the width of the peaks for the local mean photon number n_b are given by n_b^L and $2\Delta_{max} = \sqrt{P_\sigma(\kappa_\sigma - P_\sigma)}$ [155], where $\kappa_\sigma = 4g^2/\kappa$ denotes the Purcell enhanced decay of an emitter through its local cavity. A plateau in the local mean photon number is observed, when the average distance between the Bloch modes, given by $4\mathcal{J}/N$ (or $4\mathcal{J}/(N-1)$ for odd N) is greater than the width of the peaks.

Disordered Coupled-Cavity Arrays

Let us now turn to the effect of the disordered photonic frequencies on the collective lasing. To this end, the local cavity frequency is split as

$$\omega_\alpha = \omega_b + \delta\omega_\alpha, \tag{8.38}$$

where ω_b is the same for all cavities and $\delta\omega_\alpha$ encode the scattering in the photonic frequency, which is assumed to be Gaussian-distributed

$$P(\delta\omega_\alpha) = \frac{1}{\sqrt{2\pi}\sigma} \exp\left(-\frac{\delta\omega_\alpha^2}{2\sigma^2}\right). \tag{8.39}$$

Here σ is a parameter controlling the width of the fluctuations in the local mode energies.

For the set of parameters used in Fig. 8.2 (left panel), we solve the set of coupled equations of motion for the correlation functions $n_{\alpha\beta}$, $\psi_{\alpha\beta}$, and $f_{\alpha\beta}$, Eqs. (8.26)-(8.28). The disorder $\delta\omega_\alpha$ are randomly generated from the Gaussian distribution. We numerically diagonalize the photonic matrix $t_{\alpha\beta}$ to obtain the energies of the collective modes (vertical red dashed lines). The influence of the photonic disorder on the collective lasing is seen in Fig. 8.3 (left) where we plot the steady-state mean photon number of each cavity against the detuning $\omega_b - \varepsilon$ for two different widths of the fluctuations in the local mode energies: $\sigma = 10g$, and $50g$. Note that for each width, the simulation has been performed for one realization of the fluctuations.

For the particular realization of the fluctuations in case of $\sigma = 10$g, compared to the translation invariant case, the modes at the edge of the band are redshifted, while the degeneracy of the central modes are lifted. Interestingly, the collective lasing is not observed in all cavities when the collective mode enters its own lasing regime, $\Omega_k = \varepsilon$. While collective lasing can obtained at the edges of the photonic band, the third cavity does not lase when all emitters resonantly

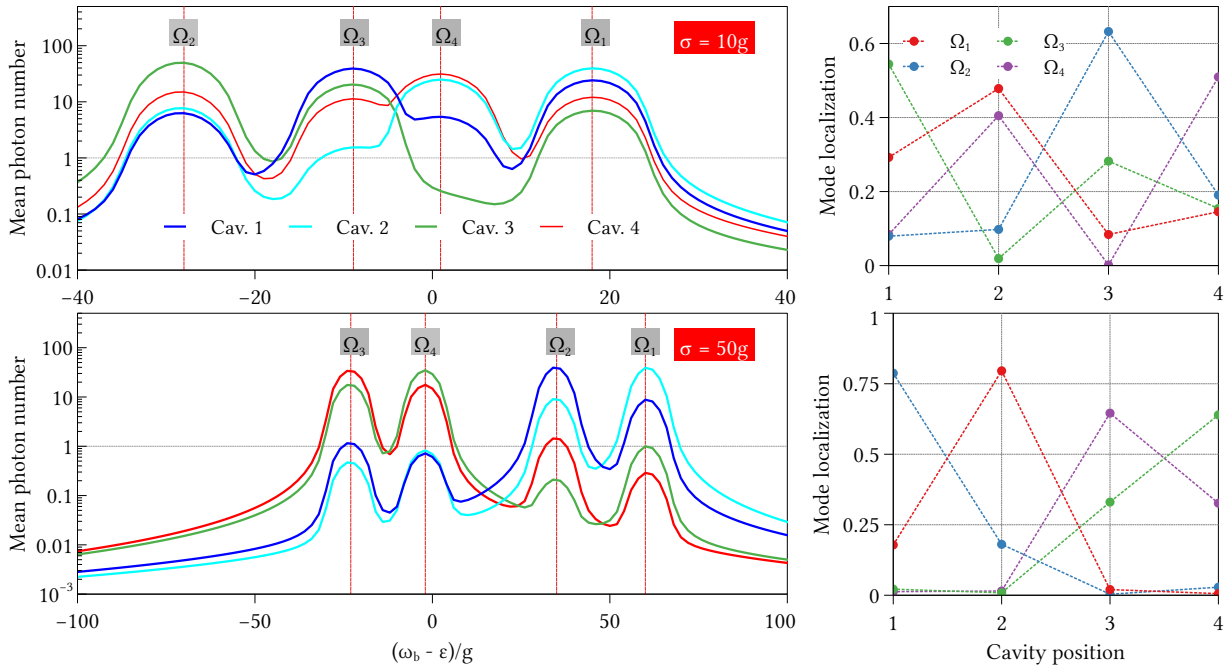

Figure 8.3 | Collective lasing in a disordered closed ring of cavities. Local mean photon number as function of the emitter frequency ε for $N = 4$ (left panel of each row), and the localization of the collective modes in each cavity (right panel of each row). The other parameters are the same as in Fig. 8.2. The vertical dotted lines are the position of the collective modes. The horizontal gray dashed line marks the threshold transition given by $\langle \hat{b}^\dagger \hat{b} \rangle = 1$.

drive the fourth collective mode. In order to understand this behavior, we plot the localization of each CM in each cavity, Fig. 8.3 (right panel). It is given by the square root of the transformation coefficients, $|S_{k\alpha}|^2$, arising from the diagonalization of the photonic matrix $t_{\alpha\beta}$, cf. Eq. (8.20). As can be observed, the collective mode Ω_4 shows the weakest localization in the third cavity, while the collective mode Ω_2 shows the highest localization. Consequently, the highest intensity is recorded in the third cavity when the second collective mode is resonant with all emitter.

For disorder higher than the photon hopping rate ($\sigma = 50g > \mathcal{J} = 10g$), when each collective mode enters its own lasing regime, the collective lasing is observed only in the first and second, or in the third and fourth cavities.

Diagonal Average Approximation

Figure 8.4 compares the results of the local mean photon obtained from the full dynamics and that based on the DAA. For photonic disorder smaller than the light-matter coupling strength, a good agreement between the full dynamics and the DAA is obtained, and results of the translation invariant array can be extended to disordered ones. In the regime $\delta\omega_\alpha > g$, where the degeneracy of the central collective modes are lifted, while the DAA reproduces qualitatively

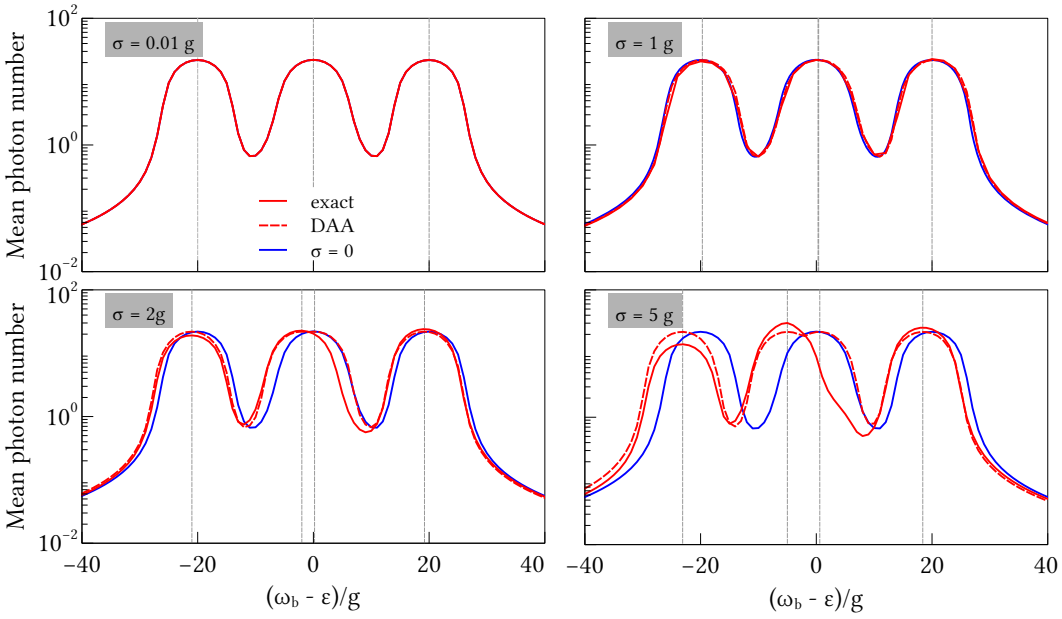

Figure 8.4 | Finess of the diagonal average approximation. Comparison of the local mean photon number obtained from the full dynamics and that from the diagonal average approximation for different values of the disorder, $\sigma = 0.01g, 1g, 2g, 5g$.

the collective lasing at the band edges, it fails to capture the feature of the central modes.

8.4 Summary

In summary, the influence of disorder in the local mode energies on the collective lasing in Jaynes-Cummings-Hubbard coupled-cavity arrays has been theoretically and numerically investigated. By introducing a diagonal average approximation, it can be show that results for translation invariant coupled cavities, i.e. homogeneous coupled cavities, can be extended for disordered array of cavities as long as the fluctuations in the local cavity frequency are smaller than the light-matter coupling strength.

9 Summary and Outlook

This chapter is intended to conclude this work and gives some future directions. Three main topics have been addressed in this thesis: (i) Non-Markovianity of lasing dynamics of InAsP/InP QDs PhC nanolaser, (ii) gain contribution of background emitters in micropillar single quantum dot nanolasers, and (iii) collective lasing in disordered coupled-cavity arrays.

For topics (i) and (ii) a semiconductor quantum dot laser theory, that makes allowances for semiconductor effects including a modification of the spontaneous emission source and filling effects, has been introduced. To that end, we first discussed the quantum Markovian master equation of Lindblad-type allowing for a genuine investigation of open quantum systems dynamics. We then described the light-matter interaction in semiconductor quantum dot systems. As a retrieval of the properties of the system under consideration in this thesis is intractable by using the Lindblad's equation of motion for the density operator, the equation of motion scheme and its inherently related hierarchy problem for the relevant observables has been discussed. To handle the hierarchy, the cluster expansion technique is usually used. To exemplify the equations of motion approach, the semiconductor luminescence equations constituting the starting point of the semiconductor quantum dot laser theory, have been derived. Upon extending the laser equations to carrier-photon correlation functions, access to the second-order photon correlation function constituting a powerful tool for characterizing the operational regimes of nanolasers was amenable.

In the framework of this laser theory, the build up of second-order coherence, associated with lasing, on a different timescale than the emission itself in a quantum-dot photonic-crystal nanolaser emitting in the telecom band has been investigated. For the investigated sample, it was possible to control the number of quantum dots overlapping with the lasing mode via the temperature. By combining the semiconductor quantum dots laser theory with the quantum regression theorem, the full two-time photon correlation function $g^{(2)}(t_1, t_2)$ under pulsed-excitation at different temperatures were calculated. Good agreement of the simulated data with the measured ones could be demonstrated. Systematical and intensive numerical calculations showed that the theoretically and experimentally observed delay of up to 250 ps in the build up of the coherence is intrinsically induced. By adiabatically eliminating the carrier-photon dynamics in the semiconductor quantum dots laser equations, that are accessible in the laser rate-equation theories, the non-Markovian effects in the emission dynamics disappear. In further calculations,

the effects was shown to depend on the quality factor Q of the microcavity and the number of emitters loaded into the former.

The second central topic was concerned with the theoretical modeling of single-emitter lasing effects in a quantum dot (QD)-microlaser under controlled variation of background gain provided by off- resonant discrete gain centers. Experimentally, the gain contribution of off-resonant QDs can be continuously tuned by using a recently proposed two-color excitation scheme that allows for precisely balancing the relative excitation power of two lasers emitting at different wavelengths. To account for the off-resonant emitters in the framework of the stripped-down semiconductor QDs laser theory, different light-matter coupling strength have been attributed to the different gain centers. Theoretical calculations based on the developed model reveal that while a single QD cannot drive the investigated micropillar into lasing, its relative contribution to the emission can be as high as 70% and it dominates the statistics of emitted photons in the intermediate excitation regime below threshold.

The last issue considered was the analytical and numerical investigation of the collective lasing in disordered coupled-cavity arrays. The emergence of collective modes in this systems has been shown to give rise to collective lasing in each building block when the emitters drive the collective modes. Fluctuations in the local cavity frequencies were demonstrated to turned off the collective in some sites depending on the localization of the collective modes in them. By introducing a diagonal average approximation, it was demonstrated that in the parameter regime where the disorder is smaller than the light-matter coupling strength, results of the translation invariant, i.e. homogeneous coupled-cavity arrays could be extended for the disordered arrays.

Prospectively, it might be interesting to measure the second-order photon correlation function in the two-color experiment to confirm our theoretical calculation. Regarding the coupled-cavity array, future works may investigate the collective lasing where the disorder is taken in full generality, meaning that all model parameters are site-dependent. Given the ability of the second-order photon correlation function to characterize the non-classical nature of the light field, it might be arresting to look at it in the disordered coupled-cavity array by resorting to the *time evolving block decimation* (TEBD) algorithm based on the powerful concept of the *matrix product state* [159, 160] to tackle the dynamics of the density matrix operator.

Appendices

A Derivation of Lindblad Equation

This appendix gives a proof of the quantum Markovian master equation of the Lindblad-type, which has been formulated in Chapter 3. To this end, it is convenient to introduce the concept of *Banach* or *Liouville space*.

A.1 Concept of Liouville Space

Let us consider some Hilbert space $\mathcal{H}$. The associated *Liouville space* $\mathcal{B}(\mathcal{H})$ is the space of Hilbert-Schmidt operators, that is the space of operators $\hat{F}$ in $\mathcal{H}$ for which $\mathrm{Tr}[\hat{F}^\dagger \hat{F}]$ is finite. By equipping the Liouville space with a scalar product given by

$$\langle \hat{F} | \hat{G} \rangle = \mathrm{Tr}[\hat{F}^\dagger \hat{G}], \tag{A.1}$$

it inherits the structure of the Hilbert space. Therefore, an orthonormal basis $\{\hat{f}_\alpha\}$ in this space fulfilling the orthogonality and the completeness relationships,

$$\langle \hat{f}_\alpha | \hat{f}_\beta \rangle = \delta_{\alpha\beta}, \quad \hat{F} = \sum_\alpha \hat{f}_\alpha \langle \hat{f}_\alpha | \hat{F} \rangle \tag{A.2}$$

can be introduced. In nutshell, the formalism of the Liouville space allows one to treat Hilbert-Schmidt operators as *vectors*. Theses vectors are easily obtained by reshaping these operators $\hat{F}$ to a large vector $|\hat{F}\rangle$ with index $\alpha \in \{1, 2 \ldots N^2\}$ where N is the dimension of the Hilbert space. An example of the Hilbert-Schmidt operators is the density operator $\hat{\rho}$.

We are now ready to proof the Lindblad equation:

Theorem A.1.1. *A linear operator $\mathcal{L}$: $\mathcal{B}(\mathcal{H}_\mathcal{S}) \to \mathcal{B}(\mathcal{H}_\mathcal{S})$ is the generator of a completely positive dynamical semigroup of $\mathcal{B}(\mathcal{H}_\mathcal{S})$ if it can be expressed in the form*

$$\mathcal{L} : \rho \to \mathcal{L}\rho = -\mathrm{i}[H, \rho] + \sum_{\alpha\beta} c_{\alpha\beta} \left(F_\alpha \rho \hat{F}_\beta^\dagger - \frac{1}{2} F_\alpha \hat{F}_\beta^\dagger \rho - \frac{1}{2} \rho F_\alpha \hat{F}_\beta^\dagger \right), \tag{A.3}$$

where $H^\dagger = H$, $\mathrm{Tr}(H) = 0$, $\mathrm{Tr}(F_\alpha) = 0$, $\mathrm{Tr}(F_\alpha \hat{F}_\beta) = \delta_{\alpha\beta}$, $(\alpha, \beta = 1, 2, .., N^2 - 1)$, and $c_{\alpha\beta}$ is positive semidefinite matrix.

Proof. To proof Eq. (A.3) we will follow Refs. [46, 50, 52]. Let us consider a complete basis of orthonormal operators $\hat{F}_\alpha, \alpha = 0, 1, .., N^2 - 1$. Such a basis set is purposely chosen so that

$$\hat{F}_0 = \frac{1}{\sqrt{N}}\mathbb{1}. \tag{A.4}$$

In this basis set, the Kraus operators appearing in the Kraus operator sum representation (KOSR) $\hat{\rho}(t) = \sum_\beta \hat{M}_\beta(t,s)\hat{\rho}(s)\hat{M}_\beta^\dagger(t,s)$, cf. Sect. 3.2.3 may be expanded as

$$\begin{aligned}\hat{M}_\beta &= \sum_{\alpha=0}^{N^2} \hat{F}_\alpha \langle \hat{F}_\alpha | \hat{M}_\beta \rangle, \\ &= \sum_{\alpha=0}^{N^2} \hat{F}_\alpha \mathrm{Tr}[\hat{F}_\alpha \hat{M}_\beta], \\ &= \frac{1}{N}\mathrm{Tr}(M_\beta)\mathbb{1} + \sum_{\alpha=1}^{N^2-1} \hat{F}_\alpha \mathrm{Tr}[\hat{F}_\alpha^\dagger \hat{M}_\beta].\end{aligned} \tag{A.5}$$

By inserting this in KOSR, we get

$$\hat{\rho}(t) = g\hat{\rho}(s) + F\hat{\rho}(s) + \hat{\rho}(s)F + \sum_{\beta\lambda} a_{\beta\lambda}\hat{F}_\beta\hat{\rho}(s)\hat{F}_\lambda^\dagger, \tag{A.6}$$

where the following short notations

$$\begin{aligned} g &= \frac{1}{N^2-1}\sum_\alpha |\mathrm{Tr}\hat{M}_\alpha|^2, \\ F &= \frac{1}{N}\sum_{\alpha\beta} \mathrm{Tr}\hat{M}_\alpha^\dagger \mathrm{Tr}[\hat{F}_\beta^\dagger \hat{M}_\alpha]\hat{F}_\beta, \\ a_{\beta\lambda} &= \sum_\alpha \mathrm{Tr}[\hat{F}_\beta^\dagger \hat{M}_\alpha]\mathrm{Tr}[\hat{M}_\alpha^\dagger \hat{F}_\lambda], \end{aligned} \tag{A.7}$$

have been introduced. The time derivative of Eq. (A.6) with respect to t at $t = s$ yields

$$\begin{aligned}\dot{\rho} &= \dot{g}\rho + \dot{F}\rho + \rho\dot{F} + \sum_{\beta\lambda} \dot{a}_{\beta\lambda}\hat{F}_\beta\rho\hat{F}_\lambda^\dagger, \\ &= -\mathrm{i}[H,\rho] + K\rho + \rho K + \sum_{\beta\lambda} c_{\beta\lambda}\hat{F}_\beta\rho\hat{F}_\lambda^\dagger,\end{aligned} \tag{A.8}$$

where the following Hermitian operators H and K, and the coefficients $c_{\alpha\beta}$ have been defined

$$\begin{cases} H &= \frac{1}{2\mathrm{i}}\left(\dot{F}^\dagger - \dot{F}\right), \\ K &= \frac{1}{2}\left(\dot{g}\mathbb{1} + \dot{F}^\dagger + \dot{F}\right), \\ c_{\beta\lambda} &= \dot{a}_{\beta\lambda} \end{cases} \tag{A.9}$$

By drawing on the trace-preserving property of the generator, the Hermitian operator K can be obtained:

$$\begin{aligned} \mathrm{Tr}\dot{\rho} &= \mathrm{Tr}\left[2K\rho + \sum_{\beta\lambda} c_{\beta\lambda}\mathrm{Tr}(\hat{F}_\beta \rho \hat{F}_\lambda^\dagger\right], \\ &= \mathrm{Tr}\left(2K + \sum_{\beta\lambda} c_{\beta\lambda}\hat{F}_\lambda \hat{F}_\beta^\dagger\right), \\ &= 0, \end{aligned} \tag{A.10}$$

This implies that

$$K = -\frac{1}{2}\sum_{\beta\lambda} c_{\beta\lambda}\hat{F}_\lambda \hat{F}_\beta^\dagger), \tag{A.11}$$

from which follows immediately the generator of QDS after renaming the indices $\beta \to \alpha, \quad \lambda \to \beta$

$$\mathcal{L}\rho = -\mathrm{i}[H,\rho] + \sum_{\alpha\beta} c_{\alpha\beta}\left(F_\alpha \rho \hat{F}_\beta^\dagger - \frac{1}{2}F_\alpha \hat{F}_\beta^\dagger \rho - \frac{1}{2}\rho F_\alpha \hat{F}_\beta^\dagger\right), \tag{A.12}$$

□

B Equations of Motion for the Correlators in Coupled-Cavity Arrays

This chapter is intented to give a detailed derivation of the equations of the motion for the correlators in coupled-cavity arrays. The equation of motion of a given correlation function $\langle \hat{G} \rangle$ reads as

$$\frac{d}{dt}\langle \hat{G} \rangle = -\mathrm{i}\langle [\hat{H}, \hat{G}] \rangle + \mathcal{D}_P[\hat{G}] + \mathcal{D}_\kappa[\hat{G}] + \mathcal{D}_\kappa[\hat{G}], \tag{B.1}$$

where

$$\begin{aligned}
\mathcal{D}_P[\hat{G}] &= \sum_\alpha P_\alpha \left\{ \langle \hat{\sigma}_\alpha \hat{G} \hat{\sigma}_\alpha^\dagger \rangle - \frac{1}{2}\langle \hat{\sigma}_\alpha \sigma_\alpha^\dagger \hat{G} \rangle - \frac{1}{2}\langle \hat{G} \hat{\sigma}_\alpha \sigma_\alpha^\dagger \rangle \right\}, \\
\mathcal{D}_\gamma[\hat{G}] &= \sum_\alpha \gamma_\alpha \left\{ \langle \hat{\sigma}_\alpha^\dagger \hat{G} \hat{\sigma}_\alpha \rangle - \frac{1}{2}\langle \hat{\sigma}_\alpha^\dagger \sigma_\alpha \hat{G} \rangle - \frac{1}{2}\langle \hat{G} \hat{\sigma}_\alpha^\dagger \sigma_\alpha \rangle \right\}, \\
\mathcal{D}_\kappa[\hat{G}] &= \sum_\alpha \kappa_\alpha \left\{ \langle \hat{b}_\alpha^\dagger \hat{G} \hat{b}_\alpha \rangle - \frac{1}{2}\langle \hat{b}_\alpha^\dagger b_\alpha \hat{G} \rangle - \frac{1}{2}\langle \hat{G} \hat{b}_\alpha^\dagger b_\alpha \rangle \right\}, \\
\hat{H} &= \sum_{\alpha\beta} t_{\alpha\beta} \hat{b}_\alpha^\dagger \hat{b}_\beta + \sum_\alpha \varepsilon_\alpha \hat{\sigma}_\alpha^\dagger \hat{\sigma}_\alpha + \sum_\alpha \left(g_\alpha \hat{b}_\alpha^\dagger \hat{\sigma}_\alpha + g_\alpha^* \hat{b}_\alpha \hat{\sigma}_\alpha^\dagger \right).
\end{aligned} \tag{B.2}$$

We start the derivation of the equations of motion (EoM) with the expectation value of the photonic quadratic product which we denote $n_{\alpha\beta} = \langle \hat{b}_\alpha^\dagger \hat{b}_\beta \rangle$.

EoM for $n_{\alpha\beta} = \langle \hat{b}_\alpha^\dagger \hat{b}_\beta \rangle$

- Photonic Hamiltonian

$$\begin{aligned}
[\hat{b}_\alpha^\dagger \hat{b}_\beta, \hat{b}_{\alpha'}^\dagger \hat{b}_{\beta'}] &= \hat{b}_\alpha^\dagger [\hat{b}_\beta, \hat{b}_{\alpha'}^\dagger] \hat{b}_{\beta'} + \hat{b}_{\alpha'}^\dagger [\hat{b}_\alpha^\dagger, \hat{b}_{\beta'}] \hat{b}_j \\
&= \hat{b}_\alpha^\dagger \hat{b}_{\beta'} \delta_{\alpha'\beta} - \hat{b}_{\alpha'}^\dagger \hat{b}_\beta \delta_{\alpha\beta'},
\end{aligned} \tag{B.3}$$

$$\boxed{-\mathrm{i} \sum_{\alpha'\beta'} t_{\alpha'\beta'} \langle [\hat{b}_\alpha^\dagger \hat{b}_\beta, \hat{b}_{\alpha'}^\dagger \hat{b}_{\beta'}] \rangle = \mathrm{i} \sum_{\alpha'} \left(t_{\alpha\alpha'}^* n_{\alpha'\beta} - n_{\alpha\alpha'} t_{\alpha'\beta}^* \right).} \tag{B.4}$$

Here $t_{\alpha\beta}^*$ is the complex conjugation of $t_{\alpha\beta}$

- The light-matter coupling Hamiltonian

$$\begin{aligned}[\hat{b}_\alpha^\dagger \hat{b}_\beta, \hat{b}_{\alpha'}^\dagger \hat{\sigma}_{\alpha'}] &= \hat{b}_\alpha^\dagger [\hat{b}_\beta, \hat{b}_{\alpha'}^\dagger] \hat{\sigma}_{\alpha'} \\ &= \hat{b}_\alpha^\dagger \hat{\sigma}_{\alpha'} \delta_{\beta\alpha'}.\end{aligned} \tag{B.5}$$

$$\boxed{-\mathrm{i} \sum_{\alpha'} \langle [\hat{b}_\alpha^\dagger \hat{b}_\beta, g_{\alpha'} \hat{b}_{\alpha'}^\dagger \hat{\sigma}_{\alpha'} + g_{\alpha'}^* \hat{b}_{\alpha'} \hat{\sigma}_{\alpha'}^\dagger] \rangle = -\mathrm{i} g_\beta \langle \hat{b}_\alpha^\dagger \hat{\sigma}_\beta \rangle + \mathrm{i} g_\alpha^* \langle \hat{b}_\beta \hat{\sigma}_\alpha^\dagger \rangle} \tag{B.6}$$

The only dissipation channel for the photonic product is the cavity loss:

$$\boxed{\mathcal{D}_\kappa [\hat{b}_\alpha^\dagger \hat{b}_\beta] = -\frac{1}{2} \left(\kappa_\alpha + \kappa_\beta \right) \langle \hat{b}_\alpha^\dagger \hat{b}_\beta \rangle} \tag{B.7}$$

By denoting $\psi_{\alpha\beta} = -\mathrm{i} g_\beta \langle \hat{b}_\alpha^\dagger \hat{\sigma}_\beta \rangle$ which encodes the inter-cavity photon-assisted polarization, the EoM for the photonic product reads

$$\boxed{\frac{\partial}{\partial t} n_{\alpha\beta} = \mathrm{i} \sum_{\alpha'} \left(t_{\alpha\alpha'}^* n_{\alpha'\beta} - n_{\alpha\alpha'} t_{\alpha'\beta}^* \right) - \frac{1}{2} \left(\kappa_\alpha + \kappa_\beta \right) \langle \hat{b}_\alpha^\dagger \hat{b}_\beta \rangle + \psi_{\alpha\beta} + \psi_{\beta\alpha}^*} \tag{B.8}$$

EoM for $\psi_{\alpha\beta} = -\mathrm{i} g_\beta \langle \hat{b}_\alpha^\dagger \hat{\sigma}_\beta \rangle$

- Photonic Hamiltonian

$$\begin{aligned}[\hat{b}_\alpha^\dagger \hat{\sigma}_\beta, \hat{b}_{\alpha'}^\dagger \hat{b}_{\beta'}] &= \hat{b}_{\alpha'}^\dagger [\hat{b}_\alpha^\dagger, \hat{b}_{\beta'}] \hat{\sigma}_\beta \\ &= -\hat{b}_{\alpha'}^\dagger \hat{\sigma}_\beta \delta_{\alpha\beta'}\end{aligned} \tag{B.9}$$

$$\boxed{-\mathrm{i} \sum_{\alpha'\beta'} t_{\alpha'\beta'} \langle [\hat{b}_\alpha^\dagger \hat{\sigma}_\beta, \hat{b}_{\alpha'}^\dagger \hat{b}_{\beta'}] \rangle = \mathrm{i} \sum_{\alpha'} t_{\alpha'\alpha} \langle \hat{b}_{\alpha'}^\dagger \hat{\sigma}_\beta \rangle = -g_\beta^{-1} \sum_{\alpha'} t_{\alpha\alpha'}^* \psi_{\alpha'\beta}} \tag{B.10}$$

- Light-matter Hamiltonian

$$\begin{aligned}[\hat{b}_\alpha^\dagger \hat{\sigma}_\beta, \hat{b}_{\alpha'} \hat{\sigma}_{\alpha'}^\dagger] &= \hat{b}_\alpha^\dagger \hat{b}_{\alpha'} [\hat{\sigma}_\beta, \hat{\sigma}_{\alpha'}^\dagger] + [\hat{b}_\alpha^\dagger, \hat{b}_{\alpha'}] \hat{\sigma}_{\alpha'}^\dagger \hat{\sigma}_\beta \\ &= \hat{b}_\alpha^\dagger \hat{b}_{\alpha'} (1 - 2\hat{\sigma}_\beta^\dagger \hat{\sigma}_\beta) \delta_{\beta\alpha'} - \delta_{\alpha\alpha'} \hat{\sigma}_{\alpha'}^\dagger \hat{\sigma}_\beta\end{aligned} \tag{B.11}$$

$$\boxed{-\mathrm{i} \sum_{\alpha'} g_{\alpha'}^* \langle [\hat{b}_\alpha^\dagger \hat{\sigma}_\beta, \hat{b}_{\alpha'} \hat{\sigma}_{\alpha'}^\dagger] \rangle = \mathrm{i} g_\alpha^\dagger \langle \hat{\sigma}_\alpha^\dagger \hat{\sigma}_\beta \rangle + \mathrm{i} g_\beta^* \langle \hat{b}_\alpha^\dagger \hat{b}_\beta (2\hat{\sigma}_\beta^\dagger \hat{\sigma}_\beta - 1) \rangle} \tag{B.12}$$

- Pump term

$$\begin{aligned}[\hat{b}_\alpha^\dagger\hat{\sigma}_\beta, \hat{\sigma}_{\alpha'}^\dagger] &= \hat{b}_\alpha^\dagger\hat{\sigma}_\beta\hat{\sigma}_{\alpha'}^\dagger - \hat{b}_\alpha^\dagger\hat{\sigma}_{\alpha'}^\dagger\hat{\sigma}_\beta, \\ &= \hat{b}_\alpha^\dagger(1 - 2\hat{\sigma}_\beta^\dagger\hat{\sigma}_\beta)\delta_{\beta\alpha'}\end{aligned} \tag{B.13}$$

$$\boxed{\mathcal{D}_P[\hat{b}_\alpha^\dagger\hat{\sigma}_\beta] = -\frac{1}{2}P_\beta\langle\hat{b}_\alpha^\dagger\hat{\sigma}_\beta\rangle} \tag{B.14}$$

- Dephasing term

$$\boxed{\mathcal{D}_\gamma[\hat{b}_\alpha^\dagger, \hat{\sigma}_\beta] = -\frac{\gamma_\beta}{2}\langle\hat{b}_\alpha^\dagger\hat{\sigma}_\beta\rangle} \tag{B.15}$$

- Cavity loss part

$$\boxed{\mathcal{D}_\kappa[\hat{b}_\alpha^\dagger\hat{\sigma}_\beta] = -\frac{\kappa_\alpha}{2}\langle\hat{b}_\alpha^\dagger\hat{\sigma}_\beta\rangle} \tag{B.16}$$

Denote

$$f_{ij} = \langle\hat{\sigma}_\alpha^\dagger\hat{\sigma}_\beta\rangle, \tag{B.17a}$$

$$\varphi_{\alpha\beta} = \langle\hat{b}_\alpha^\dagger\hat{b}_\beta\hat{\sigma}_\beta^\dagger\hat{\sigma}_\beta\rangle, \tag{B.17b}$$

$$\lambda_\beta = \gamma_\beta + P_\beta \tag{B.17c}$$

and we obtain

$$\boxed{\frac{\partial}{\partial t}\psi_{\alpha\beta} = \mathrm{i}\sum_{\alpha'} t^*_{\alpha\alpha'}\psi_{\alpha'\beta} + g^*_\alpha g_\beta f_{\alpha\beta} + |g_\beta|^2\left(2\varphi_{\alpha\beta} - n_{\alpha\beta}\right) - \frac{1}{2}\left(\kappa_\alpha + \lambda_\beta\right)\psi_{\alpha\beta}} \tag{B.18}$$

EoM for $f_{\alpha\beta} = \langle\hat{\sigma}_\alpha^\dagger\hat{\sigma}_\beta\rangle$ In a similar fashion, we obtain

$$\boxed{\frac{\partial}{\partial t}f_{\alpha\beta} = -\frac{1}{2}\left(\lambda_\alpha + \lambda_\beta\right)f_{\alpha\beta} + \frac{g_\alpha}{g_\beta}\left(2\varrho_{\alpha\beta} - \psi_{\alpha\beta}\right) + \frac{g^*_\beta}{g^*_\alpha}\left(2\varrho^*_{\beta\alpha} - \psi^*_{\beta\alpha}\right) + \delta_{ij}[P_i - 2(\varrho_{ii} + \bar{\varrho}_{ii})]} \tag{B.19}$$

Here $\varrho_{\alpha\beta} = -\mathrm{i}g_\beta\langle\hat{b}_\alpha^\dagger\hat{\sigma}_\beta\hat{\sigma}_\alpha^\dagger\hat{\sigma}_\alpha\rangle$

To obtain a closed set of EoMs, the following factorizations have been performed

$$\begin{aligned}\langle\hat{b}_\alpha^\dagger\hat{b}_\beta\hat{\sigma}_\nu^\dagger\hat{\sigma}_\nu\rangle &\approx \langle\hat{b}_\alpha^\dagger\hat{b}_\beta\rangle\langle\hat{\sigma}_\nu^\dagger\hat{\sigma}_\nu\rangle = n_{\alpha\beta}f_\nu, \\ \langle\hat{b}_\alpha^\dagger\hat{\sigma}_\beta\hat{\sigma}_\nu^\dagger\hat{\sigma}_\nu\rangle &\approx \langle\hat{b}_\alpha^\dagger\hat{\sigma}_\beta\rangle\langle\hat{\sigma}_\nu^\dagger\hat{\sigma}_\nu\rangle = \psi_{\alpha\beta}f_\nu.\end{aligned} \tag{B.20}$$

Bibliography

[1] E. M. Purcell. Spontaneous emission probability at radio frequencies. *Phys. Rev.*, 69:681, 1946.

[2] J. M. Raimond, M. Brune, and S. Haroche. Manipulating quantum entanglement with atoms and photons in a cavity. *Reviews of Modern Physics*, 73(3):565–582, August 2001.

[3] J. I. Cirac, P. Zoller, H. J. Kimble, and H. Mabuchi. Quantum State Transfer and Entanglement Distribution among Distant Nodes in a Quantum Network. *Physical Review Letters*, 78(16):3221–3224, April 1997.

[4] L.-M. Duan and H. J. Kimble. Scalable Photonic Quantum Computation through Cavity-Assisted Interactions. *Physical Review Letters*, 92(12):127902, March 2004.

[5] H. Mabuchi and A. C. Doherty. Cavity Quantum Electrodynamics: Coherence in Context. *Science*, 298(5597):1372–1377, November 2002.

[6] A. Imamog¯lu, D. D. Awschalom, G. Burkard, D. P. DiVincenzo, D. Loss, M. Sherwin, and A. Small. Quantum Information Processing Using Quantum Dot Spins and Cavity QED. *Physical Review Letters*, 83(20):4204–4207, November 1999.

[7] Hatice Altug, Dirk Englund, and Jelena Vučković. Ultrafast photonic crystal nanocavity laser. *Nature Physics*, 2(7):484–488, July 2006.

[8] Yoshitaka Kurosaka, Seita Iwahashi, Yong Liang, Kyosuke Sakai, Eiji Miyai, Wataru Kunishi, Dai Ohnishi, and Susumu Noda. On-chip beam-steering photonic-crystal lasers. *Nature Photonics*, 4(7):447–450, July 2010.

[9] Kengo Nozaki, Akihiko Shinya, Shinji Matsuo, Yasumasa Suzaki, Toru Segawa, Tomonari Sato, Yoshihiro Kawaguchi, Ryo Takahashi, and Masaya Notomi. Ultralow-power all-optical RAM based on nanocavities. *Nature Photonics*, 6(4):248–252, April 2012.

[10] Liu Liu, Rajesh Kumar, Koen Huybrechts, Thijs Spuesens, Günther Roelkens, Erik-Jan Geluk, Tjibbe de Vries, Philippe Regreny, Dries Van Thourhout, Roel Baets, and Geert Morthier. An ultra-small, low-power, all-optical flip-flop memory on a silicon chip. *Nature Photonics*, 4(3):182–187, March 2010.

[11] Matthew Pelton, Charles Santori, Jelena Vucković, Bingyang Zhang, Glenn S. Solomon, Jocelyn Plant, and Yoshihisa Yamamoto. Efficient Source of Single Photons: A Single Quantum Dot in a Micropost Microcavity. *Physical Review Letters*, 89(23):233602, November 2002.

[12] J. P. Reithmaier, G. Sęk, A. Löffler, C. Hofmann, S. Kuhn, S. Reitzenstein, L. V. Keldysh, V. D. Kulakovskii, T. L. Reinecke, and A. Forchel. Strong coupling in a single quantum dot–semiconductor microcavity system. *Nature*, 432(7014):197–200, November 2004.

[13] E. Peter, P. Senellart, D. Martrou, A. Lemaître, J. Hours, J. M. Gérard, and J. Bloch. Exciton-Photon Strong-Coupling Regime for a Single Quantum Dot Embedded in a Microcavity. *Physical Review Letters*, 95(6):067401, August 2005.

[14] P. Michler, A. Kiraz, C. Becher, W. V. Schoenfeld, P. M. Petroff, Lidong Zhang, E. Hu, and A. Imamoglu. A Quantum Dot Single-Photon Turnstile Device. *Science*, 290(5500):2282–2285, December 2000.

[15] Antonio Badolato, Kevin Hennessy, Mete Atatüre, Jan Dreiser, Evelyn Hu, Pierre M. Petroff, and Atac Imamoğlu. Deterministic Coupling of Single Quantum Dots to Single Nanocavity Modes. *Science*, 308(5725):1158–1161, May 2005.

[16] T. Yoshie, A. Scherer, J. Hendrickson, G. Khitrova, H. M. Gibbs, G. Rupper, C. Ell, O. B. Shchekin, and D. G. Deppe. Vacuum Rabi splitting with a single quantum dot in a photonic crystal nanocavity. *Nature*, 432(7014):200–203, November 2004.

[17] S. Strauf, K. Hennessy, M. T. Rakher, Y.-S. Choi, A. Badolato, L. C. Andreani, E. L. Hu, P. M. Petroff, and D. Bouwmeester. Self-Tuned Quantum Dot Gain in Photonic Crystal Lasers. *Physical Review Letters*, 96(12):127404, March 2006.

[18] S. M. Ulrich, C. Gies, S. Ates, J. Wiersig, S. Reitzenstein, C. Hofmann, A. Löffler, A. Forchel, F. Jahnke, and P. Michler. Photon Statistics of Semiconductor Microcavity Lasers. *Physical Review Letters*, 98(4):043906, January 2007.

[19] S. Reitzenstein, A. Bazhenov, A. Gorbunov, C. Hofmann, S. Münch, A. Löffler, M. Kamp, J. P. Reithmaier, V. D. Kulakovskii, and A. Forchel. Lasing in high-Q quantum-dot micropillar cavities. *Applied Physics Letters*, 89(5):051107, July 2006.

[20] Masahiro Nomura, Naoto Kumagai, Satoshi Iwamoto, Yasutomo Ota, and Yasuhiko Arakawa. Laser oscillation in a strongly coupled single-quantum-dot–nanocavity system. *Nature Physics*, 6:279–283, 2010.

[21] Z. G. Xie, S. Götzinger, W. Fang, H. Cao, and G. S. Solomon. Influence of a Single Quantum Dot State on the Characteristics of a Microdisk Laser. *Physical Review Letters*, 98(11):117401, March 2007.

[22] S. Reitzenstein, C. Böckler, A. Bazhenov, A. Gorbunov, A. Löffler, M. Kamp, V. D. Kulakovskii, and A. Forchel. Single quantum dot controlled lasing effects in high-Q micropillar cavities. *Optics Express*, 16(7):4848–4857, March 2008.

[23] M. J. Hartmann, F. G. S. L. Brandão, and M. B. Plenio. Quantum many-body phenomena in coupled cavity arrays. *Laser & Photonics Reviews*, 2(6):527–556, December 2008.

[24] Dimitris G. Angelakis, Marcelo Franca Santos, and Sougato Bose. Photon-blockade-induced Mott transitions and XY spin models in coupled cavity arrays. *Physical Review A*, 76(3):031805, September 2007.

[25] Michael J. Hartmann, Fernando G. S. L. Brandão, and Martin B. Plenio. Strongly interacting polaritons in coupled arrays of cavities. *Nature Physics*, 2(12):849–855, December 2006.

[26] Dimitris G. Angelakis and Alastair Kay. Weaving light-matter qubits into a one way quantum computer. *New Journal of Physics*, 10(2):023012, 2008.

[27] Guilherme M. A. Almeida, Francesco Ciccarello, Tony J. G. Apollaro, and Andre M. C. Souza. Quantum-state transfer in staggered coupled-cavity arrays. *Physical Review A*, 93(3):032310, March 2016.

[28] Mark Fox. *Quantum Optics, An Introduction*. Oxford University Press, 2006.

[29] Alexey V. Kavokin, Jeremy J. Baumberg, Guillaume Malpuech, and Fabrice P. Laussy. *Microcavities*. Oxford University Press, 2007.

[30] Masahiro Nomura, Naoto Kumagai, Satoshi Iwamoto, Yasutomo Ota, and Yasuhiko Arakawa. Photonic crystal nanocavity laser with a single quantum dot gain. *Optics Express*, 17(18):15975–15982, August 2009.

[31] K. Hennessy, A. Badolato, M. Winger, D. Gerace, M. Atatüre, S. Gulde, S. Fält, E. L. Hu, and A. Imamoğlu. Quantum nature of a strongly coupled single quantum dot–cavity system. *Nature*, 445(7130):896–899, February 2007.

[32] Y. Yamamoto, F. Tassone, and H. Cao. *Semiconductor Cavity Quantum Electrodynmics*. Srpinger, 2000.

[33] Daniel Kleppner. Inhibited Spontaneous Emission. *Physical Review Letters*, 47(4):233–236, July 1981.

[34] Karl H. Drexhage. IV Interaction of Light with Monomolecular Dye Layers. In E. Wolf, editor, *Progress in Optics*, volume 12, pages 163–232. Elsevier, January 1974.

[35] Y.-S. Choi, M. T. Rakher, K. Hennessy, S. Strauf, A. Badolato, P. M. Petroff, D. Bouwmeester, and E. L. Hu. Evolution of the onset of coherence in a family of photonic crystal nanolasers. *Applied Physics Letters*, 91(3):031108, July 2007.

[36] G. S. Solomon, M. Pelton, and Y. Yamamoto. Single-mode Spontaneous Emission from a Single Quantum Dot in a Three-Dimensional Microcavity. *Physical Review Letters*, 86(17):3903–3906, April 2001.

[37] S. Reitzenstein and A. Forchel. Quantum dot micropillars. *Journal of Physics D: Applied Physics*, 43(3):033001, 2010.

[38] Lucio Claudio Andreani, Giovanna Panzarini, and Jean-Michel Gérard. Strong-coupling regime for quantum boxes in pillar microcavities: Theory. *Physical Review B*, 60(19):13276–13279, November 1999.

[39] S. Rudin and T. L. Reinecke. Oscillator model for vacuum Rabi splitting in microcavities. *Physical Review B*, 59(15):10227–10233, April 1999.

[40] L. V. Keldysh, V. D. Kulakovskii, S. Reitzenstein, M. N. Makhonin, and A. Forchel. Interference effects in the emission spectra of quantum dots in high-quality cavities. *JETP Letters*, 84(9):494–499, January 2007.

[41] M. B. Plenio, S. F. Huelga, A. Beige, and P. L. Knight. Cavity-loss-induced generation of entangled atoms. *Physical Review A*, 59(3):2468–2475, March 1999.

[42] H. J. Kimble. The quantum internet, June 2008.

[43] Darrick E. Chang, Anders S. Sørensen, Eugene A. Demler, and Mikhail D. Lukin. A single-photon transistor using nanoscale surface plasmons. *Nature Physics*, 3(11):807–812, November 2007.

[44] Andreas Reinhard, Thomas Volz, Martin Winger, Antonio Badolato, Kevin J. Hennessy, Evelyn L. Hu, and Ataç Imamoğlu. Strongly correlated photons on a chip. *Nature Photonics*, 6(2):93–96, February 2012.

[45] E. Asplund. *Control of open quantum systems: A theoretical Approach to control of Surface Photochemistry*. PhD thesis, Oldenburg, 2011.

[46] G. Lindblad. On the generators of quantum dynamical semigroups. *Communications in Mathematical Physics*, 48(2):119–130, June 1976.

[47] Julio T. Barreiro, Markus Müller, Philipp Schindler, Daniel Nigg, Thomas Monz, Michael Chwalla, Markus Hennrich, Christian F. Roos, Peter Zoller, and Rainer Blatt. An open-system quantum simulator with trapped ions. *Nature*, 470(7335):486–491, February 2011.

[48] Robert Alicki and K. Lendi. *Quantum Dynamical Semigroups and Applications*. Springer, 1987.

[49] Ian Percival. *Quantum State Diffusion*. Cambridge University Press, December 1998. Google-Books-ID: AlXSmZTHxtwC.

[50] Vittorio Gorini, Andrzej Kossakowski, and E. C. G. Sudarshan. Completely positive dynamical semigroups of N level systems. *Journal of Mathematical Physics*, 17(5):821–825, May 1976.

[51] K. Hornberger. Monitoring approach to open quantum dynamics using scattering theory. *EPL (Europhysics Letters)*, 77(5):50007, 2007.

[52] H. P. Breuer and F. Petruccione. *The Theory of Open Quantum Systems*. Oxford University Press, 2002.

[53] Peter Lambropoulos and David Petrosyan. *Fundamentals of Quantum Optics and Quantum Inofrmation*. Springer-Verlag Berlin Heidelberg, 2007.

[54] Ángel Rivas and Susana F. Huelga. *Open Quantum Systems: An Introduction*. Springer Science & Business Media, October 2011. Google-Books-ID: FGCuYsIZAA0C.

[55] Gernot Schaller. *Open Quantum Systems Far from Equilibrium*. Springer, January 2014. Google-Books-ID: deS5BQAAQBAJ.

[56] A. Kossakowski. On quantum statistical mechanics of non-Hamiltonian systems. *Reports on Mathematical Physics*, 3(4):247–274, December 1972.

[57] Ronnie Kosloff, Mark A. Ratner, and William B. Davis. Dynamics and relaxation in interacting systems: Semigroup methods. *The Journal of Chemical Physics*, 106(17):7036–7043, May 1997.

[58] M. Grundmann, O. Stier, and D. Bimberg. InAs/GaAs pyramidal quantum dots: Strain distribution, optical phonons, and electronic structure. *Physical Review B*, 52(16):11969–11981, October 1995.

[59] Weidong Sheng, Shun-Jen Cheng, and Pawel Hawrylak. Multiband theory of multi-exciton complexes in self-assembled quantum dots. *Physical Review B*, 71(3):035316, January 2005.

[60] C. Cornet, A. Schliwa, J. Even, F. Doré, C. Celebi, A. Létoublon, E. Macé, C. Paranthoën, A. Simon, P. M. Koenraad, N. Bertru, D. Bimberg, and S. Loualiche. Electronic and optical properties of InAs/InP quantum dots on InP(100) and InP(311)B substrates: Theory and experiment. *Physical Review B*, 74(3):035312, July 2006.

[61] O. Stier. *Electronic and optical properties of quantum dots and wires. PhD thesis, 2000,*. PhD thesis, Technische Universität Berlin, Berlin, 2000.

[62] O. Stier, M. Grundmann, and D. Bimberg. Electronic and optical properties of strained quantum dots modeled by 8-band k\ensuremath{\cdot}p theory. *Physical Review B*, 59(8):5688–5701, February 1999.

[63] S. Schulz and G. Czycholl. Tight-binding model for semiconductor nanostructures. *Physical Review B*, 72(16):165317, October 2005.

[64] S. Schulz, S. Schumacher, and G. Czycholl. Tight-binding model for semiconductor quantum dots with a wurtzite crystal structure: From one-particle properties to Coulomb correlations and optical spectra. *Physical Review B*, 73(24):245327, June 2006.

[65] M. Bayer, O. Stern, P. Hawrylak, S. Fafard, and A. Forchel. Hidden symmetries in the energy levels of excitonic 'artificial atoms'. *Nature*, 405(6789):923–926, June 2000.

[66] U. Hohenester and E. Molinari. Role of Coulomb Correlations in the Optical Spectra of Semiconductor Quantum Dots. *physica status solidi (b)*, 221(1):19–24, September 2000.

[67] U. Merkt, J. Huser, and M. Wagner. Energy spectra of two electrons in a harmonic quantum dot. *Physical Review B*, 43(9):7320–7323, March 1991.

[68] Fanyao Qu and Pawel Hawrylak. Magnetic Exchange Interactions in Quantum Dots Containing Electrons and Magnetic Ions. *Physical Review Letters*, 95(21):217206, November 2005.

[69] T. R. Nielsen, P. Gartner, and F. Jahnke. Many-body theory of carrier capture and relaxation in semiconductor quantum-dot lasers. *Physical Review B*, 69(23):235314, June 2004.

[70] Walter Hoyer, Mackillo Kira, and Stephan W. Koch. Influence of Coulomb and phonon interaction on the exciton formation dynamics in semiconductor heterostructures. *Physical Review B*, 67(15):155113, April 2003.

[71] N. Baer, C. Gies, J. Wiersig, and F. Jahnke. Luminescence of a semiconductor quantum dot system. *The European Physical Journal B*, 50(3):411–418, April 2006.

[72] Hartmut Haug and Stephan W. Koch. *Quantum Theory of the Optical and Electronic Properties of Semiconductors*. World Scientific, 2004.

[73] R. Ravinder. *Mathematical Methods of Quantum Optics*. Springer, Berlin, 2001.

[74] Crispin Gardiner and Peter Zoller. *The Quantum World of Ultra-Cold Atoms and Light Book I: Foundations of Quantum Optics*. Imperial College Press, May 2014.

[75] Crispin Gardiner and Peter Zoller. *The Quantum World of Ultra-Cold Atoms and Light Book II: The Physics of Quantum-Optical Devices*. Imperial College Press, June 2015.

[76] H. A. M. Leymann, A. Foerster, and J. Wiersig. Expectation value based equation-of-motion approach for open quantum systems: A general formalism. *Physical Review B*, 89(8):085308, February 2014.

[77] Thorsten Köhler and Keith Burnett. Microscopic quantum dynamics approach to the dilute condensed Bose gas. *Physical Review A*, 65(3):033601, February 2002.

[78] Alexander Carmele, Marten Richter, Weng W. Chow, and Andreas Knorr. Antibunching of Thermal Radiation by a Room-Temperature Phonon Bath: A Numerically Solvable Model for a Strongly Interacting Light-Matter-Reservoir System. *Physical Review Letters*, 104(15):156801, April 2010.

[79] M. Kira, F. Jahnke, and S. W. Koch. Quantum Theory of Secondary Emission in Optically Excited Semiconductor Quantum Wells. *Physical Review Letters*, 82(17):3544–3547, April 1999.

[80] Christopher Gies. *Theory for Light-Matter Interaction in Semiconductor Quantum Dots*. PhD thesis, Universtität Bremen, Bremen, 2007.

[81] Christopher Gies, Jan Wiersig, Michael Lorke, and Frank Jahnke. Semiconductor model for quantum-dot-based microcavity lasers. *Physical Review A*, 75(1):013803, January 2007.

[82] Jens Fricke. Transport Equations Including Many-Particle Correlations for an Arbitrary Quantum System: A General Formalism. *Annals of Physics*, 252(2):479–498, December 1996.

[83] T. Feldtmann, L. Schneebeli, M. Kira, and S. W. Koch. Quantum theory of light emission from a semiconductor quantum dot. *Physical Review B*, 73(15):155319, April 2006.

[84] M. Kira, F. Jahnke, W. Hoyer, and S. W. Koch. Quantum theory of spontaneous emission and coherent effects in semiconductor microstructures. *Progress in Quantum Electronics*, 23(6):189–279, November 1999.

[85] J. Seebeck, T. R. Nielsen, P. Gartner, and F. Jahnke. Polarons in semiconductor quantum dots and their role in the quantum kinetics of carrier relaxation. *Physical Review B*, 71(12):125327, March 2005.

[86] R. Bonifacio and L. A. Lugiato. Cooperative radiation processes in two-level systems: Superfluorescence. *Physical Review A*, 11(5):1507–1521, May 1975.

[87] R. Bonifacio, P. Schwendimann, and Fritz Haake. Quantum Statistical Theory of Superradiance. I. *Physical Review A*, 4(1):302–313, July 1971.

[88] R. Bonifacio, P. Schwendimann, and Fritz Haake. Quantum Statistical Theory of Superradiance. II. *Physical Review A*, 4(3):854–864, September 1971.

[89] Vasily V. Temnov and Ulrike Woggon. Superradiance and Subradiance in an Inhomogeneously Broadened Ensemble of Two-Level Systems Coupled to a Low-Q Cavity. *Physical Review Letters*, 95(24):243602, December 2005.

[90] R. H. Dicke. Coherence in Spontaneous Radiation Processes. *Physical Review*, 93(1):99–110, January 1954.

[91] F. Jahnke, M. Kira, W. Hoyer, and S. W. Koch. Influence of Correlation Effects on the Excitonic Semiconductor Photoluminescence. *physica status solidi (b)*, 221(1):189–193, September 2000.

[92] M. Schwab, H. Kurtze, T. Auer, T. Berstermann, M. Bayer, J. Wiersig, N. Baer, C. Gies, F. Jahnke, J. P. Reithmaier, A. Forchel, M. Benyoucef, and P. Michler. Radiative emission dynamics of quantum dots in a single cavity micropillar. *Physical Review B*, 74(4):045323, July 2006.

[93] H. Yokoyama and S. D. Brorson. Rate equation analysis of microcavity lasers. *Journal of Applied Physics*, 66(10):4801–4805, November 1989.

[94] Y. Yamamoto, S. Machida, and G. Björk. Microcavity semiconductor laser with enhanced spontaneous emission. *Physical Review A*, 44(1):657–668, July 1991.

[95] Perry R. Rice and H. J. Carmichael. Photon statistics of a cavity-QED laser: A comment on the laser–phase-transition analogy. *Physical Review A*, 50(5):4318–4329, November 1994.

[96] Oliver Benson and Yoshihisa Yamamoto. Master-equation model of a single-quantum-dot microsphere laser. *Physical Review A*, 59(6):4756–4763, June 1999.

[97] Christian Wiele, Fritz Haake, and Yuri M. Golubev. Quantum-dot laser with periodic pumping. *Physical Review A*, 60(6):4986–4995, December 1999.

[98] I. E. Protsenko and M. Travagnin. Microscopic model of semiconductor laser without inversion. *Physical Review A*, 65(1):013801, December 2001.

[99] Weng W. Chow, Stephan W. Koch, and Murray III Sargent. *Semiconductor-Laser Physics*. Srpinger, Berlin, 1994.

[100] Frank Jahnke and Stephan W. Koch. Many-body theory for semiconductor microcavity lasers. *Physical Review A*, 52(2):1712–1727, August 1995.

[101] M. Travagnin. Effects of Pauli blocking on semiconductor laser intensity and phase noise spectra. *Physical Review A*, 64(1):013818, June 2001.

[102] Weng W. Chow, Frank Jahnke, and Christopher Gies. Emission properties of nanolasers during the transition to lasing. *Light: Science & Applications*, 3(8):e201, August 2014.

[103] Roy J. Glauber. Coherent and Incoherent States of the Radiation Field. *Physical Review*, 131(6):2766–2788, September 1963.

[104] Frank Jahnke, Christopher Gies, Marc Aßmann, Manfred Bayer, H. a. M. Leymann, Alexander Foerster, Jan Wiersig, Christian Schneider, Martin Kamp, and Sven Höfling. Giant photon bunching, superradiant pulse emission and excitation trapping in quantum-dot nanolasers. *Nature Communications*, 7:11540, May 2016.

[105] G. Timothy Noe Ii, Ji-Hee Kim, Jinho Lee, Yongrui Wang, Aleksander K. Wójcik, Stephen A. McGill, David H. Reitze, Alexey A. Belyanin, and Junichiro Kono. Giant superfluorescent bursts from a semiconductor magneto-plasma. *Nature Physics*, 8(3):219–224, March 2012.

[106] Armand Lebreton, Izo Abram, Rémy Braive, Nadia Belabas, Isabelle Sagnes, Francesco Marsili, Varun B. Verma, Sae Woo Nam, Thomas Gerrits, Isabelle Robert-Philip, Martin J. Stevens, and Alexios Beveratos. Pulse-to-pulse jitter measurement by photon correlation in high beta lasers. *Applied Physics Letters*, 106(3):031108, January 2015.

[107] Petru Tighineanu, Raphaël S. Daveau, Tau B. Lehmann, Harvey E. Beere, David A. Ritchie, Peter Lodahl, and Søren Stobbe. Single-Photon Superradiance from a Quantum Dot. *Physical Review Letters*, 116(16):163604, April 2016.

[108] Marc Aßmann, Franziska Veit, Manfred Bayer, Christopher Gies, Frank Jahnke, Stephan Reitzenstein, Sven Höfling, Lukas Worschech, and Alfred Forchel. Ultrafast tracking of second-order photon correlations in the emission of quantum-dot microresonator lasers. *Physical Review B*, 81(16):165314, April 2010.

[109] Melvin Lax. Quantum Noise. XI. Multitime Correspondence between Quantum and Classical Stochastic Processes. *Physical Review*, 172(2):350–361, August 1968.

[110] R. Hostein, A. Michon, G. Beaudoin, N. Gogneau, G. Patriache, J.-Y. Marzin, I. Robert-Philip, I. Sagnes, and A. Beveratos. Time-resolved characterization of InAsP/InP quantum dots emitting in the C-band telecommunication window. *Applied Physics Letters*, 93(7):073106, August 2008.

[111] A. Michon, R. Hostein, G. Patriarche, N. Gogneau, G. Beaudoin, A. Beveratos, I. Robert-Philip, S. Laurent, S. Sauvage, P. Boucaud, and I. Sagnes. Metal organic vapor phase epitaxy of InAsP/InP(001) quantum dots for 1.55 micrometers applications: Growth, structural, and optical properties. *Journal of Applied Physics*, 104(4):043504, August 2008.

[112] H. Marchand, P. Desjardins, S. Guillon, J.-E. Paultre, Z. Bougrioua, R. Y.-F. Yip, and R. A. Masut. Metalorganic vapor phase epitaxy of coherent self-assembled InAs nanometer-sized islands in InP(001). *Applied Physics Letters*, 71(4):527–529, July 1997.

[113] G. Saint-Girons, A. Michon, I. Sagnes, G. Beaudoin, and G. Patriarche. Thermodynamic description of the competition between quantum dots and quantum dashes during metalorganic vapor phase epitaxy in the InAs/InP(001)$ system: Experiment and theory. *Physical Review B*, 74(24):245305, December 2006.

[114] Galan Moody, Mawussey Segnon, Isabelle Sagnes, Rémy Braive, Alexios Beveratos, Isabelle Robert-Philip, Nadia Belabas, Frank Jahnke, Kevin L. Silverman, Richard P. Mirin, Martin J. Stevens, and Christopher Gies. Delayed formation of coherence in the emission dynamics of high-Q nanolasers. *Optica*, 5(4):395–401, April 2018.

[115] Edward B. Flagg, Sergey V. Polyakov, Tim Thomay, and Glenn S. Solomon. Dynamics of Nonclassical Light from a Single Solid-State Quantum Emitter. *Physical Review Letters*, 109(16):163601, October 2012.

[116] J. Wiersig, C. Gies, F. Jahnke, M. Aßmann, T. Berstermann, M. Bayer, C. Kistner, S. Reitzenstein, C. Schneider, S. Höfling, A. Forchel, C. Kruse, J. Kalden, and D. Hommel. Direct observation of correlations between individual photon emission events of a microcavity laser. *Nature*, 460(7252):245–249, July 2009.

[117] Christopher Gies, Jan Wiersig, and Frank Jahnke. Output Characteristics of Pulsed and Continuous-Wave-Excited Quantum-Dot Microcavity Lasers. *Physical Review Letters*, 101(6):067401, August 2008.

[118] T. Wang, G. P. Puccioni, and G. L. Lippi. How mesoscale lasers can answer fundamental questions related to nanolasers. In *Nanophotonics VI*, volume 9884, page 98840B. International Society for Optics and Photonics, April 2016.

[119] D. K. Armani, T. J. Kippenberg, S. M. Spillane, and K. J. Vahala. Ultra-high-Q toroid microcavity on a chip. *Nature*, 421(6926):925–928, February 2003.

[120] J. Liu, S. Ates, M. Lorke, J. Mørk, P. Lodahl, and S. Stobbe. A comparison between experiment and theory on few-quantum-dot nanolasing in a photonic-crystal cavity. *Optics Express*, 21(23):28507–28512, November 2013.

[121] C. Gies, F. Gericke, P. Gartner, S. Holzinger, C. Hopfmann, T. Heindel, J. Wolters, C. Schneider, M. Florian, F. Jahnke, S. Höfling, M. Kamp, and S. Reitzenstein. Strong light-matter coupling in the presence of lasing. *Physical Review A*, 96(2):023806, August 2017.

[122] Martin Winger, Thomas Volz, Guillaume Tarel, Stefano Portolan, Antonio Badolato, Kevin J. Hennessy, Evelyn L. Hu, Alexios Beveratos, Jonathan Finley, Vincenzo Savona, and Ataç Imamoğlu. Explanation of Photon Correlations in the Far-Off-Resonance Optical Emission from a Quantum-Dot–Cavity System. *Physical Review Letters*, 103(20):207403, November 2009.

[123] Matthias Florian, Paul Gartner, Alexander Steinhoff, Christopher Gies, and Frank Jahnke. Coulomb-assisted cavity feeding in nonresonant optical emission from a quantum dot. *Physical Review B*, 89(16):161302, April 2014.

[124] Mikkel Settnes, Per Kaer, Anders Moelbjerg, and Jesper Mork. Auger Processes Mediating the Nonresonant Optical Emission from a Semiconductor Quantum Dot Embedded Inside an Optical Cavity. *Physical Review Letters*, 111(6):067403, August 2013.

[125] C. Roy and S. Hughes. Influence of Electron–Acoustic-Phonon Scattering on Intensity Power Broadening in a Coherently Driven Quantum-Dot–Cavity System. *Physical Review X*, 1(2):021009, November 2011.

[126] A. Laucht, M. Kaniber, A. Mohtashami, N. Hauke, M. Bichler, and J. J. Finley. Temporal monitoring of nonresonant feeding of semiconductor nanocavity modes by quantum dot multiexciton transitions. *Physical Review B*, 81(24):241302, June 2010.

[127] N. Gregersen, T. Suhr, M. Lorke, and J. Mørk. Quantum-dot nano-cavity lasers with Purcell-enhanced stimulated emission. *Applied Physics Letters*, 100(13):131107, March 2012.

[128] S. Lichtmannecker, M. Florian, T. Reichert, M. Blauth, M. Bichler, F. Jahnke, J. J. Finley, C. Gies, and M. Kaniber. A few-emitter solid-state multi-exciton laser. *Scientific Reports*, 7(1):7420, August 2017.

[129] F. Gericke, M. Segnon, M. von Helversen, C. Hopfmann, T. Heindel, C. Schneider, S. Höfling, M. Kamp, A. Musiał, X Porte, C. Gies, and S. Reitzenstein. Controlling the gain contribution of background emitters in few-quantum-dot microlasers. *New Journal of Physics*, 20(2):023036, 2018.

[130] Matthias Florian, Paul Gartner, Christopher Gies, and Frank Jahnke. Phonon-mediated off-resonant coupling effects in semiconductor quantum-dot lasers. *New Journal of Physics*, 15(3):035019, 2013.

[131] Richard P. Feynman. Simulating physics with computers. *International Journal of Theoretical Physics*, 21(6):467–488, June 1982.

[132] H. S. J. van der Zant, F. C. Fritschy, W. J. Elion, L. J. Geerligs, and J. E. Mooij. Field-induced superconductor-to-insulator transitions in Josephson-junction arrays. *Physical Review Letters*, 69(20):2971–2974, November 1992.

[133] Alexander van Oudenaarden and J. E. Mooij. One-Dimensional Mott Insulator Formed by Quantum Vortices in Josephson Junction Arrays. *Physical Review Letters*, 76(26):4947–4950, June 1996.

[134] Matthew P. A. Fisher, G. Grinstein, and S. M. Girvin. Presence of quantum diffusion in two dimensions: Universal resistance at the superconductor-insulator transition. *Physical Review Letters*, 64(5):587–590, January 1990.

[135] Matthew P. A. Fisher, Peter B. Weichman, G. Grinstein, and Daniel S. Fisher. Boson localization and the superfluid-insulator transition. *Physical Review B*, 40(1):546–570, July 1989.

[136] C. Bruder, R. Fazio, and G. Schön. The Bose-Hubbard model: from Josephson junction arrays to optical lattices - Bruder - 2005 - Annalen der Physik - Wiley Online Library. August 2005.

[137] D. Jaksch, C. Bruder, J. I. Cirac, C. W. Gardiner, and P. Zoller. Cold Bosonic Atoms in Optical Lattices. *Physical Review Letters*, 81(15):3108–3111, October 1998.

[138] Markus Greiner, Olaf Mandel, Tilman Esslinger, Theodor W. Hänsch, and Immanuel Bloch. Quantum phase transition from a superfluid to a Mott insulator in a gas of ultracold atoms. *Nature*, 415(6867):39–44, January 2002.

[139] Belén Paredes, Artur Widera, Valentin Murg, Olaf Mandel, Simon Fölling, Ignacio Cirac, Gora V. Shlyapnikov, Theodor W. Hänsch, and Immanuel Bloch. Tonks–Girardeau gas of ultracold atoms in an optical lattice. *Nature*, 429(6989):277–281, May 2004.

[140] D. Jaksch, H.-J. Briegel, J. I. Cirac, C. W. Gardiner, and P. Zoller. Entanglement of Atoms via Cold Controlled Collisions. *Physical Review Letters*, 82(9):1975–1978, March 1999.

[141] Hatice Altug and Jelena Vučković. Two-dimensional coupled photonic crystal resonator arrays. *Applied Physics Letters*, 84(2):161–163, January 2004.

[142] Andrew D. Greentree, Charles Tahan, Jared H. Cole, and Lloyd C. L. Hollenberg. Quantum phase transitions of light. *Nature Physics*, 2(12):856–861, December 2006.

[143] Peter Lodahl, Sahand Mahmoodian, and Søren Stobbe. Interfacing single photons and single quantum dots with photonic nanostructures. *Reviews of Modern Physics*, 87(2):347–400, May 2015.

[144] Mika A. Sillanpää, Jae I. Park, and Raymond W. Simmonds. Coherent quantum state storage and transfer between two phase qubits via a resonant cavity. *Nature*, 449(7161):438–442, September 2007.

[145] J. Majer, J. M. Chow, J. M. Gambetta, Jens Koch, B. R. Johnson, J. A. Schreier, L. Frunzio, D. I. Schuster, A. A. Houck, A. Wallraff, A. Blais, M. H. Devoret, S. M. Girvin, and R. J. Schoelkopf. Coupling superconducting qubits via a cavity bus. *Nature*, 449(7161):443–447, September 2007.

[146] Pierre Nataf and Cristiano Ciuti. Protected Quantum Computation with Multiple Resonators in Ultrastrong Coupling Circuit QED. *Physical Review Letters*, 107(19):190402, November 2011.

[147] Chui-Ping Yang, Qi-Ping Su, and Franco Nori. Entanglement generation and quantum information transfer between spatially-separated qubits in different cavities. *New Journal of Physics*, 15(11):115003, 2013.

[148] Lan Zhou, Z. R. Gong, Yu-xi Liu, C. P. Sun, and Franco Nori. Controllable Scattering of a Single Photon inside a One-Dimensional Resonator Waveguide. *Physical Review Letters*, 101(10):100501, September 2008.

[149] B. Peng, Ş K. Özdemir, S. Rotter, H. Yilmaz, M. Liertzer, F. Monifi, C. M. Bender, F. Nori, and L. Yang. Loss-induced suppression and revival of lasing. *Science*, 346(6207):328–332, October 2014.

[150] Dimitris G. Angelakis, Marcelo F. Santos, Vassilios Yannopapas, and Artur Ekert. A proposal for the implementation of quantum gates with photonic-crystal waveguides. *Physics Letters A*, 362(5):377–380, March 2007.

[151] D. G. Angelakis, S. Bose, and S. Mancini. Steady-state entanglement between hybrid light-matter qubits. *EPL (Europhysics Letters)*, 85(2):20007, 2009.

[152] Jaeyoon Cho, Dimitris G. Angelakis, and Sougato Bose. Heralded generation of entanglement with coupled cavities. *Physical Review A*, 78(2):022323, August 2008.

[153] Michael J. Hartmann, Fernando G. S. L. Brandão, and Martin B. Plenio. Effective Spin Systems in Coupled Microcavities. *Physical Review Letters*, 99(16):160501, October 2007.

[154] Neil Na and Yoshihisa Yamamoto. Massive parallel generation of indistinguishable single photons via the polaritonic superfluid to Mott-insulator quantum phase transition. *New Journal of Physics*, 12(12):123001, 2010.

[155] J. Ruiz-Rivas, E. del Valle, C. Gies, P. Gartner, and M. J. Hartmann. Spontaneous collective coherence in driven dissipative cavity arrays. *Physical Review A*, 90(3):033808, September 2014.

[156] Amnon Yariv, Yong Xu, Reginald K. Lee, and Axel Scherer. Coupled-resonator optical waveguide:?a proposal and analysis. *Optics Letters*, 24(11):711–713, June 1999.

[157] Christian Nietner. *Quantum Phase Transition of Light in the Jaynes-Cummings Lattice*. Diploma thesis, Freie Universität Berlin, September 2010.

[158] Roy J. Glauber and M. Lewenstein. Quantum optics of dielectric media. *Physical Review A*, 43(1):467–491, January 1991.

[159] Ulrich Schollwöck. The density-matrix renormalization group in the age of matrix product states. *Annals of Physics*, 326(1):96–192, January 2011.

[160] Guifré Vidal. Efficient Classical Simulation of Slightly Entangled Quantum Computations. *Physical Review Letters*, 91(14):147902, October 2003.

Publications and Conference Contributions

List of Publications

- *Controlling the gain contribution of background emitters in few-quantum-dot microlasers*, F. Gericke, **M. Segnon**, M. von Helversen, C. Hopfmann, T. Heindel, C. Schneider, S. Höfling, M. Kamp, A. Musiał, X Porte, C. Gies, and S. Reitzenstein, New Journal of Physics, **20**(2):023036, 2018.

- *Delayed formation of coherence in the emission dynamics of high-Q nanolasers*, Galan Moody, **Mawussey Segnon**, Isabelle Sagnes, Rémy Braive, Alexios Beveratos, Isabelle Robert-Philip, Nadia Belabas, Frank Jahnke, Kevin L. Silverman, Richard P. Mirin, Martin J. Stevens, and Christopher Gies, Optica, **5**(4):395–401, April 2018.

List of Conference Contributions

- *Controlling the influence of background emitters on lasing in quantum dot micropillars*
  DPG spring meeting condensed matter section, Dresden (2017)
  Fabian Gericke, **Mawussey Segnon**, Martin von Helversen, Tobias Heindel, Christian Schneider, Frank Jahnke, Sven Höfling, Anna Musial, Xavier Porte, Martin Kamp, Christopher Gies, and Stephan Reitzenstein

- *Non-markovian delay in the formation of coherence in a pulsed quantum-dot crystal laser*
  DPG spring meeting condensed matter section, Dresden (2017)
  Mawussey Segnon, Galan Moody, Frank Jahnke, Marty Stevens und Christopher Gies

- *Non-Markovian delay in the formation of coherence in quantum-dot nanolasers operating in the cavity-QED regime*
  International Conference on Numerical Simulation of Optoelectronic Devices (NUSOD), Denmark (2017)
  Mawussey Segnon, Galan Moody, Frank Jahnke, Marty Stevens and Christopher Gies

- *Emitter-emitter correlation mediated by collective modes in coupled cavity arrays*
  DPG spring meeting condensed matter section, Berlin (2018)
  Mawussey Segnon, Isa Grothe, Paul Gartner, and Christopher Gies

Acknowledgements

First and foremost, I would like to thank my supervisor Prof. Dr. Frank Jahnke for giving me the possibility to prepare this thesis in his group, and for providing me the opportunity to attend the NUSOD conference in Denmark.
Furthermore, I am indebted to Dr. Christopher Gies and Dr. Paul Gartner for their stimulating discussions and the fruitful cooperation without which this thesis would not have been possible.
I would also like to express my thanks to Dr. Galan Moody, and the team of Prof. Dr. Stephan Reitzenstein for many interesting discussions and the constructive cooperation between experiment and theory.
Very special thanks to Prof. Dr. Tim Wehling for accepting to be my second advisor.
I would like to express my gratitude to Dr. Christopher Gies, Dr. Alex Steinhoff, Christian Carmesin, Daniel Erben, and Frederick Lohof for proofreading parts of this thesis.
Finally, I would like to thank my beloved wife Doélé and my family, im particular my brother Dr. Mawuli Segnon for their unconditional support.